

**UCSF**

**UC San Francisco Electronic Theses and Dissertations**

**Title**

Optogenetic Manipulation of Zebrafish Physiology and Behavior

**Permalink**

<https://escholarship.org/uc/item/3wn2c8p4>

**Author**

Arrenberg, Aristides B.

**Publication Date**

2010

Peer reviewed|Thesis/dissertation

**Optogenetic Manipulation of Zebrafish  
Physiology and Behavior**

by Aristides B. Arrenberg

DISSERTATION

Submitted in partial satisfaction of the requirements for the degree of

DOCTOR OF PHILOSOPHY

in NEUROSCIENCE in the

GRADUATE DIVISION

of the

UNIVERSITY OF CALIFORNIA, SAN FRANCISCO

© Copyright 2010

by

Aristides B. Arrenberg

## **Acknowledgements**

I would like to thank my thesis advisor, Herwig Baier, for his guidance and support. I am grateful to the members of the Baier laboratory for their advice and the exchange of ideas, foremost to Ethan K. Scott, who helped me to start in the Baier laboratory.

I would like to acknowledge my Thesis Committee, Herwig Baier, David Copenhagen, Michael Stryker and John Rubenstein, who have contributed meaningfully to my project; and Russell Fernald, who helped to evaluate my work in its final stage.

The text of this thesis is partially i) a reprint of a manuscript published in PNAS (Arrenberg et al., 2009), ii) a reprint of a manuscript published in the Journal of Neuroscience (Schoonheim et al.) and iii) a manuscript in preparation for submission. The senior authors listed in these publications directed and supervised the research that forms the basis for the thesis.

The author contributions in the published material are as follows.

i) PNAS 2009 (Arrenberg et al., 2009) (chapter 2): Aristides B. Arrenberg performed experiments and analyzed data. Filippo Del Bene contributed

zebrafish lines for *UAS:ChR2(H134R)-eYFP* and *UAS:mCherry-kras*. Aristides B. Arrenberg and Herwig Baier wrote the manuscript.

ii) Journal of Neuroscience 2010 (Schoonheim et al.) (chapter 3): Aristides B. Arrenberg developed the movie theater setup, performed the optogenetic experiments (Fig. 1, Fig. 2, Fig. 3, Fig. 11) and analyzed the *didy* recovery (Fig. 7). Peter J. Schoonheim characterized the mutant (Fig. 4, Fig. 5, Fig. 6, Fig. 8, Fig. 9, Fig. 10). Aristides B. Arrenberg and Peter J. Schoonheim analyzed data. Filippo Del Bene contributed the *UAS:ChR2(H134R)-eYFP* line. Herwig Baier wrote the manuscript, which was drafted by Peter Schoonheim.

iii) Manuscript in preparation (chapter 4): The optogenetic idea, transgenic lines and original observation originated in Herwig Baier's lab; follow-up experiments were carried out in Didier Y.R. Stainier's lab as an equal collaboration between Aristides B. Arrenberg and Jan Huisken. All authors worked on the manuscript, which was drafted by Aristides B. Arrenberg and Jan Huisken.

The work presented in these manuscripts is equivalent to a standard thesis.

# Optogenetic Manipulation of Zebrafish

## Physiology and Behavior

Aristides B. Arrenberg

### **Abstract**

Expression of halorhodopsin (NpHR), a light-driven microbial chloride pump, allows for optical control of membrane potential and reversible silencing of transfected neurons and muscle cells (“optogenetics”). Zebrafish are ideal model organisms for experiments involving localized light delivery, since they are optically clear, genetically tractable and display many behaviors within the first two weeks of life.

Here, the optogenetic approach was adapted to zebrafish by creating transgenic zebrafish lines coding for light-activatable pumps (NpHR) and channels (channelrhodopsin-2, ChR2) and by implementing optical methods for the precise application of light. We studied the neural circuits underlying the generation of fast eye movements (saccades) during the optokinetic response (OKR). The OKR is a visual behavior, which minimizes retinal slip during rotating motion. Applying light through thin optic fibers positioned above the animal's head enabled us to target small groups of cells and to simultaneously test the effect of their silencing on the generation of saccades during the OKR. We identified a cell population in rhombomere 5 that is required and sufficient for the generation of saccades in zebrafish larvae. The discovered similarities between zebrafish and

mammalian oculomotor circuitry are in line with a possible homology of the saccade generator in fish and mammals.

Furthermore, we studied the cardiac conduction system throughout development using these tools. By automated sequential illumination of small areas of the developing heart with a digital micromirror device (DMD), while simultaneously monitoring heart contractions, we identified the regions responsible for initiating and relaying cardiac conduction. By directly targeting the pacemaker areas with well-defined light pulses, we were able to induce disease-like states (tachycardia, bradycardia, AV blocks).

Together, our studies have introduced a versatile optogenetic toolkit for precise loss-of-function and gain-of-function analysis of neural circuits, behavior, and physiology.

# Table of Contents

<i>Optogenetic Manipulation of Zebrafish Physiology and Behavior</i>	<i>i</i>
<i>Acknowledgements</i>	<i>iii</i>
<i>Abstract</i>	<i>v</i>
<i>Table of Contents</i>	<i>vii</i>
<i>List of Figures</i>	<i>xi</i>
<b>Chapter 1 - Introduction</b>	<b>1</b>
<b>1.1 Conceptual Approach</b>	<b>1</b>
<b>1.2 The zebrafish as a model system</b>	<b>2</b>
<b>1.3 Genetically defined populations of neurons</b>	<b>4</b>
<b>1.4 Tools for the manipulation of neuronal activity in zebrafish</b>	<b>6</b>
<b>1.5 Optical methods for light application</b>	<b>9</b>
<b>Chapter 2 - Optical control of zebrafish behavior with halorhodopsin</b>	<b>12</b>
<b>2.1 Authors</b>	<b>12</b>
<b>2.2 Abstract</b>	<b>12</b>
<b>2.3 Publication</b>	<b>13</b>
<b>2.4 Introduction</b>	<b>14</b>
<b>2.5 Results</b>	<b>16</b>
2.5.1 Enhanced Halorhodopsin (eNpHR) is targeted to the cell surface of zebrafish neurons <i>in vivo</i>	



2.5.2	Single-unit electrophysiology confirms silencing <i>in vivo</i> _____	18
2.5.3	Swimming Behavior is inhibited by NpHR stimulation and triggered by rebound from inhibition _____	20
2.5.4	Fiber optics enables targeted, high-resolution silencing of neuronal activity _____	21
2.5.5	NpHR-assisted optogenetic scanning identifies swim command neurons in the hindbrain _	23
2.5.6	“Reversible spinalization” can be used as a method to study descending swim commands _	25
2.5.7	ChR2, co-expressed with NpHR and activated separately, can be used to control locomotor behavior _____	27
<b>2.6</b>	<b>Discussion</b> _____	<b>29</b>
<b>2.7</b>	<b>Materials and Methods</b> _____	<b>34</b>
2.7.1	Electrophysiology _____	34
2.7.2	Optic fiber setup _____	35
2.7.3	Additional Methods _____	35
<b>2.8</b>	<b>Acknowledgements</b> _____	<b>35</b>
<b>2.9</b>	<b>Supporting Information</b> _____	<b>36</b>
2.9.1	Plasmids and Transgenic Fish Lines _____	36
2.9.2	Electrophysiology _____	37
2.9.3	Modeling _____	38
2.9.4	Optic fiber Setup _____	39
2.9.5	Swimming Behavior _____	40
2.9.6	Statistics _____	41
2.9.7	Supporting Figures _____	43
<b>Chapter 3 - Optogenetic localization and genetic perturbation of saccade-generating neurons in zebrafish</b> _____		<b>50</b>
<b>3.1</b>	<b>Authors</b> _____	<b>50</b>

<b>3.2</b>	<b>Abstract</b>	<b>50</b>
<b>3.3</b>	<b>Publication</b>	<b>51</b>
<b>3.4</b>	<b>Introduction</b>	<b>52</b>
<b>3.5</b>	<b>Materials and methods</b>	<b>55</b>
3.5.1	Fish maintenance and genotypes of wildtype strains, mutants, and transgenics	55
3.5.2	Optokinetic response assay	56
3.5.3	Manipulation of neural activity with NpHR and ChR2	56
3.5.4	Positional cloning and genotyping	57
3.5.5	Morpholino phenocopy and <i>in situ</i> RNA hybridization	58
3.5.6	Site-directed mutagenesis	59
3.5.7	Two-electrode voltage-clamp recordings from <i>Xenopus</i> oocytes	59
<b>3.6</b>	<b>Results</b>	<b>60</b>
3.6.1	A small hindbrain region in rhombomere 5 is necessary for saccade generation	60
3.6.2	Optical stimulation of a small hindbrain area is sufficient for saccade generation	62
3.6.3	Optical stimulation of abducens motor neurons in a specific enhancer trap line does not produce saccades	66
3.6.4	<i>didy</i> mutants fail to sustain saccads during the OKR in a direction-specific manner	67
3.6.5	The <i>didy</i> mutation does not affect vision, saccade ballistics, or eye muscles	68
3.6.6	The saccade generation defect does not depend on stimulus velocity and recovers over time	70
3.6.7	Genetic and functional identification of <i>didy</i> <sup>s52</sup> as a null allele of <i>scn11lab</i>	71
3.6.8	The <i>didy</i> saccade deficit is reversed by activating ChR2 in the putative saccade generator	74
<b>3.7</b>	<b>Discussion</b>	<b>77</b>
<b>3.8</b>	<b>Acknowledgements</b>	<b>82</b>
<b>Chapter 4 - Optogenetic control of cardiac function</b>		<b>84</b>
<b>4.1</b>	<b>Authors</b>	<b>84</b>

<b>4.2</b>	<b>Abstract</b>	<b>84</b>
<b>4.3</b>	<b>Results and Discussion</b>	<b>86</b>
<b>4.4</b>	<b>Methods</b>	<b>98</b>
<b>4.5</b>	<b>Acknowledgements</b>	<b>98</b>
<b>4.6</b>	<b>Author contributions</b>	<b>98</b>
<b>4.7</b>	<b>Author Information</b>	<b>99</b>
<b>4.8</b>	<b>Supplementary Methods</b>	<b>99</b>
4.8.1	Transgenic fish	99
4.8.2	DMD stimulation	100
4.8.3	Analysis	101
4.8.4	Supplementary Figures	102
<b><i>Chapter 5 - Discussion</i></b>		<b><i>106</i></b>
<b>5.1</b>	<b>Optogenetics in zebrafish</b>	<b>106</b>
<b>5.2</b>	<b>Limitations</b>	<b>107</b>
<b>5.3</b>	<b>Outlook</b>	<b>109</b>
<b><i>Chapter 6 - Bibliography</i></b>		<b><i>111</i></b>
<b><i>Signed library release form</i></b>		<b><i>121</i></b>

## List of Figures

<i>Figure 1</i>	2
<i>Figure 2</i>	4
<i>Figure 3</i>	5
<i>Figure 4</i>	6
<i>Figure 5</i>	9
<i>Figure 6</i>	11
<i>PNAS Figure 1</i>	17
<i>PNAS Figure 2</i>	20
<i>PNAS Figure 3</i>	23
<i>PNAS Figure 4</i>	25
<i>PNAS Figure 5</i>	27
<i>PNAS Figure 6</i>	28
<i>PNAS Supplementary Figure 1</i>	43
<i>PNAS Supplementary Figure 2</i>	43
<i>PNAS Supplementary Figure 3</i>	44
<i>PNAS Supplementary Figure 4</i>	44
<i>PNAS Supplementary Figure 5</i>	45
<i>PNAS Supplementary Figure 6</i>	46
<i>PNAS Supplementary Figure 7</i>	47
<i>PNAS Supplementary Figure 8</i>	48
<i>PNAS Supplementary Figure 9</i>	49
<i>J Neuro Figure 1</i>	62

<i>J Neuro Figure 2</i>	65
<i>J Neuro Figure 3</i>	66
<i>J Neuro Figure 4</i>	68
<i>J Neuro Figure 5</i>	69
<i>J Neuro Figure 6</i>	69
<i>J Neuro Figure 7</i>	71
<i>J Neuro Figure 8</i>	73
<i>J Neuro Figure 9</i>	74
<i>J Neuro Figure 10</i>	74
<i>J Neuro Figure 11</i>	76
<i>J Neuro Figure 12</i>	79
<i>Manuscript figure 1</i>	88
<i>Manuscript figure 2</i>	90
<i>Manuscript figure 3</i>	93
<i>Manuscript figure 4</i>	96
<i>Manuscript supplementary figure 1</i>	102
<i>Manuscript supplementary figure 2</i>	103
<i>Manuscript supplementary figure 3</i>	104
<i>Manuscript supplementary figure 4</i>	105

# **Chapter 1 - Introduction**

## ***1.1 Conceptual Approach***

The task of neuroscience is to relate activity within the brain to the behavior the organism produces. From a developmental perspective, scientists ask how the neuronal assembly reaches its organizational state and from a functional perspective, we strive to unravel how the organism makes use of its neuronal assembly to generate behavior. The presented work has been accumulated in an environment that addresses both of these questions in the zebrafish animal model. We are interested in the molecular and cellular mechanisms underlying animal behavior and try to distill knowledge by manipulating single genes in the organism and document the resulting effects. Our research emphasizes behavioral analysis and genes that alter the behavior in specific ways in the hope of facilitating the understanding of the complex network of neurons and genes in the developing and mature organism. In addition we use targeted manipulations of neuronal activity and study the resulting effects on behavioral performance to identify neuronal circuits involved in generating behaviors. To assess their functional role, these manipulations are performed in spatially or genetically defined populations of neurons.

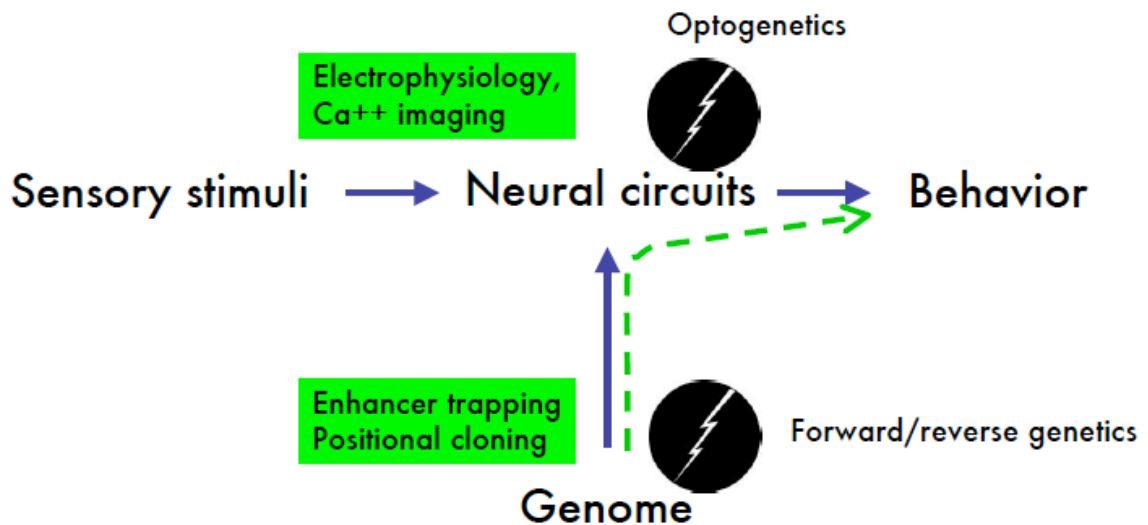


**Figure 1**

**Conceptual Approach.** We use genetic approaches to circuit assembly and function for phenotype-driven systems neuroscience. Sensory stimuli and the genome shape the activity patterns in the neural circuits that in turn drive the behavior. At the neural circuit level, we use sensors (e.g. electrophysiology, Ca<sup>2+</sup> imaging) and actuators (e.g. genetically encoded, light-activatable ion channels, “optogenetics”) to read out and manipulate neural activity. At the genome level, forward and reverse genetics enable us to study the function of genes and enhancer trapping provides a means for targeting specific neural tissues (see text body below).

## **1.2 The zebrafish as a model system**

Zebrafish are the animal model of choice for the presented studies, because the fish life cycle combines a couple of important advantages. First, transgenic lines can be generated efficiently in a relatively short time (3-4 months). Since zebrafish develop externally (outside the parental fish), genetic manipulations are easily performed at single-cell stage. Second, within five days the egg develops into a larva that shows a plethora of complex behaviors. The larvae are already heavily dependent on vision at this stage and use eye movements to stabilize the image of the outer world on the retina (Optokinetic Response, OKR) and bring objects into the field of view. They use vision to stay geostationary in moving

waters (Optomotor response, OMR) and to feed on dead and living food. One of the most complex identified visual behaviors is hunting, in which larvae orient towards, follow and capture moving prey (e.g. paramecia). To a neuroscientist the availability of behavioral paradigms is critical, since the understanding of the brain is limited by our ability to measure behavioral performances, which are the outcome of the computations in the brain. Third, larval zebrafish are small and transparent which is convenient for several reasons: It allows to perform fluorescent labeling and imaging experiments *in vivo*. We can study morphologies (cell contacts, cell shapes and projections) and also time-dependent processes, like the growth of neurons and the activity of neurons during behavior (e.g. Calcium imaging). Furthermore, we can manipulate neuronal activity using spatially defined light pulses (see below). Lastly, zebrafish are amenable to large-scale, high-throughput screens for disruptions of behavior (Brockhoff et al., 1995; Granato et al., 1996), as our laboratory has recently shown (Muto et al., 2005).



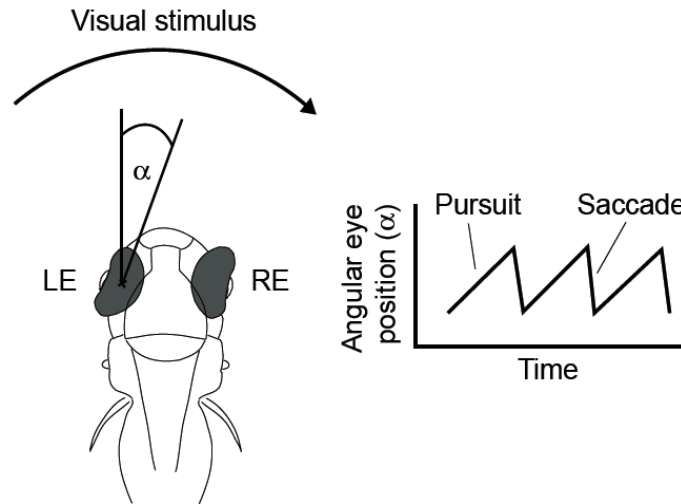


**Figure 2**

**The Optokinetic Response (OKR).** The OKR is one of the many visual behaviors the animal starts performing already at larval stage. Animals perform the OKR when a large visual stimulus is rotated about them (arched arrow). The OKR consists of alternating tracking eye movements in the direction of motion and quick saccadic eye movements in the other direction. Humans perform similar eye movements, e.g. sitting in a train and watching objects pass by through the window. Note that zebrafish do not have a fovea (retinal area of sharpest sight). Therefore, the slow phases (tracking) of the OKR aim at minimizing the slip on the retina and not at following a specific visual object.

### **1.3 Genetically defined populations of neurons**

In the presented studies, I will make use of the zebrafish lines generated by the large-scale enhancer trap screen that our laboratory performed from 2005 to 2007 (Scott et al., 2007; Mason, 2009). Enhancer trapping is a technique in which constructs containing a basal promoter and a marker transgene are randomly integrated into the organism's genome. The "trapped" enhancers of endogenous genes then express the marker in a pattern similar to that of the endogenous gene. This approach has been very useful in the *Drosophila* model system, as it allowed researchers to visualize and manipulate discrete tissues.

The insertions can be used to identify and mutate the genes expressed in subpopulations of cells (Bourbon et al., 2002; Gerlitz et al., 2002), and to manipulate the labeled tissues (Martin et al., 1999; Dubnau et al., 2001; Martin et al., 2002). Our large-scale enhancer trap screen made use of the Gal4/UAS expression system (see Figure 3). Trapped enhancers drive the expression of GAL4, and fish carrying this insertion can be crossed to fish expressing fluorescent fluorophores, e.g. *UAS:Kaede* transgenic fish, in order to characterize the expression pattern of the trapped enhancer.

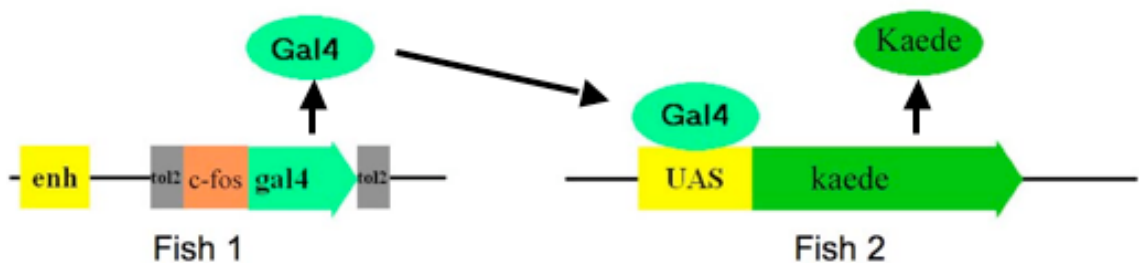


### Figure 3

**The Gal4/UAS system used in our enhancer trap approach.** During the enhancer trap screen hundreds of Gal4 fish (fish 1) are generated. The DNA construct (within the *tol2* sites) integrates in proximity of an enhancer (*enh*) in the fish genome. The (tissue specific) enhancer in turn drives the expression of the yeast transcription factor Gal4. A fish (fish 2) transgenic for the Gal4 binding DNA element, UAS, is crossed to the Gal4 fish to drive the expression of the fluorophore Kaede in offspring larvae that are transgenic for both constructs. The Kaede expression pattern is dictated by the trapped enhancer.

We generated approximately 180 enhancer trap lines with unique and restricted expression patterns (Scott et al., 2007; Mason, 2009). A selection of the lines is illustrated in Figure 4. These lines can be subjected behavioral assays in order to investigate the function of each of the targeted tissues and cell types.

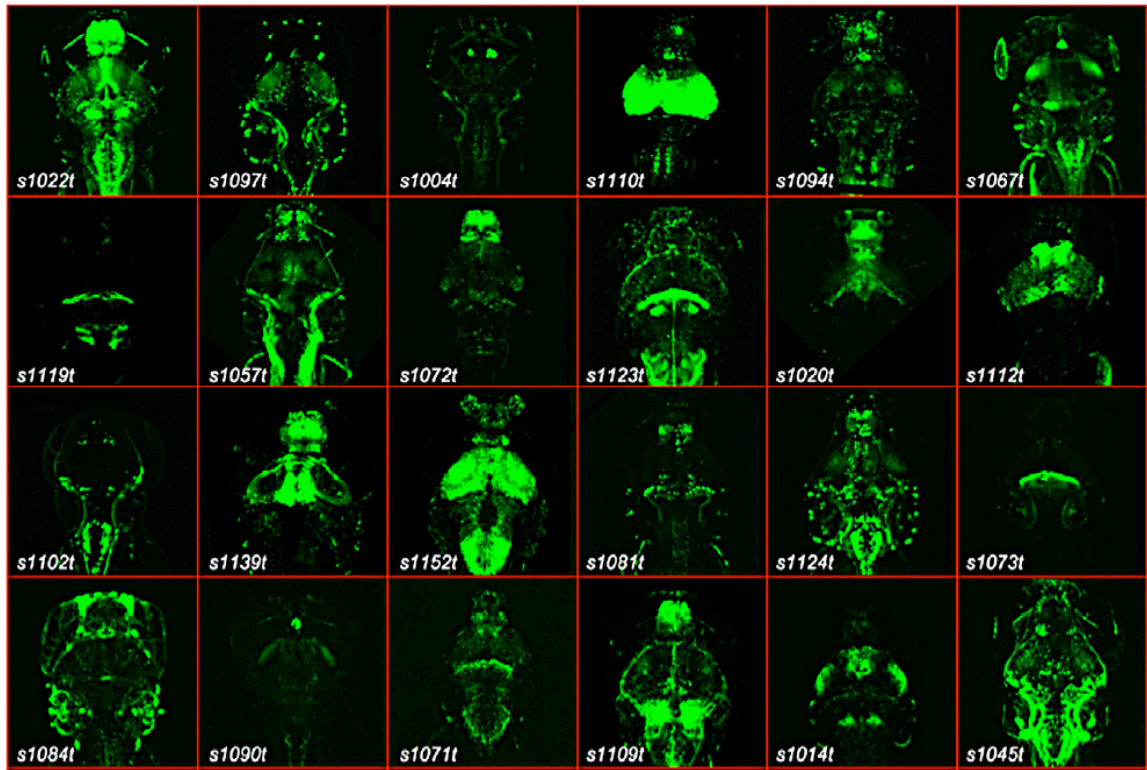


#### Figure 4

##### Examples of Gal4-VP16 driver lines labeling subsets of neurons in the zebrafish brain.

Panels show 24 examples of UAS:Kaede expression patterns picked up in a recent ET screen, with the Gal4-VP16 line number indicated. All are dorsal images of 5 or 6 dpf live larvae, mounted in agarose. Reprinted from (Baier and Scott, 2009).

### 1.4 Tools for the manipulation of neuronal activity in zebrafish

A powerful approach for the causal analysis of neural circuits underlying behaviors is the manipulation of neuronal function. Tools that allow to do this in spatially and temporally controlled ways are very useful for a great number of research projects. Generally, manipulation approaches include pharmacological perturbations, mutant animals with defects in neuronal activity (Gnuegge et al., 2001; Grubb et al., 2003; McLaughlin et al., 2003) and genetically introduced manipulations that alter activity, block synaptic transmission (Gnuegge et al.,

2001; Suster et al., 2003; Yamamoto et al., 2003) or ablate cell populations (Padungchaichot et al., 2000; Wong et al., 2000). Many approaches are limited, because precise spatial and temporal control is not feasible. In invertebrates, a temperature-sensitive blocker of synaptic transmission, *shibire*<sup>ts</sup>, has advanced *Drosophila* research considerably (Kitamoto, 2002). Other activity blockers have been reported, including an IVM-gated chloride channel from *C.elegans*, GluCl, that has been used to hyperpolarize and inactivate neurons (Slimko et al., 2002). These two blockers of neural activity are attractive because they are inducible and reversible. More recently, novel ion channels (Nagel et al., 2003) and pumps (Schobert and Lanyi, 1982; Kalaidzidis et al., 1998; Han and Boyden, 2007; Zhang et al., 2007; Gradinaru et al., 2008; Zhao et al., 2008) that are activatable by light have been introduced to neuroscience. Light activatable channels provide the advantage of even more precise temporal control (milliseconds) than achievable with previous tools. Furthermore light can be shaped spatially using optics (see below), which provides an additional way of controlling activation spatially. While light-activatable channels were already available for some time, the recent channels channelrhodopsin-2 (ChR2) and halorhodopsin (NpHR, it is actually a pump) have found broad use in neuroscience since 2007, since they worked very well (high currents) and studies using them caught attention in prominent journals.

Before we set out to generate transgenic fish for light-activatable channels, the toolbox for zebrafish had been limited. Pharmacology and mutant analyses had been used as mentioned above and two pioneering studies had been published

using a light-gated glutamate receptor (LiGluR) (Szobota et al., 2007) and channelrhodopsin-2 in transient expression (Douglass et al., 2008) in zebrafish. Furthermore tools for permanent activity manipulations became available (tetanus toxin transgenic fish (Asakawa et al., 2008)) and genetically specified ablations were possible (using Nitroreductase (Curado et al., 2007; Davison et al., 2007; Pisharath et al., 2007)). Our laboratory had previously (up to 2007) tried to establish transgenic tools coding for the temperature-sensitive synaptic transmission blocker dnDynamin and for the synaptic transmission blocker dnVAMP (dominant negative vesicle-associated membrane protein) as well as for a potassium channel (Kir2.1) and for GluCl. These approaches did not turn out to be fruitful for various reasons (data not shown) and the introduction of light activatable channels in zebrafish was appreciated in our laboratory for its success in the manipulation of neural activity and behaviors. The light-activatable ion channels allow for conditional, tissue-specific blockage of neural activity in zebrafish. Filling this gap in our technical capabilities has a profound effect on the types of questions that vertebrate neurobiologists can address. For instance, systems neurobiologists interested in the function of a particular area or nucleus in zebrafish can hope to find a mutant with a specific defect, or can ablate the tissue physically. Either approach carries caveats related to the inability to reverse the effects of the lesion. Furthermore, observations can usually only be started a while after the introduction of the defect which complicates the interpretation of results. This is just one example for studies that would benefit

greatly from the ability to block neural activity at controlled times and in specified tissues.

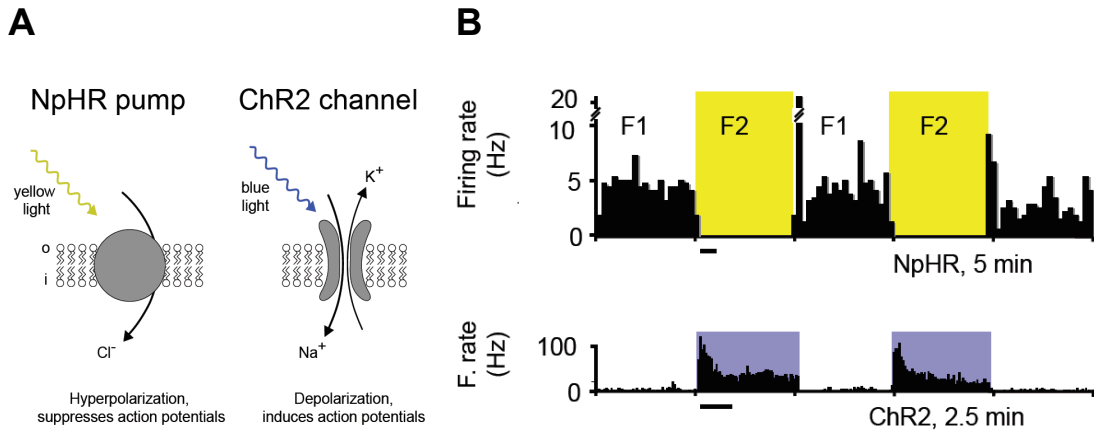


**Figure 5**

**Light-activatable ion pumps and channels.** (A) The bacterial *Natronomonas Pharaonis* halorhodopsin (NpHR) and the algal channelrhodopsin-2 (ChR2) allow ions to move across the plasma membrane of a cell. (B) Firing rate histograms for two zebrafish neurons expressing NpHR (top row) or ChR2 (bottom row). The colored box indicates illumination with yellow and blue light, respectively. NpHR stimulation effectively suppressed spiking, while ChR2 stimulation induced spiking. Fig. 3B is reprinted from (Arrenberg et al., 2009).

### 1.5 Optical methods for light application

Spatial control of ion channel activation can be achieved in two ways in genetically encoded light-activatable ion channels. First, the expression of the ion channels can be limited to tissues and cell types of interest. Two examples for this expression restriction are the use of specific promoters or enhancer trap lines. Second, the light that is used to activate the channels can be shaped to only illuminate brain regions and cells of interest. In the presented studies we make use of the spatial restriction via light in most instances. When designing the optical setup for stimulation, two parameters are of utmost importance: light

intensity and spatial spread (resolution). Sufficient light intensities ( $> 1 \text{ mW/mm}^2$ ) have to be used to activate the contemporary light-gated channels. High power light sources are needed (e.g. lasers) and oftentimes the light needs to be focused on an immobilized animal. The spatial spread of the light needs to be precisely controlled to ensure that only desired neurons are activated and other neurons are left non-perturbed. Most of the tools do not allow stimulation of single specified cells within the brain (exception: two photon activation). In the presented studies I used fiber optics and digital-micro-mirror (DMD) stimulation. The former is an inexpensive, versatile approach that allows good resolution in the xy plane, but little or no resolution in the z direction. The latter provides superior spatial resolution and can be used to activate a tissue volume defined by the user. More laborious methods with even better spatial resolution exist (e.g. holographics (Lutz et al., 2008), 2P temporal focusing (Papagiakoumou et al., 2008)) and might find application in future zebrafish studies.

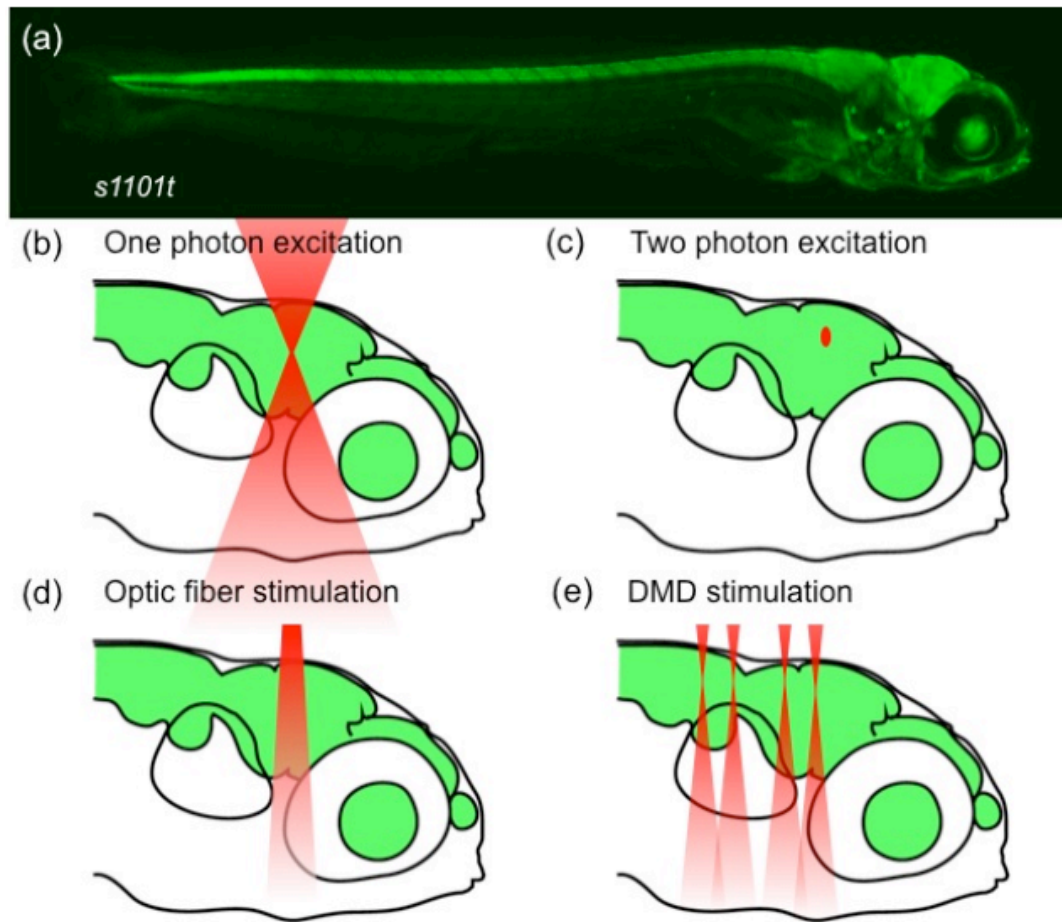


### Figure 6

**Options for the spatially confined delivery of light into the brain of a zebrafish larva.** (a) Side view of a 6 day post fertilization (dpf) zebrafish larva, carrying the pan-neuronal Et(E1b:Gal4)s1101t driver and Tg(UAS:Kaede). (b-e) Four methods for the local excitation of fluorophores and light-activated ion channels. The images show the zebrafish head with a schematic depiction of illumination volumes (red) for each method. Reprinted from (Baier and Scott, 2009).



## **Chapter 2 - Optical control of zebrafish behavior with halorhodopsin**

### **2.1 Authors**

Aristides B. Arrenberg, Filippo Del Bene and Herwig Baier

### **2.2 Abstract**

Expression of halorhodopsin (NpHR), a light-driven microbial chloride pump, enables optical control of membrane potential and reversible silencing of targeted neurons. We generated transgenic zebrafish expressing enhanced NpHR under control of the Gal4/UAS system. Electrophysiological recordings showed that eNpHR stimulation effectively suppressed spiking of single neurons in vivo. Applying light through thin optic fibers positioned above the head of a semi-restrained zebrafish larva enabled us to target groups of neurons and to simultaneously test the effect of their silencing on behavior. The photostimulated volume of the zebrafish brain could be marked by subsequent photoconversion of co-expressed Kaede or Dendra. These techniques were employed to localize swim command circuitry to a small hindbrain region, just rostral to the *commissura infima Halleri*. The kinetics of the hindbrain-generated swim command was investigated by combined and separate photo-activation of NpHR and Channelrhodopsin-2 (ChR2), a light-gated cation channel, in the same neurons. Together this “optogenetic toolkit” allows loss-of-function and gain-of-function analyses of neural circuitry at high spatial and temporal resolution in a behaving vertebrate.

### **2.3 *Publication***

Optical control of zebrafish behavior with halorhodopsin. Arrenberg AB, Del Bene F, Baier H. Proc Natl Acad Sci U S A. 2009 Oct 20;106(42):17968-73. Epub 2009 Oct 2. PMID: 19805086

## **2.4 Introduction**

Technology for the inactivation of neurons in vivo has been developed (van der Bliet and Meyerowitz, 1991; Burrone et al., 2002; Slimko et al., 2002; Sorensen et al., 2002; Hua et al., 2005; Pitman et al., 2006; Lerchner et al., 2007; Hong et al., 2008), allowing for variable degrees of temporal and spatial control. The light-gated chloride pump halorhodopsin (NpHR) from the archaeobacterium *Natronomonas pharaonis* has recently been introduced into neuroscience along with enhanced derivatives (Schobert and Lanyi, 1982; Kalaidzidis et al., 1998; Han and Boyden, 2007; Zhang et al., 2007; Gradinaru et al., 2008; Zhao et al., 2008) and enables superior temporal and spatial control. Other light-controlled silencing methods are being developed (Banghart et al., 2004; Chambers et al., 2006; Fortin et al., 2008), but require covalent attachment of a photo-switchable affinity label. NpHR silencing has been demonstrated electrophysiologically (Zhang et al., 2007; Zhao et al., 2008) and has been used to reversibly paralyze *Caenorhabditis elegans* expressing NpHR in motor peripheries (Zhang et al., 2007). Despite its promise, however, NpHR has so far found only limited applications for circuit analysis in vivo. In this study, we have devised a versatile and cost-effective optical stimulation strategy for manipulation of animal behavior with this probe. These advances were made possible by our choice of zebrafish as the experimental paradigm.

Zebrafish are ideal models for testing and applying light-controlled channels and pumps in vertebrates, since they are translucent and display a number of quantifiable behaviors during the first two weeks of larval development (Borla et

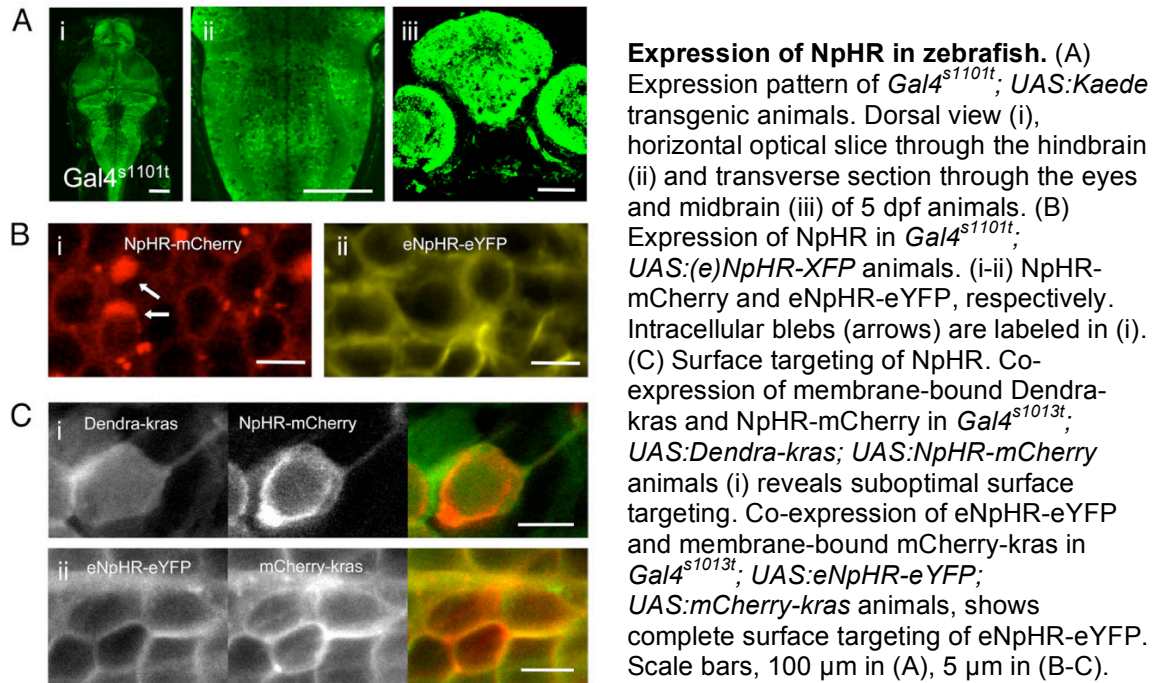
al., 2002; Orger et al., 2004; Masino and Fetcho, 2005; Burgess and Granato, 2007). Accordingly, Szobota et al. (Szobota et al., 2007) employed a re-engineered, light-gated glutamate receptor (LiGluR), to interfere with zebrafish touch responses. Douglass et al. (Douglass et al., 2008) succeeded in triggering escape responses by activating ChR2 in single zebrafish mechanosensory cells. The adaptation of the Gal4/UAS method from *Drosophila melanogaster* (Brand and Perrimon, 1993) to zebrafish enables targeting transgene expression to specific brain areas and cell types (Scheer and Campos-Ortega, 1999; Davison et al., 2007; Scott et al., 2007; Asakawa and Kawakami, 2008; Asakawa et al., 2008) and will further contribute to the refinement of an optogenetic toolkit in this system.

Here we report on the generation of UAS:NpHR transgenic zebrafish lines. Using a Gal4 line that drove NpHR broadly in neurons, we show that enhanced NpHR (eNpHR) was targeted efficiently to the surface of neurons in vivo and mediated light-induced suppression of spikes. We then employed a non-invasive fiber optics approach to stimulate small (ca. 30  $\mu$ m) CNS areas, while simultaneously monitoring the fish's behavioral responses. We combined NpHR silencing with ChR2-mediated excitation, to identify a critical role for a small cell group in the caudal hindbrain in the control of forward swimming. The ability to selectively silence neurons in vivo with precise temporal and spatial control is likely to have broad applications for the study of functional neuroanatomy and neuronal plasticity.

## **2.5 Results**

### **2.5.1 Enhanced Halorhodopsin (eNpHR) is targeted to the cell surface of zebrafish neurons *in vivo***

Different versions of NpHR have been reported to vary in their intracellular distribution and surface localization. To compare their properties in zebrafish, we generated four transgenic lines, *UAS:NpHR-eYFP*, *UAS:NpHR-mCherry*, *UAS:eNpHR-eYFP*, and *UAS:eNpHR-mCherry*. Transgenic fish were crossed to carriers from the enhancer trap line *Gal4<sup>S1101t</sup>*, which expresses the transcriptional activator Gal4-VP16 broadly in most neurons (Scott et al., 2007) (Fig. 1A). eNpHR was engineered to have improved surface targeting properties compared to NpHR (Zhao et al., 2008). As expected, eNpHR-eYFP proteins (Fig. 1B) trafficked to the cell surface and did not form the intracellular blebs that were observed for NpHR-eYFP (Fig. S1) and NpHR-mCherry (Fig.1B).



### PNAS Figure 1

Two lines (NpHR-mCherry and eNpHR-eYFP) were further investigated for surface localization by co-expressing membrane-targeted fluorophores, Dendra-kras or mCherry-kras, respectively (Fig. 1C). While most of the NpHR-mCherry protein remained intracellular, a fraction co-localized with Dendra-kras at the cell surface. In contrast, virtually all eNpHR-eYFP signal was co-localized with mCherry-kras at the plasma membrane. Membrane targeting was also demonstrated by the crisp and intense labeling of cell morphologies including neurites (Fig. S2 shows radial glial cells in the optic tectum). For unknown reasons, fusion proteins containing the identical opsin but different fluorescent tags were sometimes distributed in apparently different cellular compartments (Fig. S1 and Fig. 1B). Together, eNpHR-eYFP appeared to be the superior

probe, as it combined excellent surface localization with effectiveness in suppressing spikes (see below).

### **2.5.2 Single-unit electrophysiology confirms silencing *in vivo***

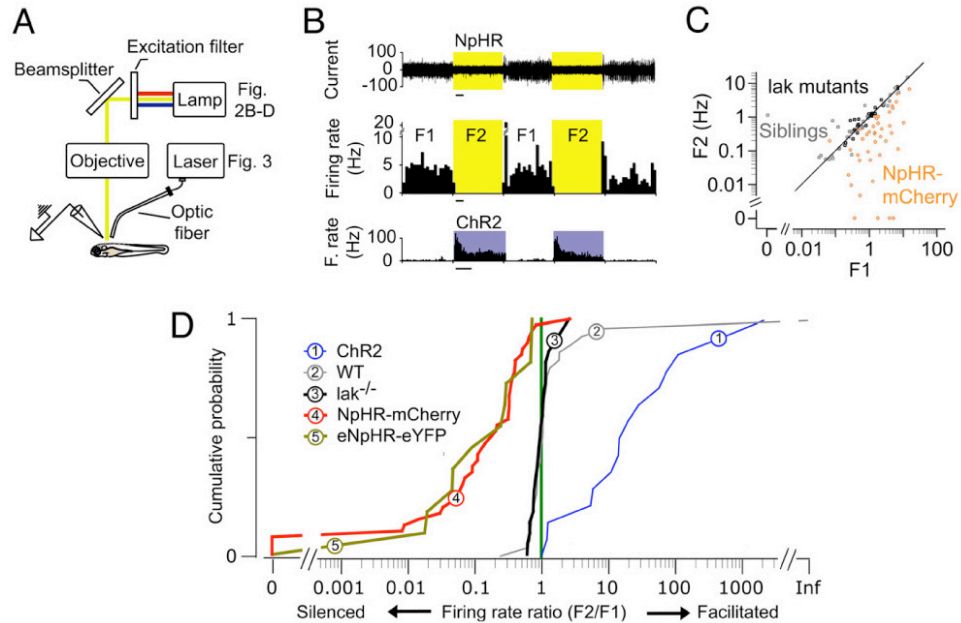
To determine whether NpHR stimulation suppressed spiking we performed loose-patch recordings in hindbrain neurons. In order to activate NpHR, a bandpass filter centered on its activation spectrum maximum (HQ 585/70, Fig. 2A) was used. The neuron in Fig. 2B (top two traces) was silenced during illumination periods, and no spikes were generated. After stimulation, the cell resumed firing at a rate comparable to the average firing rate before stimulation. This experiment suggested that NpHR was an effective and reversible silencer of neuronal activity in larval zebrafish. Conversely, the activation of the light-gated cation channel ChR2 in *Gal4<sup>s1101t</sup>; UAS:ChR2-eYFP* animals induced firing rates up to 130 Hz for many seconds (Fig. 2B bottom trace).

We next assessed the magnitude of the silencing effect across the population of recorded hindbrain neurons. NpHR expressing cells had much lower firing rates during illumination (F2) than without illumination (F1; Fig. 2C). For quantification, the distributions of firing rate ratios (F2/F1) of NpHR expressing cells and NpHR non-expressing cells (wildtype, Fig. 2D and Fig. S3) were compared. The silencing effect in NpHR expressing cells was highly significant ( $p < 0.0001$  for both eNpHR-eYFP and NpHR-mCherry, Ranksum and KS test). Furthermore, the median firing rate ratio (F2/F1) was 0.2 for both eNpHR-eYFP and NpHR-mCherry (see Fig. S4 for the light intensity dependence of the effect). This

means that NpHR photostimulation suppressed, on average, 80% of all spontaneous spikes. A fraction of cells (~15 %) were not significantly inactivated; very few even increased their spike rate (permutation test with  $\alpha=0.01$ , Fig. S5).

In control experiments with wildtype cells, we noted that illumination had a small effect on firing rate in 26 % (8/31) of the cells (permutation test,  $p<0.01$ ). These light responses could be due to synaptic input from the visual system. We therefore recorded from blind *lakritz/atoh7* mutant fish, in which retinal ganglion cells do not form (Kay et al., 2001), and found that the fraction of cells reproducibly responsive to light decreased to 14% (3/23; Fig 2D). Since the hindbrain of *lakritz/atoh7* mutants receives no input from the retina, the significant firing rate change in the few light-responsive cells could stem from inputs from the pineal organ, from intrinsic photosensitivity of the recorded cells, or from a thermal effect of the illumination.





## PNAS Figure 2

**Analysis of silencing efficacy in the hindbrain.** (A) Schematic of the electrophysiological setup. The optics of a microscope was used for NpHR activation in Fig. 2B-D (mercury lamp, excitation filter HQ 585/70, beamsplitter 90/10). For Fig. 3, a laser (532 nm) was coupled to an optic fiber to activate NpHR. (B) Unprocessed current trace (top) and corresponding single unit firing rate histogram (middle) show a cell of a NpHR-mCherry expressing animal that was silenced during illumination (yellow shaded boxes, 21 mW/mm<sup>2</sup>). Bottom: A cell from a ChR2-eYFP expressing animal fired at a higher rate upon stimulation with blue light (blue shaded boxes). Scale bars, 10 s. (C) Scatter plot of the firing rate during stimulation (F2) vs. the firing rate without stimulation (F1). NpHR-mCherry cells had a reduced firing rate F2, while cells from non-expressing siblings and blind *lakritz/ato7* mutants clustered around the line of unity (black, F2=F1). (D) Cumulative probabilities of firing rate ratios F2/F1 (with/without stimulation) in cells from different lines. Cells from NpHR lines were silenced (curve shift to the left) and cells from the ChR2 line were facilitated (shift to the right). The differences between wildtype and eNpHR-eYFP or NpHR-mCherry were highly significant ( $p < 0.0001$ , KS test and Ranksum test).

### 2.5.3 Swimming Behavior is inhibited by NpHR stimulation and triggered by rebound from inhibition

The *Gal4<sup>S1101t</sup>* transgene drives *NpHR-mCherry* broadly in CNS neurons. We therefore expected an extensive and almost instantaneous inhibition of movements upon global activation of NpHR in the entire animal. Indeed, when a dish containing zebrafish larvae was illuminated with a high-power LED (617 nm), larvae frequently stopped moving and lost coordination (Movie S1 for NpHR-expressing animals and Movie S2 for their non-expressing siblings).

Strikingly, the offset of illumination triggered a single bout of forward swimming (swim scoot) synchronized across the population (Movie S1). A similar response could be elicited in agarose-embedded larvae whose tails were left free to move (Fig. 3A and Movie S3). The frequency (35 Hz) and amplitude ( $\sim 55^\circ$ ) of the induced tail movement were in the range of those previously reported for routine swim scoots (Budick and O'Malley, 2000).

Since the forward swims were induced by switching the illumination off, it seemed likely that cells rebounding from inhibition triggered the behavior. Indeed, a heightened firing rate (up to tenfold) in the first second after light offset was observed in the majority (60%) of the recorded hindbrain cells (Fig. 3B; the remaining 40 % of cells did not show detectable changes). While we did not attempt to relate the neuronal rebound kinetics to the onset of the behavioral response in the same animal, recordings similar to those in Fig. 2 showed that rebound spiking could start within tens of milliseconds after light offset, which is in agreement with the fast NpHR kinetics (Zhang et al., 2007) ( $\tau_{\text{OFF}} = 40$  ms). The forward swimming could last up to 5 s, unless the illumination was turned back on, which again blocked all swimming movements (see below; Movie S3).

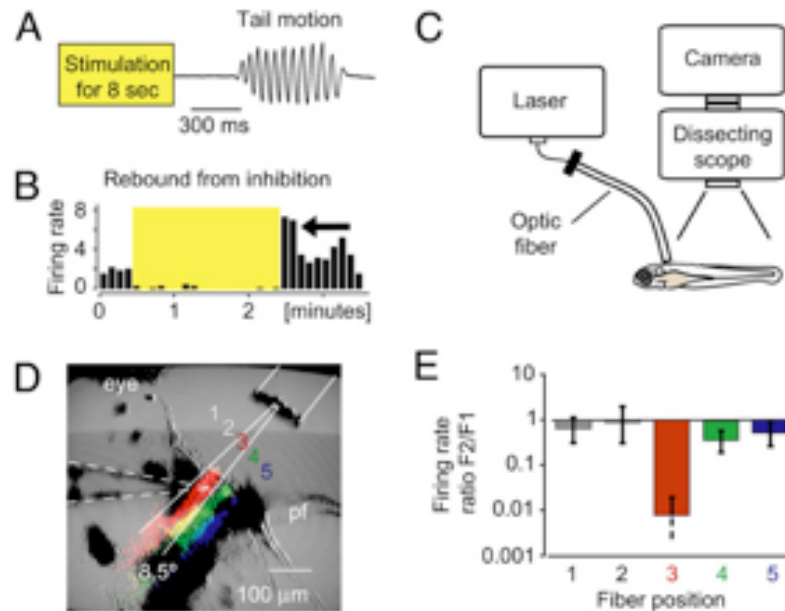
#### **2.5.4 Fiber optics enables targeted, high-resolution silencing of neuronal activity**

To investigate which neural structure was triggering the rebound swim behavior, we decided to map its origin in the zebrafish CNS using fiber optics, a method we termed “optogenetic scanning”. First, we needed to determine the spatial

resolution achievable with this method. For local activation of NpHR we used multimode optical fibers that were coupled to lasers. To verify that the light was confined to a small cone exiting the fiber we moved the fiber (10 or 50  $\mu\text{m}$  in diameter) about a recorded cell and measured the firing rate ratio F2/F1 for each position (Fig. 3D-E). In three of eight cells recorded in this manner, silencing only occurred when they were directly illuminated. (In the remaining five cells, firing rates were influenced by illuminating neighboring positions away from the cell bodies, possibly due to local interconnectivity.) Aiming the optic fiber to a position just 30  $\mu\text{m}$  away from the tip of the recording pipette had no influence on the firing rate of the cell in Fig. 3E. This observation suggests that non-invasive fiber optics used for silencing has a spatial resolution of 30  $\mu\text{m}$  or better in vivo.

To determine the approximate penetration depth and the extent of light scatter within the tissue as the stimulus light passes through the tissue, we employed a photoconvertible fluorescent protein. Fish carrying both *UAS:Dendra-kras* and *Gal4<sup>S1101t</sup>* expressed the membrane-targeted Dendra protein in most neurons. These larvae were embedded in agarose and illuminated with an optic fiber (50  $\mu\text{m}$ ) coupled to a blue laser for several minutes. Selective-plane illumination microscopy (Huisken et al., 2004) (SPIM) was used to image the distribution of green-to-red photoconverted Dendra in the hindbrain from two orthogonal directions (Fig. S6). As expected, red cells formed a narrow column whose width was 50  $\mu\text{m}$  at the surface and widened slightly with increasing depth. The divergence angle of the cone of converted cells matched the theoretical value for low numerical-aperture optic fibers ( $12^\circ$ , NA= 0.22). This experiment shows that

blue light emitted from thin optic fibers penetrates the entire depth of the zebrafish brain with little scattering.



### PNAS Figure 3

**NpHR induced locomotion.** (A) Release from NpHR activation induced locomotion in head-restrained animals. The tail deflection is plotted over time. (B) The recorded cell showed an above-average firing rate directly after the stimulation (yellow shaded box) was stopped (arrow). (C) Fiber-optic setup for the mapping of the locomotion phenotype. An optic fiber was coupled to a laser and placed over the head-restrained larva with a micromanipulator. (D, E) Spatially defined light application was feasible with optic fibers. (D) The optic fiber (10 μm inner core diameter) was moved about the recorded cell in five steps. False-colored stripes in the image represent the scattered light that was detected by the camera when light was sent through the fiber at positions 3 to 5. The stripes of scattered light approximately match the theoretical divergence angle of the fiber (8.5°, white solid lines). Dashed lines outline the position of the electrode. pf, pectoral fin. (E) The firing rate ratio F2/F1 of a single cell is plotted for different fiber positions. The cell was only silenced when it was directly illuminated, which demonstrated the precise light application with optic fibers.

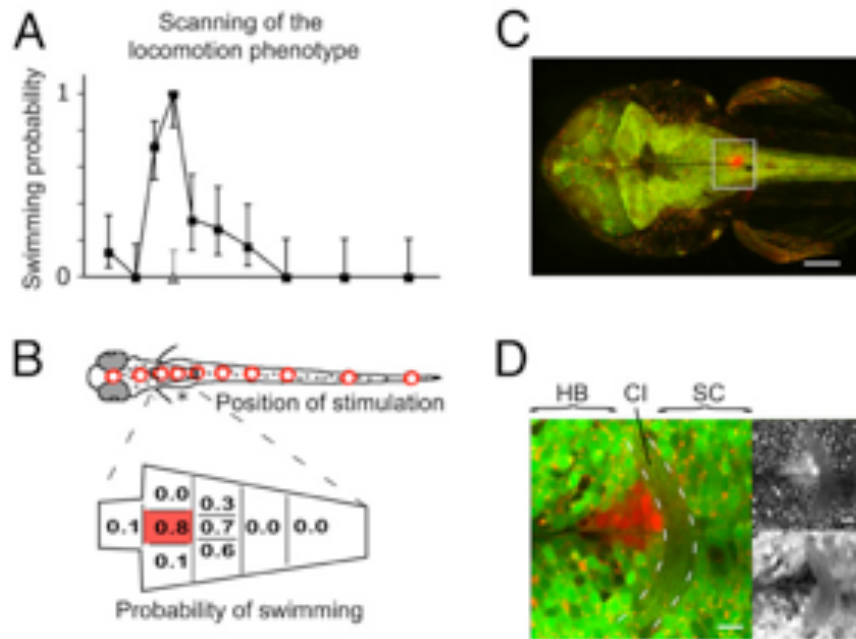
### 2.5.5 NpHR-assisted optogenetic scanning identifies swim command neurons in the hindbrain

Having shown that photostimulation with optic fibers is spatially precise, we set out to map the rebound swimming behavior to particular locations in the zebrafish

CNS. Reticulospinal neurons in the midbrain and hindbrain project to the spinal cord and activate an array of segmentally repeated neural circuits, called central pattern generators (CPGs), which drive muscles via motoneurons (Grillner et al., 2008). We placed a thick fiber (200  $\mu\text{m}$  in diameter) on the dorsal surface of the animal and photostimulated various positions in the brain (Fig. 3C). The probability of evoking swimming was maximal after offset of hindbrain illumination (Fig. 4A,  $P = 1.0$ ,  $n=17$  trials, 95 % confidence interval [0.82 1.00]) and small ( $P < 0.3$ ) after forebrain, midbrain, or spinal cord were illuminated. Non-expressing siblings did not show swimming behavior correlated to the light pulse ( $P = 0.0$ ,  $n=23$  trials, 95 % confidence interval [0 0.14]). The difference between expressors and controls was significant ( $p < 0.01$ , z-test for proportions).

A thin fiber (diameter 50  $\mu\text{m}$ ) was used to map the swim-inducing neurons in the hindbrain with greater precision (Fig. 4B). The maximum response probability ( $P = 0.8$ ) was seen following illumination of a small area just caudal to the pectoral fins and along the midline of the animal. We used the *UAS:Kaede* transgene and a UV laser to label the illumination position via photoconversion of Kaede from green to red (Fig. 4C-D). The cells that triggered the behavior with a probability of  $P=0.8$  were located in the caudal-most part of the reticular formation (Kimmel et al., 1982; Metcalfe et al., 1986), just rostral to the *commissura infima Halleri* (Herrick, 1908; Myers, 1985). This commissural tract defines the division between spinal cord and hindbrain. At the caudally adjacent positions, it was also possible to sometimes elicit swimming behavior ( $P=0.3-0.7$ ), but regions further down the spinal cord or more rostral in the brain did not affect swimming ( $P=0.0$ ).

The caudal hindbrain contains previously identified groups of neurons that extend axons into the spinal cord (Kimmel et al., 1985; Mendelson, 1986) (Fig. S7).



#### PNAS Figure 4

##### Mapping of the locomotion phenotype that was induced by rebound from NpHR silencing

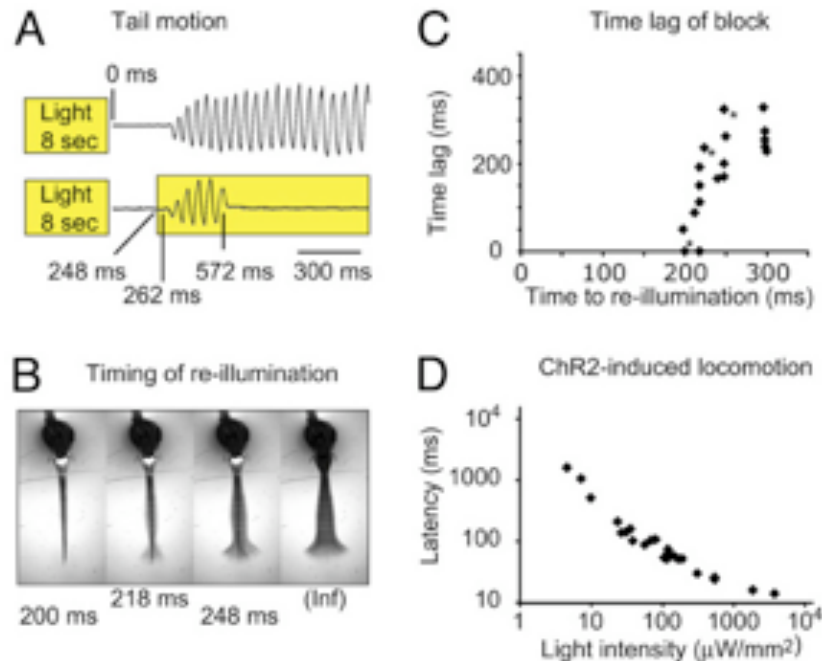
(A) The probability of observing a forward swim is plotted versus the position of stimulation (200  $\mu\text{m}$  optic fiber) in 3 dpf zebrafish. Mean probabilities of NpHR-mCherry expressors (black) and siblings (gray, only 3<sup>rd</sup> position) are shown with 95% confidence intervals (Wilson score interval for binomial distributions). (B) The hindbrain region in (A) (asterisk) was mapped in detail with a 50  $\mu\text{m}$  fiber. The probability was maximal in a small area along the midline just caudal to the pectoral fins. A total of 295 trials was analyzed in (A) and (B) ( $n=7$  animals). (C) The phenotype was mapped in an animal transgenic for *Gal4<sup>S1101t</sup>; UAS:NpHR-mCherry; UAS:Kaede*. The region where the animal responded reliably was illuminated with UV light to photo-convert Kaede. (D) Close-up of the box in (C). A narrow column of tissue was converted, labeling only few cells in every optical section. The maximal response probability was found in the region of the commissura infima Halleri (CI, dashed lines), which demarcates the border between spinal cord (SC) and hindbrain (HB). The upper right shows the red channel and the lower right the green channel. Scale bars, 100  $\mu\text{m}$  in (C) and 10  $\mu\text{m}$  in (D).

#### 2.5.6 “Reversible spinalization” can be used as a method to study descending swim commands

Spinal cord CPGs are able to generate normal locomotor muscle activations following surgical lesion of the descending connections (spinalization) (Graham-

Brown, 1911; Wallen and Williams, 1984; McDearmid and Drapeau, 2006). In our experiment, these connections were left physically intact, but reversibly inactivated. This allowed us to ask to what extent swimming, once started, was an autonomous function of the spinal CPGs. We found that rebound-evoked swimming behavior could be blocked by turning the NpHR stimulation back on during or after buildup of activity in the caudal hindbrain (n = 5 animals; Fig. 5A). This indicates that there is a defined time during which the swimming command is sensitive to hindbrain perturbations.

To begin to investigate the kinetics of this control, we used an animal (5 dpf) with long-lasting induced forward swims ( $3.6 \pm 0.3$  sec, SEM; 35 Hz swim cycle frequency). The latency of the first tail undulation following light-offset was highly reproducible ( $267 \pm 14.0$  ms, standard deviation, n=17). When the animal was re-illuminated 0 to 200 ms after turning the illumination off, the forward swim was always blocked (Fig. 5B, C). With longer time intervals, the animal initially started swimming. However, the amplitude (Fig. 5B; Movie S4) and the number of tail undulations were dependent on the re-illumination time point. The later the animal was illuminated, the stronger and longer was the swimming response. Intervals longer than 300 ms did not result in more vigorous swimming movements. Resetting CPG activity by hindbrain inputs, once set in motion, appeared to be almost immediate for low locomotor activity and took a few hundreds of milliseconds ( $\sim 300$  ms) for higher levels of locomotor activity (Fig. 5B and C).



### PNAS Figure 5

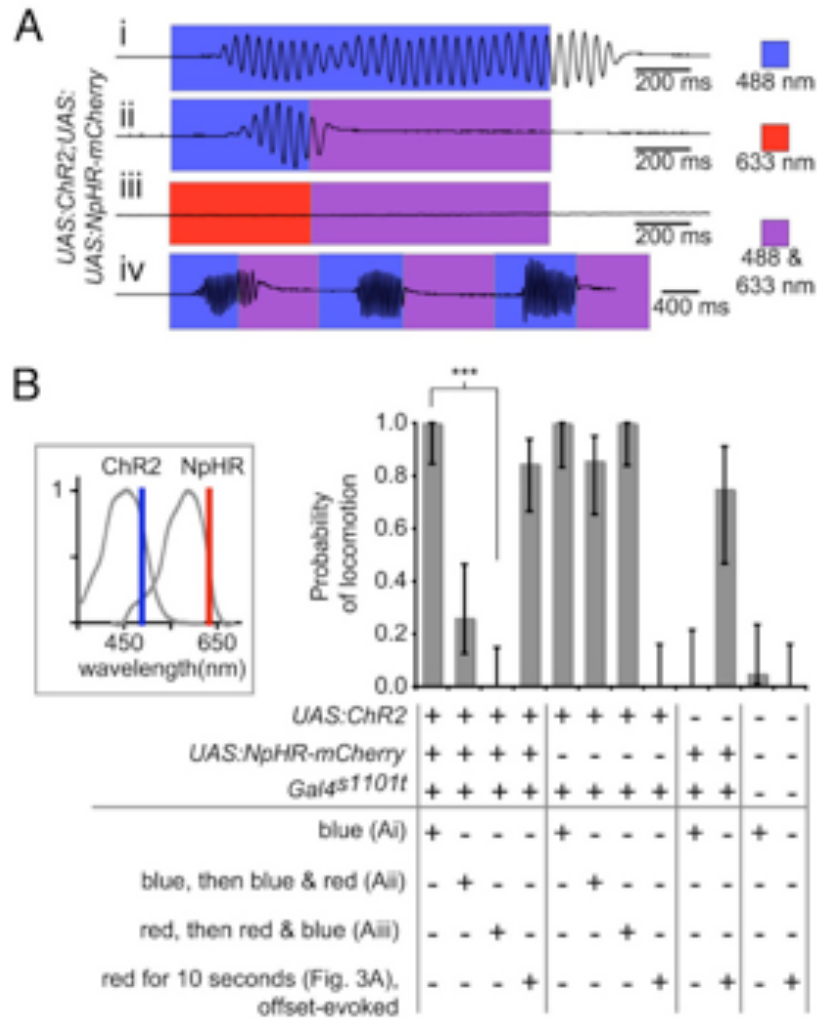
**Kinetics of the rebound-evoked swim command.** (A) The NpHR induced forward swimming was blocked by reactivating NpHR. Top: Without reactivation of NpHR, the animal (5 dpf) started to move 267 ± 3.5 ms (SEM) after the light had been turned off and continued to swim for 3.6 ± 0.3 s (SEM). Bottom: When the animal was re-illuminated after 248 ms, the locomotion that had started after 262 ms was blocked at t=572 ms. (B) The amplitude and duration of the tail contractions depended on the re-illumination time point. Early re-illuminations permitted only smaller amplitudes (see also Movie S4). Images are an average-z-projection of four consecutive minimum-intensity-z-projections. (C) The time difference between the cessation of locomotion and the re-illumination is plotted versus the re-illumination time point. Intervals shorter than 190 ms never permitted tail contractions. Between 190 ms and 250 ms the time difference increased rapidly and approached a maximum value of 263 ± 14 ms (SEM) at 300 ms. Trials in (B) are labeled with an asterisk in (C). (D) In ChR2 expressing animals, the response latency depended on the illumination intensity. Stronger illuminations elicited shorter latencies. Trials from a single 3 dpf animal are plotted.

### 2.5.7 ChR2, co-expressed with NpHR and activated separately, can be used to control locomotor behavior

We tested whether ChR2 activation in the caudal hindbrain could trigger locomotion in a fashion similar to rebound from NpHR inhibition (Fig. 5D, Fig. S8 and Movie S5). We found that the latency and amplitude of locomotion were correlated with the magnitude of the induced depolarization. For high light intensities, the latency was 10 ms; for very low intensities, the latency was >1000



ms. These results suggest that the amount of activity in the caudal hindbrain specifies the intensity of the ensuing locomotion.



### PNAS Figure 6

**NpHR and ChR2 can be combined and activated separately.** (A) Animals transgenic for *Gal4<sup>S1101t</sup>*; *UAS:NpHR-mCherry*; *UAS:ChR2-eYFP* were illuminated with red or blue light, or both. Illumination with blue light induced locomotion (i), which could be blocked when red light was added (ii). When red light was followed by blue and red light, no locomotion was induced (iii). In (vi), blue light evoked locomotion was blocked with red light three consecutive times. (B) Experiments in (A) were highly reproducible. The probability of locomotion is plotted for four different genotypes (divided by vertical lines) and four different stimulation protocols. Error bars are 95 % confidence intervals for binomial distributions (Wilson score,  $n=238$  trials in total,  $n \geq 2$  animals for each genotype). For triple transgenic animals, the blue-evoked locomotion probability was significantly different between trials with (Aiii) and without (Ai) red illumination ( $p < 0.0004$ , z-test for proportions). The inset shows the activation spectra of ChR2 and NpHR (after ref. (Zhang et al., 2007)) and the laser lines for ChR2 (488 nm) and NpHR (633 nm).

In a previous report (Zhang et al., 2007), ChR2 and NpHR were expressed in the same cells and activated separately. The activation spectra of ChR2 and NpHR (Fig. 6B, inset) partially overlap and we tested whether independent activation was possible in triple-transgenic *Gal4<sup>S1101t</sup>; UAS:NpHR-mCherry; UAS:ChR2-eYFP* animals (Fig. 6). Since ChR2 is activatable with much lower light intensities than NpHR, we used a red laser (633 nm) instead of a green one for NpHR activation (Fig. 6B inset). Using the locomotor behavior described above, we found that ChR2 induced locomotion and NpHR-rebound induced locomotion could be triggered independently by using medium intensity blue light (488 nm, 30 mW/mm<sup>2</sup>) and high intensity red light (633 nm, 710 mW/mm<sup>2</sup>), respectively. Furthermore, the ChR2-evoked locomotion could be interrupted by additionally activating NpHR (Fig. 6A ii-iv). The behavioral output was very reliable for all stimulation protocols, as the probability of seeing locomotion was either close to 0 or close to 1 (Fig. 6B). These experiments confirmed that ChR2 and NpHR can be activated independently in the same neurons.

## **2.6 Discussion**

We have generated zebrafish lines for four NpHR variants, making use of the Gal4/UAS system. Judging by its cell-surface localization, eNpHR-eYFP is the fusion protein of choice for use in the zebrafish system, although NpHR-mCherry was equally effective in silencing of neurons. Our electrophysiological experiments demonstrated effective and rapid suppression of spikes in NpHR-expressing cells, including in brain areas in which the probe was broadly

expressed. Interestingly, firing rate changes upon NpHR activation were highly variable (see Fig. 2). This could be due to differences in expression level or in intensity of illumination, which varies somewhat with position in the tissue. Another source of variability is the intrinsic connectivity of the network. The relative weights of excitatory and inhibitory synaptic connections to a recorded cell should impact its response; in rare cases, the firing rate ratio ( $F2/F1$ ) may even be  $>1$  if overall reduction of the cell's inputs leads to a net increase in excitation. We confirmed this intuition by modeling the silencing of a random network of neurons receiving external inputs of varying magnitude (Fig. S9). Global hyperpolarization of all network neurons produced variable changes in firing rates, suggesting that intrinsic network properties alone should produce a broad range of responses.

A requirement for the dissection of behavioral circuitry with NpHR is the spatial restriction of activated NpHR. This can in principle be achieved by genetic targeting (e. g., using cell-type specific Gal4 lines) (Davison et al., 2007; Scott et al., 2007; Asakawa and Kawakami, 2008; Asakawa et al., 2008) in combination with global illumination. However, Gal4 expression patterns are rarely limited to one defined cell population. Moreover, global illumination inadvertently activates the visual and other photosensitive systems and influences behavior. We therefore relied on optical targeting to restrict the light-activated volume. This was done initially in a broadly expressing line, but could be combined in the future with specific Gal4 drivers to accomplish additional levels of spatial control. Our setup is particularly useful for behavioral studies, because, (i) the position of the

light beam can be varied independently from the imaging region; (ii) optic fibers are inexpensive and provide great flexibility in behavioral setups; (iii) light application can be controlled and synchronized with simple electronics; and (iv) the size of the brain region that is stimulated can be large or small depending on the fiber diameter (10 to 1500  $\mu\text{m}$ ). Notably, alternative light application methods with superior spatial resolution (Lutz et al., 2008) exist, e.g. digital micromirror devices (Wang et al., 2007) and laser-scanning units (Ayling et al., 2009) and will be used to expand this approach further.

We employed Kaede and Dendra to mark the photostimulated cells and estimate light scatter and penetration depth. Light delivered by the optic fiber photoconverted a narrow column, whose diameter increased with depth and extended several 100  $\mu\text{m}$  into the brain tissue. The divergence angle of the cone of converted cells matched the theoretical value for low numerical-aperture optic fibers ( $12^\circ$ ,  $\text{NA} = 0.22$ ). Thus, light scatter appears to be negligible. One caveat is that the photoconverted volume is not identical to the photostimulated volume, because Kaede and NpHR require different wavelengths and intensities. The radial spread of light application, however, will be slightly larger for Kaede than for NpHR, because scattering is stronger for shorter wavelengths, e.g. by a factor of 5 for 405 compared to 633 nm (Mie theory of scattering). We calculated that the divergence angle difference is small ( $<1\%$  for 405 compared to 633 nm). The photoconverted volume is therefore expected to provide a very close, upper-bound estimate for the radial extent of photostimulation.

To demonstrate the utility of this toolkit for functional neuroanatomy, we employed an unbiased "optogenetic scanning" approach. A thin optic fiber was positioned above the head of a semi-restrained animal, expressing NpHR in almost all neurons. By moving the fiber across the surface of the brain, we photostimulated various regions, while simultaneously monitoring the animal's behavior. Using this method, we identified a small region in the caudal hindbrain, just rostral to the *commissura infima Halleri*, that initiates a locomotor command when released from inhibition. The swim-inducing region identified by this approach contains bilaterally symmetric groups of neurons called IC, CC and T that project axons into the spinal cord (Kimmel et al., 1985; Mendelson, 1986). Because photostimulation of the region immediately rostral to the maximally responsive position showed no effect, we consider it extremely unlikely that the behavior was triggered by activity of *en passant* axons originating from more rostrally positioned cells. While identified reticulospinal cells (O'Malley et al., 1996; Liu and Fetcho, 1999; Gahtan et al., 2002; Gahtan and Baier, 2004; Gahtan et al., 2005; Orger et al., 2008) have been assigned functions in specific behaviors, including fast start (escape response), turning, and pursuit of prey, we know of no other study that has implicated cells of the caudal reticular formation in the control of forward swimming. The observation that activity in the brain region containing these neurons is necessary and sufficient for swim scoots makes them prime candidates for locomotor command neurons.

We made use of the temporal resolution of NpHR and ChR2 to study the kinetics of rebound-induced swimming. NpHR-assisted "spinalization" of animals in a

reversible manner showed that CPGs in the spinal cord are under tight control of descending projections. After light offset, swimming starts with a delay of a little less than 300 ms (267 ms in the animal shown in the Results). This latency is the composite of several processes that occur in the hindbrain, spinal cord, and muscle. In the hindbrain, NpHR needs to cease its chloride pump activity, the neurons need to rebound from hyperpolarization and generate spikes, and enough neurons need to be recruited to form a “swim command”. To determine the sum of all activities localized in the hindbrain, we turned the light off and then back on after various intervals, while monitoring the animal’s behavior. We found that up to a certain interval length (200 ms in the tested animal), the swim command appeared to be completely dependent on hindbrain activity; i. e., the fish never started swimming when the light was turned back on within 200 ms. After this time, for intervals of 200-300 ms, enough activity appeared to be building up to drive the CPGs, i. e., the fish swam. Longer intervals (>300 ms) did not lead to more vigorous swimming. This suggests that the rebounding swim command builds up over roughly 300 ms and for the first 200 ms is completely hindbrain-dependent.

The fact that the fish start swimming less than 300 ms after light offset (of which a large part, roughly 200 ms, is attributable to hindbrain) suggests that spinal circuits and muscle respond very fast to a descending input. This was confirmed by photoactivation of the caudal hindbrain with ChR2 – here swimming could be elicited within 10 ms after light onset. We reasoned that CPG activity would continue for some time after hindbrain silencing. Indeed, the time lag between re-

illumination time and the cessation of the behavior was up to 330 ms (see Fig. 5C). Notably, the delayed response could not be explained by the NpHR rise time alone (Zhang et al., 2007) ( $\tau_{\text{ON}} = 36$  ms). We interpret this finding to indicate that, while the CPGs do not require continuous excitation, their autonomous activity is not sustained for longer than a fraction of a second in the absence of reticulospinal drive.

Our preliminary analysis of the topography and kinetics of information transfer from hindbrain to CPGs was confirmed by optic fiber stimulation of ChR2, alone or in combination with NpHR. First, as expected, activation of the caudal-most hindbrain with ChR2 elicited vigorous swimming, which could be blocked by wavelength-separated activation of NpHR in the same neurons. The latency of ChR2-induced swimming onset scaled inversely with light intensity and was as short as 10 ms for the brightest light. In summary, we have shown here, using electrophysiology and behavior, that the microbial opsins NpHR and ChR2 are potent and versatile tools for the dissection of circuit function in an intact vertebrate nervous system.

## ***2.7 Materials and Methods***

### ***2.7.1 Electrophysiology***

For NpHR activation, a light intensity of 21 mW/mm<sup>2</sup> was used. The stimulation protocol consisted of alternated (no stimulus, with stimulus) repeated trials lasting 5-20 minutes in total.

### **2.7.2 Optic fiber setup**

For NpHR activation, a laser system of a confocal microscope was used and the light intensity was adjusted via an analog voltage signal to the AOTF. The single mode fiber of the AOTF was coupled into multimode fibers using an FC-to-SMA adapter. Fibers were prepared according to ref. (Campagnola et al., 2008) and the maximal output intensities were 58 mW/mm<sup>2</sup> (200 μm fiber, 633 nm) and 712 mW/mm<sup>2</sup> (50 μm fiber).

### **2.7.3 Additional Methods**

Descriptions of plasmids, transgenic fish lines, electrophysiology, modeling, optic fiber setup, swimming behavior and statistics are available in the supporting information (SI Materials and Methods).

## **2.8 Acknowledgements**

We thank Mu-ming Poo and Germán Sumbre (UC Berkeley) for providing us with the electrophysiological setup used in this study and Karl Deisseroth (Stanford) for the halorhodopsin plasmid. Jan Huisken helped with the laser setup and performed the SPIM imaging. Filippo del Bene made the *UAS:ChR2(H134R)-eYFP* and the *UAS:mCherry-kras* lines. We are thankful to Christian Machens and Pedro Gonçalves for designing the linear firing rate model. A. B. A. was supported by a Boehringer-Ingelheim foundation fellowship (B.I.F.). This work was funded by grants and fellowships to H.B. from the NIH (R01–NS053358), the NIH Nanomedicine Development Center for the Optical Control of Biological



Function (PN2 EY018241), the David and Lucile Packard Foundation, a Sandler Opportunity Award, and the Byers Award for Basic Science.

## **2.9 Supporting Information**

### **2.9.1 Plasmids and Transgenic Fish Lines**

A *NpHR-mCherry* fragment was ligated into the Tol2 vector pT2KXIG (a gift from K. Kawakami) containing an *UAS* site. The *UAS:NpHR-mCherry* construct was injected into one cell stage TL embryos together with transposase mRNA. *UAS:NpHR-eYFP* and *UAS:eNpHR-eYFP* fish were generated similarly. For *UAS:eNpHR-mCherry*, the *UAS:eNpHR-eYFP* plasmid was used and the eYFP sequence was switched with a mCherry sequence that contained the C-terminal ER export sequence of eNpHR-eYFP. To identify germ line carriers with strong and faithful expression, *UAS:NpHR* founders were crossed to the enhancer trap line *Gal4<sup>S1101t</sup>* or other lines which carry an insertion encoding the transcription factor Gal4-VP16. The line for *NpHR-mCherry* had minimal mosaicism and acceptable plasma membrane targeting. The eNpHR-eYFP line had much better plasma membrane targeting but the expression was somewhat mosaic, not every Gal4 positive cell expressed *NpHR* with this line. Double-transgenic *Gal4<sup>S1101t</sup>*; *UAS:NpHR-mCherry* zebrafish could not always be raised to adulthood, however, they showed no overt morphological or behavioral deficits at room light. Besides the broadly expressing *Gal4<sup>S1101t</sup>* line, additional Gal4-VP16 driver lines were used, and the expression of *NpHR* in these patterns did not affect viability, and double-transgenic fish could be raised to adulthood effortlessly. Although we

had no evidence for NpHR activation under room light, experimental animals were raised in the dark most of the times. For the UAS:Dendra-kras fish line, a previously generated UAS:Dendra plasmid was used and the k-ras tag was inserted at the C terminus. Dendra-kras is monomeric and can be converted from green to red under intense blue light (Gurskaya et al., 2006) while low intensities can be used to image without conversion.

### **2.9.2 Electrophysiology**

Loose-patch recordings from hindbrain neurons were performed on 3 dpf to 8 dpf zebrafish. Animals were mounted in low-melting agarose (2 %). The recording chamber and the electrodes (~2  $\mu\text{m}$  tip diameter) were filled with Evans solution (Drapeau et al., 1999). Data was low-pass filtered (5 kHz, Axopatch 200B) and digitized (Digidata 1322A, Axon instruments).  $\alpha$ -bungarotoxin (2.5  $\mu\text{M}$  or more) was added to paralyze the animal and the skin over the brain area of interest was incised to open a small window. To activate NpHR, a mercury lamp (U-ULS 100HG, 100W; microscope: Olympus BX50WI) was used in combination with a bandpass filter centered on the action spectrum maximum of NpHR (HQ 585nm/70). A 90/10 beam splitter enabled visual inspection of the illuminated area. The field diaphragm slider and neutral density filters were used to adjust the illuminated area (diameter of approximately 300  $\mu\text{m}$ ) and the light intensity. For NpHR activation, a light intensity of 21  $\text{mW}/\text{mm}^2$  was used. Using more light (83  $\text{mW}/\text{mm}^2$ ) was not necessary, since the silencing effect reached saturation between 21 and 83  $\text{mW}/\text{mm}^2$  (Fig. S4). The stimulation protocol consisted of

alternated (no stimulus, with stimulus) repeated (1-8 repeats) trials, each 30 seconds to 2 minutes long. The multi-unit recordings were spike-sorted using Matlab and Wave Clus (Quiroga et al., 2004) to identify single units. One to two single units were identified for most recordings. Units with very low firing rates (<50 spikes over the course of minutes) were excluded from analysis. Two to four animals were recorded in each group. For a small fraction of the recordings the first pair of trials was discarded because the spike shape changed. Since NpHR was functional, the endogenous concentration of all-trans retinal, a necessary cofactor of NpHR, appeared to be sufficiently high in zebrafish.

### 2.9.3 Modeling

The silencing of a random network of neurons was modeled in a linear firing rate model. The dynamics of the  $i$ -th neuron's firing rate ( $x_i$ ) without NpHR activation was defined as follows:

$$\dot{x}_i = -x_i + \sum_{j=1}^n (A_{ij}x_j) + h_i \quad (1)$$

where  $A$  was the connectivity matrix,  $n=500$  neurons, and  $(h_i)$  was the external input to the  $i$ -th neuron. The weight matrix  $A$  was generated by using the following equation:

$$A = UDU^{-1} \quad (2)$$

where  $U$  was an invertible random matrix,  $D$  was a diagonal matrix with the eigenvalues of  $A$  as entries. The eigenvalues of  $A$  were chosen to be below 1

to ensure that the firing rates would reach a stable state. The steady state of firing rates was calculated with (F2) and without (F1) NpHR activation as follows:

$$F1_i = x_i(t) = - \sum_{j=1}^n (B^{-1})_{ij} h_j \quad (3)$$

$$F2_i = x_i(t) = - \sum_{j=1}^n (B^{-1})_{ij} (h_j + halo_j) \quad (4)$$

where  $B=A-I$ , and  $I$  was an  $n \times n$  identity matrix. Each network neuron carried the same NpHR current upon NpHR activation ( $halo_j$ ). Neurons with  $F1=0$  were removed in Fig. S9, since electrophysiological recordings were only made from neurons that showed spontaneous activity.

#### 2.9.4 Optic fiber Setup

For NpHR activation, a laser system of a confocal microscope (Krypton, 568 nm, HeNe, 633 nm, Argon, 488 nm) was used and the light intensity was adjusted via an analog voltage signal to the AOTF. The single mode fiber of the AOTF was coupled into multimode fibers using an FC-to-SMA adapter and SMA multimode fibers of different diameters. Low numerical aperture multimode fibers of 200  $\mu\text{m}$  diameter (NA=0.22, BFL22-200, custom patch cable, [www.thorlabs.com](http://www.thorlabs.com)), 50  $\mu\text{m}$  diameter (NA=0.22, AFS50/125Y) and 10  $\mu\text{m}$  diameter (NA=0.1, HPSC10) were prepared by cutting them with a cable strip tool, removing the protective tubing and burning the buffer with a lighter (Campagnola et al., 2008). Subsequently, the naked fiber was scored using a diamond scribe and broken to obtain a blunt surface. The output light intensities used in the mapping experiments were 58

mW/mm<sup>2</sup> (633 nm) for the 200 μm fiber and 712 mW/mm<sup>2</sup> for the 50 μm fiber. In a few experiments the 568 nm laser was used. In pilot experiments, high-power LEDs (III star, 590 nm, 617 nm, [luxeonstars.com](http://luxeonstars.com)) were bluntly coupled to multimode fibers (200 μm) to achieve output intensities of 1.9 mW/mm<sup>2</sup> (590 nm) and 8 mW/mm<sup>2</sup> (617 nm). These light intensities were oftentimes sufficient to evoke the behavioral phenotypes reported in this study. However, the laser setup was more reliable for evoking behaviors. For the experiments in Fig. 2C a portable laser (532 nm, 100 mW, [www.dragonlasers.com](http://www.dragonlasers.com)) was coupled bluntly into the SMA connector of the fiber.

The divergence half-angle of the emitted light was approximately 12 degrees for the low NA (NA=0.22) fibers. While zebrafish larvae are transparent and transmission loss from absorption is minimal, transmission loss from scattering is significant (Aravanis et al., 2007). Therefore, light intensities calculated from the fiber diameter, the divergence angle, the penetration depth, and the output light power are only upper bound estimates (e.g. 9 mW/mm<sup>2</sup> at 200 μm tissue penetration with a 200 μm / 0.22 NA fiber and with an output intensity of 58 mW/mm<sup>2</sup>).

### **2.9.5 Swimming Behavior**

Larvae (3 dpf for mapping, 5-6 dpf for locomotion analysis) were mounted in low-melting agarose, egg-water was added, and agarose was removed from the tail. Larvae used for mapping were treated with PTU, an inhibitor of pigment synthesis, to increase optical accessibility of neural tissues. The optic fiber was

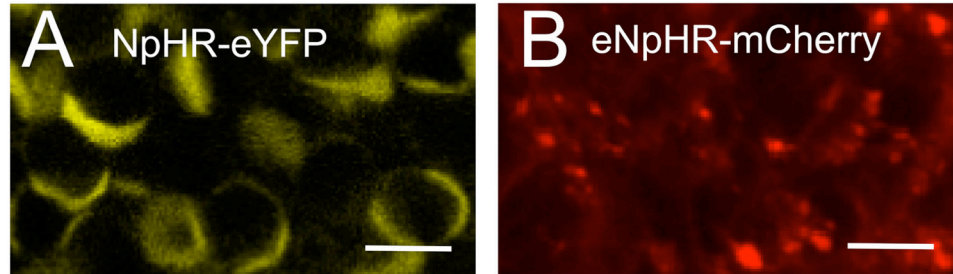
inserted into a pasteur pipet and placed close ( $\sim 50\text{-}100\ \mu\text{m}$ ) to the dorsal surface of the animal using a stereoscope and a micromanipulator. After 8 seconds of stimulation, the light was turned off and the behavior of the animals was recorded. In some animals ( $\sim 30\%$ ) light offset did not induce locomotion and these animals were excluded from analysis. However, the behavior was highly reproducible in animals that showed the response (75-100% of trials, also see Fig. 6). For mapping, each experiment consisted of two or three trials 15 seconds apart and animals rested for at least one minute in between trials. The total number of trials was  $n = 295$ , and 7 animals were used (3 NpHR expressors, 4 non-expressing siblings). Statistical analysis was performed on the calculated probabilities (95% Wilson confidence intervals for proportions). For locomotion analysis, larvae were imaged at 500 frames/s (M1 Redlake Motion, [www.redlake.com](http://www.redlake.com)). Millisecond timing of re-illumination was achieved by gating the analog input voltage of the laser with a TTL-transistor. The TTL pulse was generated using a DAQ box and Labview.

### **2.9.6 Statistics**

Since the firing rate ratios ( $F2/F1$ ) in Fig. 2D were not normally distributed, we used the non-parametric KS-test and Ranksum test to compare firing rate distributions from different transgenic genotypes. In order to judge whether individual units had a firing rate ratio different from 1 (see text body), we used the non-parametric permutation test: firing rate histograms (bin width 1s) were randomized and two times 5000 firing rate histograms  $F1$  and  $F2$  were drawn.

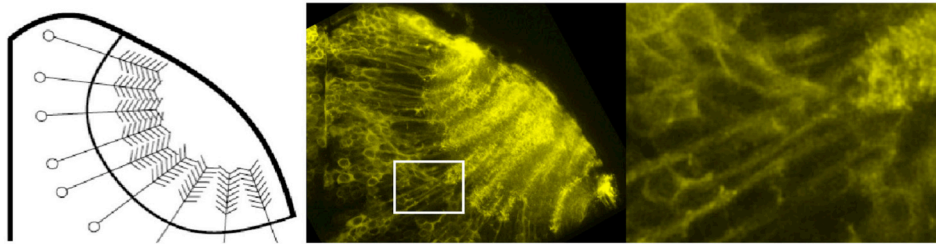
The real firing rate ratio ( $F2/F1$ ) was then compared to two times 5000 permuted ones to estimate how likely it is to obtain the observed  $F2/F1$  by chance ( $\alpha=0.01$ , two-tailed). The significance levels did not change qualitatively when different histogram bin widths were used. In a similar manner, the certainty of a firing rate ratio ( $F2/F1$ ) was assessed by calculating its 95% bootstrap interval (Fig. S5): two times 5000 random samples were drawn with replacement from each  $F1$  and  $F2$ . In Fig. 4A, probabilities of observing a swim event are reported. Since these probabilities are proportions (ranging from 0 to 1), we employed a binomial proportion confidence interval, the Wilson score interval, to calculate error bars. This test assumes a binomial distribution of proportions and performs well even for the extreme proportions close to 0 and 1 found in our study. To compare proportions for NpHR expressors and wildtype animals (Fig. 4A), we used the z-test for two proportions. Since the proportions were extreme (1 and 0, respectively), the test could not be used to calculate the exact p-value due to our small sample sizes ( $n=17$  and  $n=23$  at position 4) and the requirement  $n \cdot P > 5$  and  $n \cdot (1-P) > 5$  for both samples. Instead, the statistical significance reported ( $p < 0.01$ ) is based on a safe upper bound estimate, in which the requirement is fulfilled ( $P=0.7$  and  $P=0.2$ ). The exact binomial test for individual proportions gave similar results. In Fig. 6B, error bars and significances were calculated in the same manner as for Fig. 4A (Wilson score interval and z-test for two proportions, respectively).

## 2.9.7 Supporting Figures



### PNAS Supplementary Figure 1

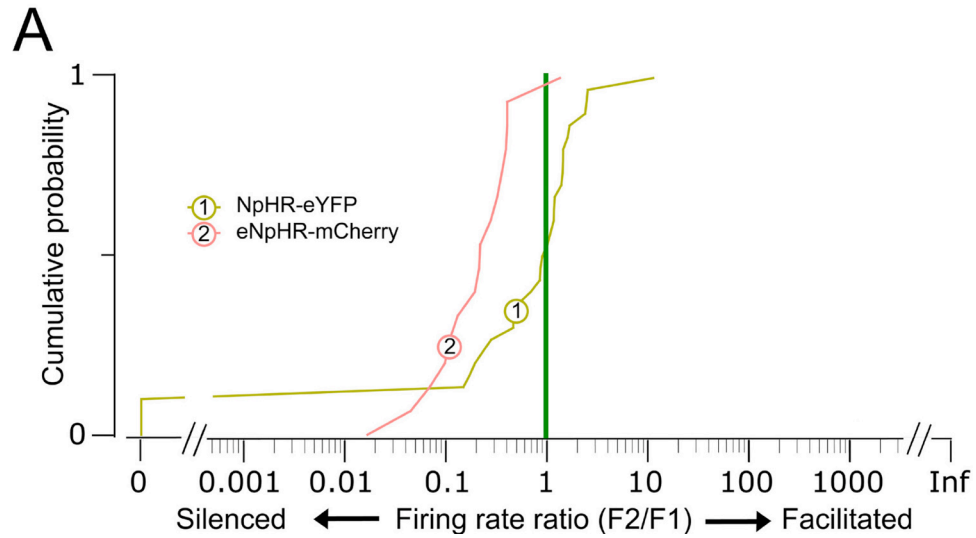
**Expression of NpHR in zebrafish.** (A) Expression of NpHR in  $Gal4^{s1101t}$ ;  $UAS:NpHR-eYFP$  animals and (B)  $Gal4^{s1101t}$ ;  $UAS:eNpHR-mCherry$  animals . Scale bars, 5  $\mu$ m.



### PNAS Supplementary Figure 2

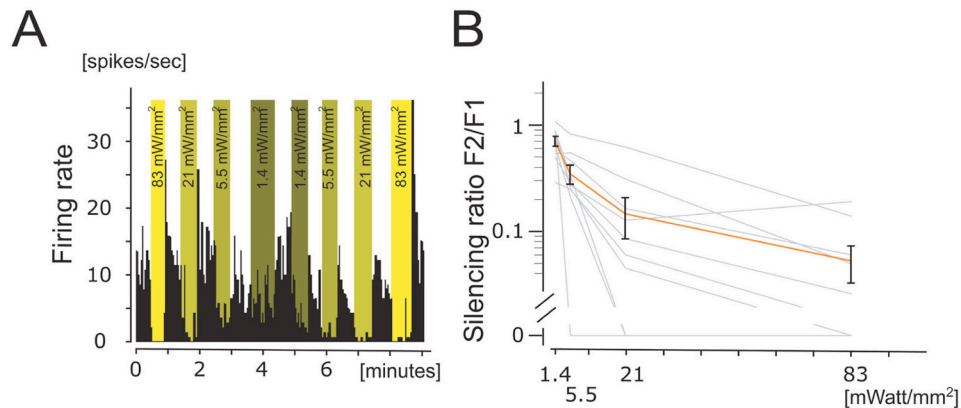
**Expression of eNpHR-eYFP in the tectum.** Expression of NpHR in  $Gal4^{s1013t}$ ;  $UAS:eNpHR-eYFP$  animals in the optic tectum. Left: Schematic showing the locations of cell bodies and cell processes in the optic tectum. Middle: Z-projected image of eNpHR-eYFP expression. Right: Magnified view of the white box.





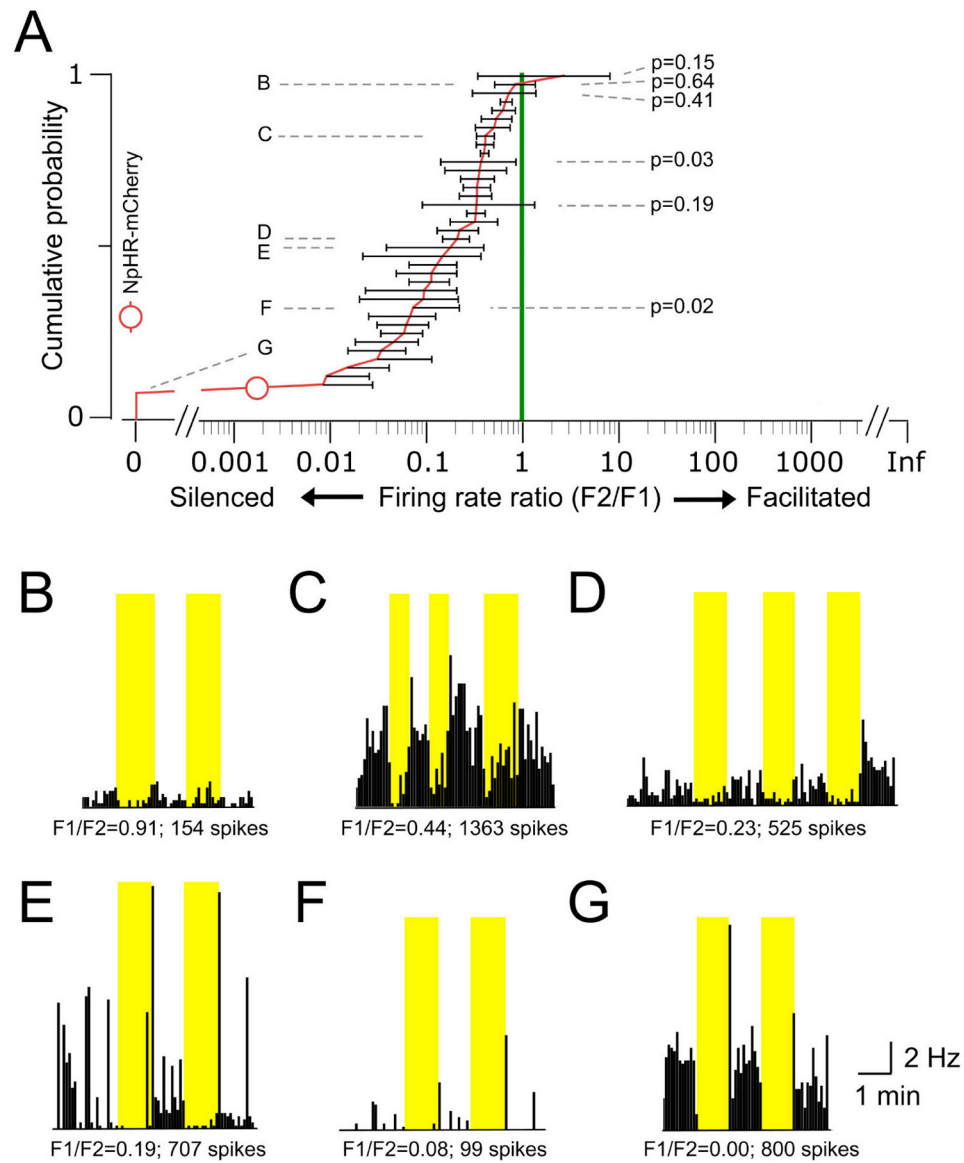
### PNAS Supplementary Figure 3

**Analysis of silencing efficacy in the hindbrain.** (A) Cumulative probabilities of firing rate ratios F2/F1 (with/without stimulation) in cells from NpHR-eYFP and eNpHR-mCherry animals.



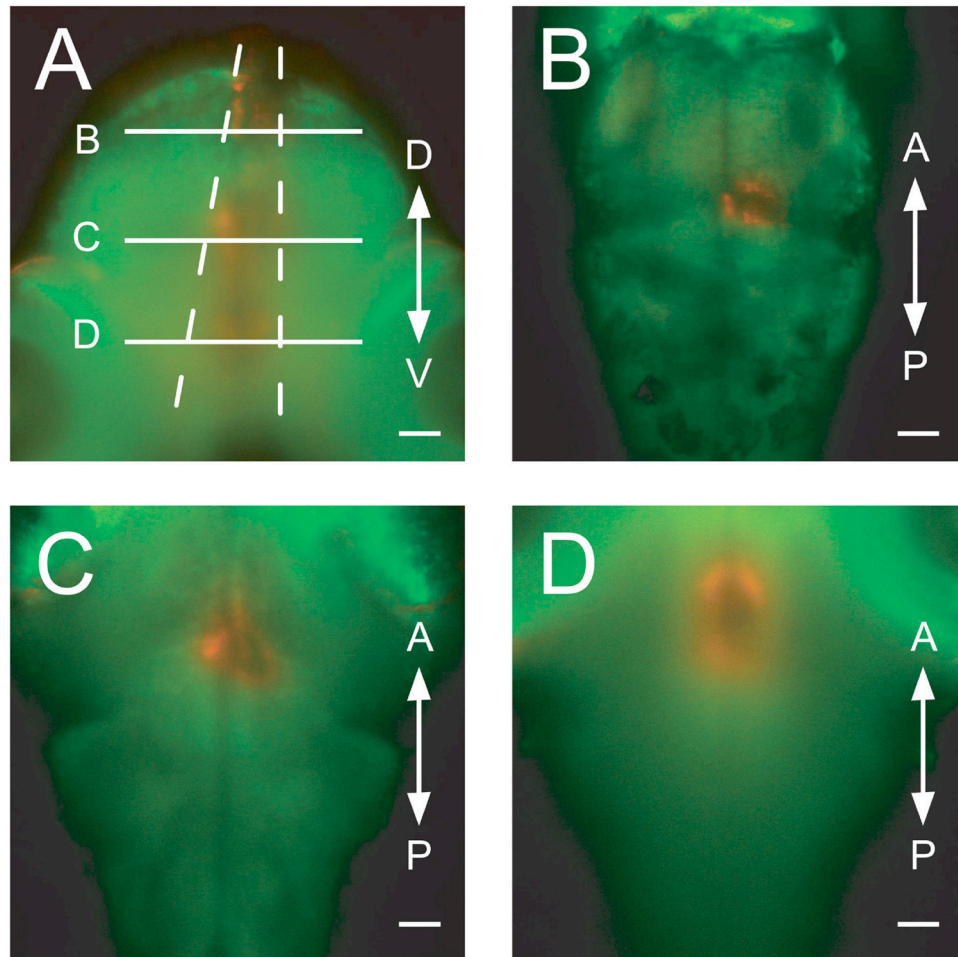
### PNAS Supplementary Figure 4

**Silencing efficacy is proportional to light intensity.** (A) Four light intensities were tested (83, 21, 5.5, and 1.4 mW/mm<sup>2</sup>) in hindbrain neurons with broad CNS expression driven from *Gal4<sup>s1101t</sup>*. Yellow shaded boxes mark the illumination periods during the recording. (B) A light intensity of 21 mW/mm<sup>2</sup>, as used in Fig. 2, reduced the firing rate by 86%. Four-fold brighter light (83 mW/mm<sup>2</sup>) reduced the firing rate further to 95% from baseline. Neurons were silenced to 66% and 30% when the light intensity was reduced to 5.5 or 1.4 mW/mm<sup>2</sup>, respectively. These data indicated that the silencing effect reached saturation between 21 and 83 mW/mm<sup>2</sup>.



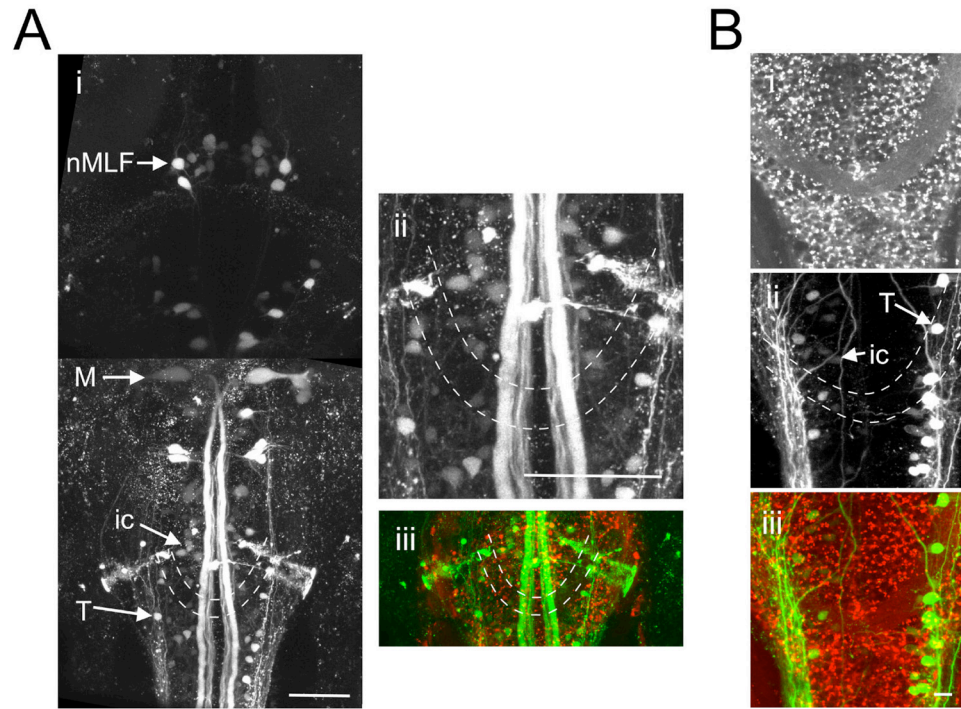
### PNAS Supplementary Figure 5

**Statistical Analysis of firing rate changes.** (A) Cumulative probability of firing rate ratios ( $F2/F1$ ) for the NpHR-mCherry line ( $n=41$  cells, data from Fig. 2). The 95% bootstrap intervals are plotted for each cell. P-values (permutation test) are indicated for all cells with  $p>0.01$  (firing rate change not significant). (B-G) Firing rate histograms for selected cells in (A). Yellow boxes indicate the period of illumination. The scale bars to the lower right apply to all plots and total spike numbers are indicated for each plot. The bandwidth is 5 s.



**PNAS Supplementary Figure 6**

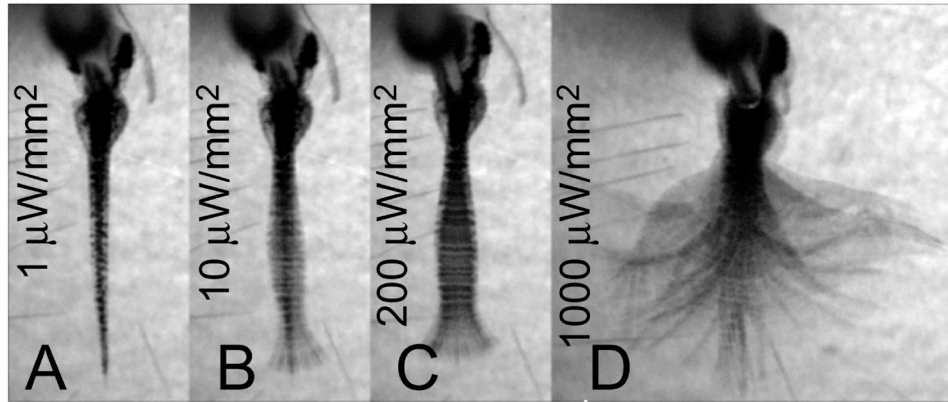
**Confirmation of precise light application with optic fibers.** (A) A *Gal4<sup>st101t</sup>; UAS:Kaede* animal was imaged (z-projection) after Kaede had been converted with optic fibers (left: 10 μm diameter, right: 50 μm diameter) placed over the dorsal surface of the animal. (B) The animal was imaged from the side to reveal the photo-converted column in the hindbrain (fiber diameter: 10 μm). (C) Side view of the photo-converted column in the midbrain (fiber diameter: 50 μm). Each slice of the z-stack was contrast enhanced and a single transformed xz slice is shown.



### PNAS Supplementary Figure 7

**The caudal reticular formation is located in the vicinity of the commissura infima Halleri.**

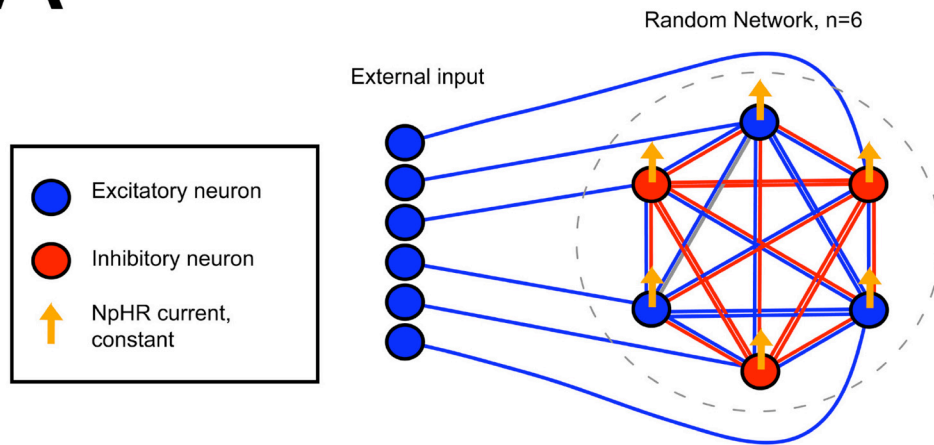
(A-B) Two *Gal4<sup>s1101t</sup>; UAS:NpHR-mCherry* animals in which a green dextran-conjugated dye was injected into the spinal cord to label reticulospinal cells. (Ai) Dorsal view, extending from the rostral spinal cord (bottom) to the midbrain (top). ic and T cells of the caudal reticular formation are located in close proximity to the commissura infima Halleri (dashed lines). M, mauthner cell, nMLF, nucleus of the medial longitudinal fasciculus. (ii) Magnified view of the region containing the ic and T cells. (iii) Merged channels image. (B) Red channel (i), green channel (ii) and merged channels (iii).



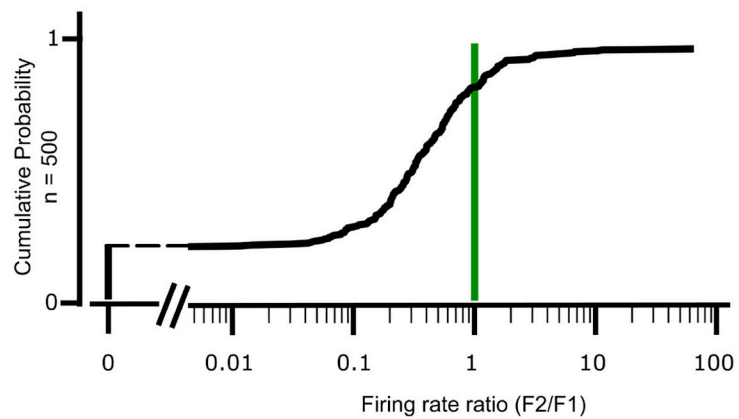
**PNAS Supplementary Figure 8**

**Locomotion latency and amplitude is dependent on light intensity in ChR2 animals.** (A-D) The caudal hindbrain of a *Gal4<sup>S1101t</sup>; UAS:ChR2-eYFP* animal was illuminated (200 μm optic fiber) with different light intensities. Images are an average-z-projection of four consecutive minimum-intensity-z-projections. See Supplementary Movie 5.

# A



# B



## PNAS Supplementary Figure 9

**Model for the silencing of a random neural network.** (A) Overview of the connectivity in the model. Network neurons are recurrently connected and receive excitatory input from external neurons. Network neurons express a constant NpHR current. (B) Firing rate ratios (before illumination/after illumination) of the model neurons. Only neurons with  $F1 \neq 0$  are plotted.

## **Chapter 3 - Optogenetic localization and genetic perturbation of saccade-generating neurons in zebrafish**

### **3.1 Authors**

Peter J. Schoonheim\*, Aristides B. Arrenberg\*, Filippo Del Bene, and Herwig Baier

\* Equal contribution

### **3.2 Abstract**

The optokinetic response (OKR) to a visual stimulus moving at constant velocity consists of a series of two alternating components, a slow phase, during which the eyes follow the stimulus, and a quick phase, which resets the eyes to begin a new response cycle. The quick phases of the OKR resemble the saccades observed during free viewing. It is unclear to what extent the premotor circuitry underlying these two types of jerky, conjugate eye movements is conserved among vertebrates. Zebrafish (*Danio rerio*) larvae, broadly expressing Halorhodopsin (NpHR) or Channelrhodopsin-2 (ChR2) in most neurons, were employed to map the location of neurons involved in this behavior. By blocking activity in localized groups of NpHR-expressing neurons with an optic fiber positioned above the head of the fish and by systematically varying the site of photostimulation, we discovered that activity in a small hindbrain area in rhombomere 5 was necessary for saccades to occur. Unilateral block of activity

at this site affected behavior in a direction-specific manner: Inhibition of the right side suppressed rightward saccades of both eyes, while leaving leftward saccades unaffected, and vice versa. Photostimulation of this area in ChR2-transgenic fish was sufficient to trigger saccades that were precisely locked to the light pulses. These extra saccades could be induced both during free viewing and during the OKR and were distinct in their kinetics from eye movements elicited by stimulating the abducens motor neurons. Zebrafish *double indemnity* (*didy*) mutants were identified in a chemical mutagenesis screen based on a defect in sustaining saccades during OKR. Positional cloning, molecular analysis, and electrophysiology revealed that the *didy* mutation disrupts the voltage-gated sodium channel *Scn1lab* (*Nav1.lb*). ChR2 photostimulation of the putative hindbrain saccade generator was able to fully reconstitute saccades in the *didy* mutant. Our studies demonstrate that an optogenetic approach is useful for targeted loss-of-function and gain-of-function manipulations of neural circuitry underlying eye movements in zebrafish and that the saccade-generating circuit in this species shares many of its properties with that in mammals.

### **3.3 Publication**

Optogenetic localization and genetic perturbation of saccade-generating neurons in zebrafish. Schoonheim PJ, Arrenberg AB, Del Bene F, Baier H. J Neurosci. 2010 May 19;30(20):7111-20. PMID: 20484654



### **3.4 Introduction**

Quick eye movements, or saccades, assist vision by redirecting the gaze and thus expanding, or adjusting, the field of view. The neural mechanisms responsible for eye position and saccade initiation have been studied extensively in mammals (Fuchs and Kaneko, 1981; Scudder et al., 2002; Glimcher, 2003). Here the nucleus prepositus (NPH) and the vestibular nucleus (MVN) in the brainstem are important for horizontal eye movements and contain neurons with eye position and velocity signals (Lopez-Barneo et al., 1982; Tomlinson and Robinson, 1984). Horizontal saccades are generated by a neural circuit called the burst generator, which consists of excitatory burst neurons (EBNs) in the paramedian pontine reticular formation (PPRF), inhibitory burst neurons (IBNs) and omnipause neurons (OPNs) (Strassman et al., 1986b; Strassman et al., 1986a). Preceding a saccade, the high constant firing rate of OPNs is inhibited by glycinergic inputs (Kanda et al., 2007). This pause of OPN inhibition gives rise to a period of short rapid firing of both EBNs and IBNs (Scudder et al., 2002). Both types of burst neurons directly synapse with the abducens motor neurons (Yoshida et al., 1982). The EBNs project to the ipsilateral abducens nucleus to excite agonist motor neurons (Strassman et al., 1986b), whereas the IBNs inhibit antagonist motor neurons in the contralateral abducens nucleus (Strassman et al., 1986a). Together, this activation pattern results in a quick, synchronous (conjugate) movement of both eyes in the same direction.

The task of voluntary saccades during free viewing in primates and cats is to bring the image of an eccentric visual target into the fovea. In contrast, the eyes

of commonly studied teleost fish do not possess a fovea. However, these animals exhibit spontaneous 'scanning' saccades during free viewing. Little is known about the teleost hindbrain circuitry for saccade generation. In adult goldfish, brain regions that control eye movements were named Area I and Area II (Pastor et al., 1994; Aksay et al., 2000; Aksay et al., 2001; Aksay et al., 2007). It was shown that Area I predominantly sends projections to the abducens nucleus (Aksay et al., 2000; Aksay et al., 2001) in contrast to Area II, which is exclusively precerebellar (Beck et al., 2006; Straka et al., 2006). Inactivation of Area I neurons using lidocaine results in a dramatic eye drift and velocity bias but does not inhibit saccade initiation. In contrast, when lidocaine is injected between Area I and Area II, saccades are no longer generated, consistent with the existence of a burst generator at this position (Pastor et al., 1994). Although Area I and II combined carry out a similar function to the NPH in primates and cats, their homology to mammalian nuclei is uncertain (Beck et al., 2006).

Both mammals and teleosts exhibit another type of jerky, conjugate eye movement as part of their vestibulo-ocular reflex (VOR) (Marsh and Baker, 1997). These reflex movements resemble saccades in speed and amplitude and punctuate periods during which the visual image is stabilized on the retina. Such 'resetting saccades' can be elicited by visual stimulation alone, resulting in the well-known optokinetic response (OKR). A drifting grating, composed of black and white stripes, that rotates around an agarose-embedded zebrafish larva at constant speed, evokes a series of highly regular eye-following movements, which counteract the perceived retinal slip (Easter and Nicola, 1996; Beck et al.,

2004). In regular intervals, as the eyes move to an extreme viewing angle, saccade-like movements then reset their orientation, and the cycle begins anew. Despite a longstanding interest in the zebrafish OKR as a sensitive readout of visual function (Brockerhoff et al., 1995; Neuhauss et al., 1999; Muto et al., 2005), little is known about the underlying neural pathway. While the pathways generating eye movements converge on a shared set of oculomotor neurons in all vertebrates, it is not known if different types of saccades are produced by the same premotor circuits and whether teleosts possess a region that is homologous to the mammalian burst generator. To gain insight into this issue, we have chosen here a functional approach in zebrafish (Arrenberg et al., 2009). We generated transgenic zebrafish larvae expressing Halorhodopsin (NpHR) in the entire CNS. Small areas of the brain were then photostimulated with a thin optic fiber, while the animal's OKR to a drifting grating was monitored with a video camera. NpHR stimulation blocked saccades at only one position in the hindbrain. This region shares several characteristics with the burst generator of mammals. Activation of the identical region with Channelrhodopsin (ChR2) evoked conjugate saccades in wildtype. The same treatment also restored saccades in *didy* mutants, which fail to sustain saccades during long exposure to a moving grating due to mutation of a voltage-gated sodium channel. These experiments help to localize an important brain function in zebrafish larvae, invite further work on homologies between teleost and mammalian hindbrain circuits, and show that optogenetic intervention can be successfully employed to reverse a neurological defect in an animal model.

### **3.5 Materials and methods**

#### **3.5.1 Fish maintenance and genotypes of wildtype strains, mutants, and transgenics**

Zebrafish (*Danio rerio*) of the standard laboratory strains TL (Tüpfel long fin), TLN (melanin-deficient TL fish that carry *mitf/nacre*<sup>s170</sup> and *mitf/nacre*<sup>s184</sup> mutations), and WIK were maintained at 28.5 °C on a 14h light and 10h dark cycle. For behavioral experiments, we used a mix of TL and TLN. For genetic mapping of the mutation, we obtained a hybrid between the TL and WIK strains. The Committee on Animal Research of the University of California, San Francisco, approved all experiments.

Two alleles of the *double indemnity* (*didy*) mutant, *didy*<sup>s552</sup> and *didy*<sup>s390</sup>, were discovered in a chemical mutagenesis screen using the OKR as a screening assay (Muto et al., 2005). Transgenic lines *Et(E1b:Gal4-VP16)s1101t*, *Et(hsp(600bp):Gal4-VP16)s1020t*, *Tg(UAS:Kaede)s1999t*, *Tg(UAS:NpHR-mCherry)s1989t*, *Tg(UAS:NpHR-eYFP)s1987t*, and *Tg(UAS:ChR2(H134R)-eYFP)s1990t* were previously described (Scott et al., 2007; Arrenberg et al., 2009). *Tg(UAS:ChR2(H134R)-mCherry)s1986t* was newly generated for this project by established procedures. Line and allele designations follow zebrafish nomenclature conventions (<http://zfin.org/>).

### 3.5.2 Optokinetic response assay

A miniature surround movie theater was built for visual stimulation. Four 72 mm LCD monitors (Aeicom) were arranged in a square and driven by one TripleHead2Go box (Matrox) and a dual-head GPU. A moving pattern of stripes ( $10^\circ/\text{s}$ , 18 cycles/ $360^\circ$ , maximal contrast) was generated in Matlab (MathWorks, MA) with the Psychtoolbox suite ([www.psychtoolbox.org](http://www.psychtoolbox.org), (Brainard, 1997; Pelli, 1997)). The pattern was warped in such a way that the temporal frequency and angular velocity were constant around the virtual circular perimeter of the movie theater. Larvae (5 days post fertilization, dpf) were mounted in either 1.5 % low-melting agarose or 2.5 % methylcellulose, the agarose surrounding the eyes was removed, and larvae were placed on a stage in the movie theater. A white, high-power LED was used as backlight for the CCD video camera. Frame rate was 15 frames/s for saccade velocity measurements and 2 frames/s for all other experiments. Spatial frequency, contrast, and time of reversal of the sine-wave gratings were adjusted using a custom-made LabVIEW program (National Instruments). The velocity of the eyes was calculated by performing linear regression of the eye movement between two eye reversals (either a saccade or stimulus-induced directional change of the eye). To calculate the gain of the OKR slow phase, the velocity of the eyes was divided by the velocity of the stimulus.

### 3.5.3 Manipulation of neural activity with NpHR and ChR2

Zebrafish carrying either *Tg(UAS:ChR2(H134R)-eYFP)s1990t*, *Tg(UAS:ChR2(H134R)-mCherry)s1986t* or *Tg(UAS:NpHR-mCherry)s1989t* were

mated to zebrafish carrying *Et(E1b:Gal4-VP16)s1101t*. For adult carriers of the TLN/TL hybrid strain, 25% of the larvae were melanophore-deficient (homozygous *nacre*). Light stimulation and simultaneous behavioral analysis of zebrafish (5 dpf) larvae were performed as described previously (Arrenberg et al., 2009). Briefly, the multimode, low numerical aperture 50  $\mu\text{m}$  fiber (AFS50/125Y; Thorlabs) was coupled to the single-mode fiber of a laser source (UV; 365nm, Argon; 488nm, Krypton; 568, HeNe: 633 nm). Placement of the fiber was performed using a micromanipulator. For some animals, stimulation of the hindbrain did not evoke saccades, and these animals were excluded from analysis. The *Tg(UAS:ChR2(H134R)-eYFP)s1990t* line exhibits random variegation which may result in diminished ChR2 expression in the putative saccade generator in a subset of the animals.

#### **3.5.4 Positional cloning and genotyping**

To identify the *didy* gene, we used microsatellite mapping as described before (Shimoda et al., 1999). Initially, genomic DNA was isolated from 24 pooled mutant or wildtype sibling larvae. Subsequently, linked markers were used to determine the recombination frequencies, and thus the putative distances to the mutation, in DNA isolated from 600 individual larvae. Mutant larvae were selected by their black appearance, which is indicative of a neuroendocrine deficit in controlling pigment aggregation. The markers *z6601-6* and *z6601-8* were identified by interrogation of the genomic sequence for simple sequence repeats (SSRs). Candidate SSRs were empirically tested for whether they were

polymorphic between the WIK and TL strains. Oligonucleotides for these new markers are: *z6601-6F* (5'-gcc aga gtt aag ggt ttc aaa gca c-3'), *z6601-6Rv* (5'-gag ttg ggc tgt ggt cag gtt tc-3'), *z6601-8Fw* (5'tag atg tgg gga cat ttg gtc tcc-3'), and *z6601-8Rv* (5'-agt ctt ttc tca tgt gcc tgt ttg c-3').

Genotyping of *didy* mutants was performed by means of a restriction fragment length polymorphism (RFLP) marker. The *didy*<sup>s552</sup> mutation introduces a novel *AcuI* restriction site into *scn1lab*. Digestion of a PCR fragment spanning the *didy*<sup>s552</sup> mutation with *AcuI* results in two smaller fragments in fish carrying the *didy*<sup>s552</sup> allele.

### **3.5.5 Morpholino phenocopy and *in situ* RNA hybridization**

Phenocopy of the *didy*<sup>s552</sup> loss-of-function mutation was performed by morpholino-mediated knock-down of *scn1lab*. A morpholino targeted to the atg translation start site of *scn1lab* (5'-agc tga gca gcc ata ttg aca tcc t-3') was kindly provided by Angie Ribera (University of Colorado Health Sciences). The morpholino was injected into wildtype TL embryos at 1- to 2-cell stages at a concentration of 2 mM. Pictures were taken using a Leica MZFLIII dissecting microscope connected to a Zeiss Axiocam MRc camera.

Expression analysis by *in situ* RNA hybridization of the *scn1lab* gene was performed as previously described (Smear et al., 2007). An isoform-specific region within the *scn1lab* gene was chosen as previously described (Novak et al., 2006).

### 3.5.6 Site-directed mutagenesis

A plasmid containing the wildtype *RnScn2a* gene positioned between the 5' and 3' noncoding regions of the *Xenopus*  $\beta$ -globin gene downstream of a T7 RNA polymerase promoter and upstream of a poly-A tail region was a kind gift of Alan L. Goldin (UC Irvine). The codon change recreating the *didy*<sup>s552</sup> mutation was introduced into the *RnScn2a* construct with a single PCR-digest step. The *BglII* and *BlnI* restriction site were used to cut out ~500 bp of the *RnScn2a* region, containing the site of interest. The mutation was introduced into the *RnScn2a* gene using PCR with the following oligonucleotides: *RnScn2aFW* (5'-acc gct gga aga tct gaa taa caa g-3') and *RnScn2aRV-(didy<sup>s552</sup>)* (5'-cac cac tgc tga gca gaa tcc taa-3'). The PCR product was digested with *BglII* and *BlnI* restriction enzymes and subsequently ligated into the digested construct. Sequencing was performed to confirm the presence of the mutation in the *RnScn2a* construct and to ensure that no additional mutations were introduced during the cloning procedures.

### 3.5.7 Two-electrode voltage-clamp recordings from *Xenopus* oocytes

Capped cRNA was transcribed *in vitro* from a *NotI* linearized plasmid with the T7 mMessage mMachine kit (Ambion, Austin, TX). The quality of the cRNA was confirmed by electrophoresis, and quantity was determined by photospectrometry (OD260). Stage V oocytes were removed from adult female *Xenopus laevis* frogs, prepared as previously described (Goldin, 1991). Approximately 20 ng of cRNA was injected into *Xenopus* oocytes using a microinjector. Oocytes were incubated for >48 hours at 16°C in ND96 medium.



Sodium currents were recorded by using two-electrode voltage clamp set up in ND96 medium in the absence or presence of 400 nM tetrodotoxin (TTX). Capacitive transients and leak currents were eliminated by subtraction of currents remaining after TTX treatment. The voltage dependency of the sodium currents was determined by performing a voltage-injection protocol with steps between -95 mV and +50 mV, with a holding potential of -100 mV and increments of 5 mV. Data analysis was performed using pClamp 8.0 software (Axon Instruments, Foster City, CA, USA). Peak currents were analyzed and plotted against their voltage.

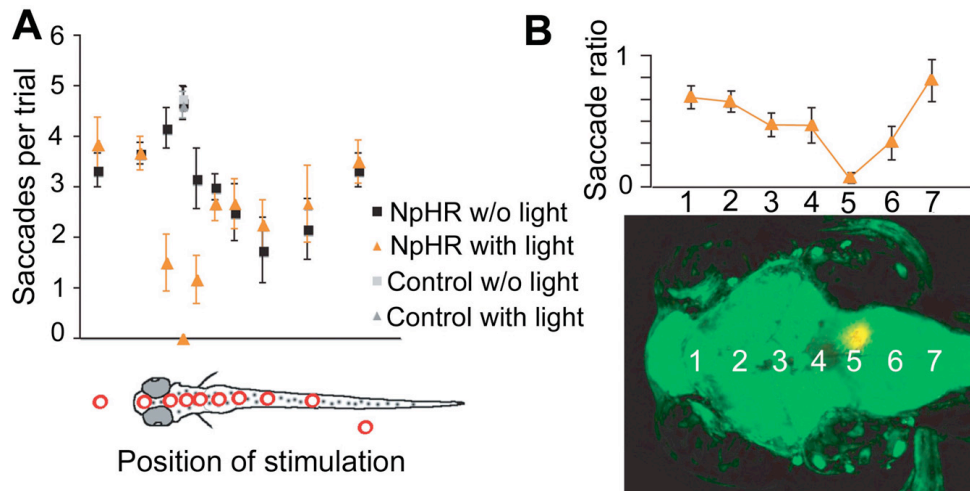
### **3.6 Results**

#### **3.6.1 A small hindbrain region in rhombomere 5 is necessary for saccade generation**

To localize the neural circuitry responsible for saccade initiation in the larval zebrafish brain, we employed an optogenetic stimulation approach (Fig. 1). Fish larvae (5 dpf) were mounted in agarose, placed inside a custom-built surround video-theater, and assayed for their eye movements in response to visual motion. We used the broadly expressing *Et(E1b:Gal4-VP16)s1101t* transgenic line (Scott et al., 2007; Scott and Baier, 2009) to drive the expression of NpHR-mCherry in almost all neurons of the zebrafish CNS (Arrenberg et al., 2009). An optic fiber was coupled to a laser (633 nm) and positioned close to the surface of the brain. This configuration allowed us to simultaneously stimulate small brain

areas and monitor eye movements, while the animal was exposed to the visual stimulus presented on the surround video screens.

We first used a 200  $\mu\text{m}$  fiber to coarsely map the brain and to control for the effect of scattered light reaching the retina (Fig. 1A). Finer mapping was then carried out with a 50  $\mu\text{m}$  fiber (Fig. 1B). In most regions of the brain and spinal cord, OKR saccades were unaltered or only mildly affected by optical stimulation. In particular, illumination of the pretectum and tectum had no effect (Fig. 1A, B; Supplementary Movie 1). Only at one position in the hindbrain, a small region in rhombomere 5 between the ears and near the midline, was our protocol successful in blocking OKR-associated saccades (Fig. 1A, B; Fig. 2B, C; Supplementary Movie 2). This position is distinct from the swim-inducing neurons in the caudal hindbrain discovered by us previously (Arrenberg et al., 2009). Light stimulation of strictly the right side of this region resulted in inhibition of saccades to the right, while saccades to the left were not affected, and vice versa (Fig. 1B, 2B; Supplementary Movie 3). Slow eye movements were not blocked by inhibition of these cells either bilaterally or unilaterally (Fig. 2B, C).



### J Neuro Figure 1

**Optogenetic scanning with fiber optics identifies a hindbrain region necessary for saccade generation.** (A) Coarse mapping of the brain using a 200  $\mu\text{m}$  diameter optic fiber to locate regions in the brain that are important for horizontal eye movements during OKR. During trials, animals were continuously visually stimulated with a moving grating (conditions in all panels: contrast 100%, velocity  $10^\circ/\text{s}$ , spatial frequency  $0.05 \text{ cycles}/^\circ$ ), and the fiber light was alternately turned on and off for periods of 20 s each. The number of saccades during one trial was measured for either wildtype larvae (gray) or siblings carrying *Et(E1b:Gal4-VP16)s1101t*, *Tg(UAS:NpHR-eYFP)s1987t* (black and orange). The drawing in the lower panel of (A) shows the corresponding brain regions that were illuminated during the trial. A total of 158 trials were analyzed for the mapping experiments and 5 animals were used (3 NpHR expressors, 2 non-expressing siblings). Error bars represent SEM. (B) Detailed mapping of the saccade phenotype along the midline in the brain. A 50  $\mu\text{m}$  diameter optic fiber was used. The saccade ratio (number of saccades during NpHR activation divided by number of saccades without NpHR activation) approached 0 for position number 5. Positions are shown in a z-projected confocal stack of a *Et(E1b:Gal4-VP16)s1101t*, *Tg(UAS:NpHR-eYFP)s1987t*, *Tg(UAS:Kaede)s1999t* carrying larvae. The asterisk indicates a photoconverted position corresponding to the experiment in Fig. 2B.

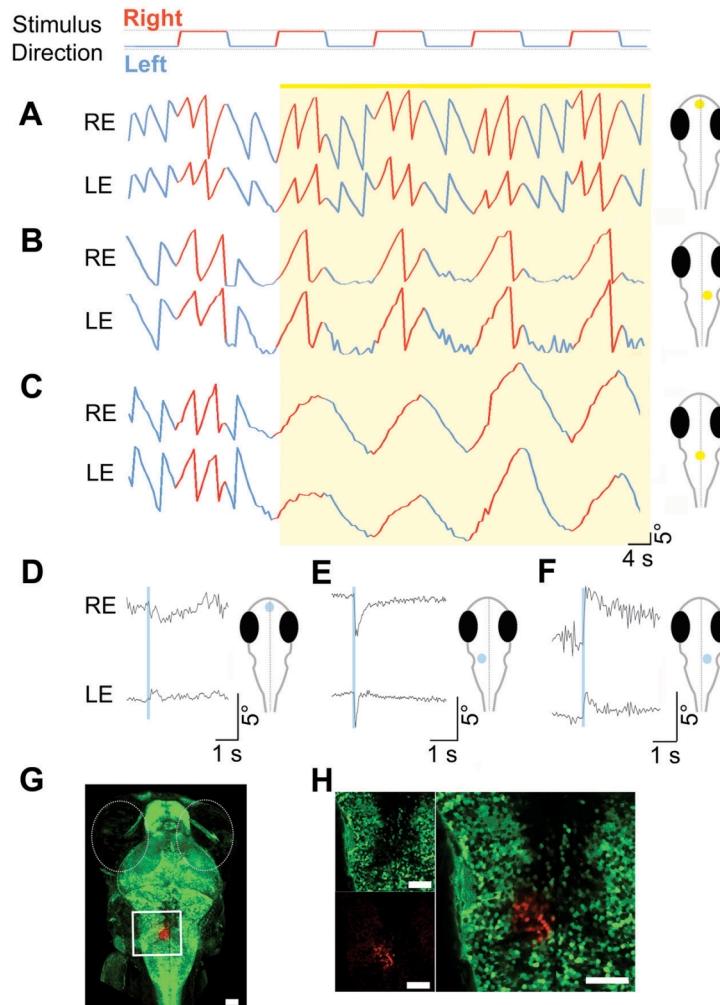
### 3.6.2 Optical stimulation of a small hindbrain area is sufficient for saccade generation

We next used ChR2 (ChR2(H134R)) to activate the neurons at the identified position. Light stimulation of *ChR2-eYFP* expressing larvae was initially performed in the absence of visual stimulation. ChR2 activation elicited conjugate (binocularly coordinated) saccades in the ipsi- and contralateral eye in the direction of the stimulated side (Fig. 2E, F; Supplementary Movie 4). Optically induced saccades were on average less vigorous than naturally occurring

saccades ( $54.4 \pm 8.2^\circ/\text{s}$  vs.  $102.6 \pm 6.4^\circ/\text{s}$ ), but substantially faster than the fastest OKR slow phase measured ( $10.5^\circ/\text{s}$ ). The latency between ChR2 activation and initial eye movement was  $\sim 28$  ms. No other behavior was observed, such as tail movements or escapes, despite vicinity to the Mauthner cells in rhombomere 4. Illumination of other brain regions did not elicit rapid eye movements (Fig. 2D; Supplementary Movie 5), with the exception of small areas rostral to the identified region (Supplementary Movies 6 and 7). Stimulating these regions evoked short, jerky eye movements ( $28.5 \pm 2.5^\circ/\text{sec}$ ), which were restricted to the eye ipsilateral to the stimulation, in striking contrast to the bilateral saccades observed earlier.

To label the region responsible for saccade initiation, we used the photoconvertible fluorescent protein Kaede. Triple transgenic zebrafish larvae carrying *Et(E1b:Gal4-VP16)s1101t*, *Tg(UAS:Kaede)s1999t*, and either *Tg(UAS:NpHR-mCherry)s1989t* (Fig. 1B) or *Tg(UAS:ChR2(H134R)-eYFP)s1990t* (Fig. 2G) were first optically stimulated to locate the saccade-generating region. The input to the optic fiber was then switched to an ultraviolet laser (UV, 365 nm), without altering its position, and the larva was illuminated with UV. We reported previously, that this photoconversion protocol yields a very close estimate of the illuminated volume, because the difference in scattering between the two wavelengths is negligible (Arrenberg et al., 2009). The red-converted Kaede highlights the stimulated region in the zebrafish larval hindbrain, approximately 20  $\mu\text{m}$  lateral from the midline (Fig. 2G). Imaging of this area with 40x magnification showed that a narrow column of less than 100 cells ( $\sim 15$  in one optical plane) was

converted by the UV light (Fig. 2H). Together, these data show that a small number of neurons in the larval hindbrain are necessary and sufficient to elicit a saccade, consistent with the existence of a burst generator in the larval fish brain.



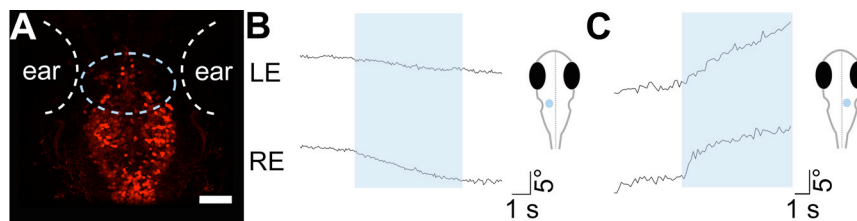
## J Neuro Figure 2

### Optical manipulation of the hindbrain saccade-generating circuit with NpHR and ChR2.

OKR stimulus conditions in panels (A-C) were: contrast 100 %, velocity  $\pm 10^\circ/\text{s}$ , spatial frequency 0.05 cycles/ $^\circ$ . Larvae transgenic for *Et(E1b:Gal4-VP16)s1101t*, *Tg(UAS:NpHR-eYFP)s1987t* were visually stimulated with a direction-changing, drifting grating (Top). Eye traces (RE, LE, right and left eye) during optogenetic stimulation of (A) telencephalon, (B) unilateral hindbrain, and (C) bilateral hindbrain are plotted. Yellow shading corresponds to the illumination of the brain region shown on the right next to the eye traces. Direction of the stimulus is color-coded in the eye traces (red, right; blue, left direction). The location of stimulation in (B) is shown and photoconverted in Fig. 1B bottom (asterisk). (D) Telencephalon and (E,F) lateral hindbrain stimulation of *Et(E1b:Gal4-VP16)s1101t*, *Tg(UAS:Kaede)s1999t*, *Tg(UAS:ChR2(H134R)-eYFP)s1990t* larvae in the absence of a visual stimulus. Light pulses are shown in blue shading. Representative traces are shown ( $n \geq 8$  animals were tested in each condition). (G) Low magnification image (10x objective) of the expression pattern of Kaede in the animal tested in (D-F). Kaede (unconverted, green) is expressed in most neurons. UV illumination with the same 50  $\mu\text{m}$  optic fiber at the identical location that is used for optical manipulation experiments in (E), results in local photoconversion of Kaede (red) within a 50  $\mu\text{m}$  wide column. (H) Higher magnification (40x) of converted area. Scale bars: 50  $\mu\text{m}$ .

### 3.6.3 Optical stimulation of abducens motor neurons in a specific enhancer trap line does not produce saccades

We asked if activation of abducens motor neurons alone could result in saccade-like eye movements. For this experiment, we used the enhancer trap line *Et(hsp(600bp):Gal4-VP16)s1020t*, which drives expression in Olig2 expressing neurons (Wyart et al., 2009). Olig2 is a transcription factor that marks the abducens motor neurons in zebrafish (Zannino and Appel, 2009). Photostimulation of ChR2 in the abducens motor neurons labeled by *Et(hsp(600bp):Gal4-VP16)s1020t* (Fig. 3A) did not evoke rapid eye movements, even when much greater light intensities were tested. Instead, activation of these neurons resulted in eye movements that were slower and more variable (Fig. 3B, C) than those seen in the broadly expressing *Et(E1b:Gal4-VP16)s1101t* line (see Fig. 2E, F). This result indicated that the saccade-generating neurons identified in rhombomere 5 of the *Et(E1b:Gal4-VP16)s1101t* line are different from, and likely upstream of, the abducens motor neurons.



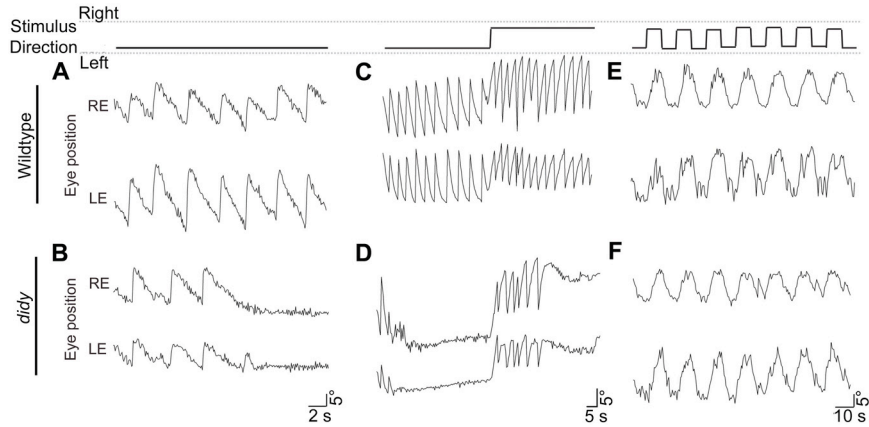
#### J Neuro Figure 3

**Optogenetic activation of the abducens motor neurons with ChR2 using a 50  $\mu$ m optic fiber.** (A) Z-projected confocal stack (40x objective) of the expression pattern of ChR2-mCherry in *Et(hsp(600bp):Gal4-VP16)s1020t*, *Tg(UAS:ChR2(H134R)-mCherry)s1986t*. The blue dashed oval between the ears indicates the region of photostimulation. Scale bar: 50  $\mu$ m. (B,C) Lateral hindbrain stimulation of *Et(hsp(600bp):Gal4-VP16)s1020t*, *Tg(UAS:ChR2(H134R)-mCherry)s1986t* larvae. Light pulses are shown in blue shading. Blue dots between the ears indicate the region of photostimulation.

### **3.6.4 *didy* mutants fail to sustain saccads during the OKR in a direction-specific manner**

Two alleles of the *didy* gene were discovered in a large-scale screen for ethylnitrosourea-induced mutations disrupting the OKR (Muto et al., 2005). While wildtype larvae perform full-blown OKR behavior in response to a unidirectional moving large-field grating for many minutes, *didy*<sup>s552</sup> mutants execute approximately four (three to six) initial saccades and then lock their eyes in the most extreme peripheral position at the end of a slow phase (Fig. 4A, B). When the motion stimulus is ended, the mutants' eyes slowly drift to the position that is parallel to the body axis. When the direction of the field motion stimulus is reversed, *didy* mutants perform a slow phase to the opposite side and subsequently perform another series of about four saccades, before the eyes become arrested again in the most extreme "pursuit" position (Fig. 4C, D). The occurrence of another series of saccades upon direction reversal shows that the saccade exhaustion in *didy* mutants is specific to the direction tested, i.e. the eye movement defect does not transfer between stimulus directions. When the direction of the motion stimulus was reversed every 8 seconds, the slow phase of the OKR was indistinguishable between wildtype and *didy* mutants (Fig. 4E, F). Thus, the oculomotor system is not generally weakened, and the mutants are well capable of detecting the motion stimulus.





## J Neuro Figure 4

### Optokinetic responses reveal a saccade-generation defect in *didy*<sup>s552</sup> mutants (5 dpf).

Stimulus conditions: contrast 100%, velocity  $\pm 10^\circ/\text{s}$ , spatial frequency  $0.05 \text{ cycles}^\circ$ . (A, B) Representative traces of the horizontal position of the left (LE) and right eye (RE) of a wildtype and a *didy* larva in response to a drifting grating (Top) with a single direction, plotted as a function of time. Mutant larvae respond initially like wildtype, but then cease to generate saccades. (C, D) Representative eye movement traces in response to a drifting grating with a single reversal of stimulus direction. (E, F) Representative eye movement traces in response to an oscillating motion stimulus. Stimulus direction was changed every 8 s. No difference is seen between wildtype and mutant.

### 3.6.5 The *didy* mutation does not affect vision, saccade ballistics, or eye muscles

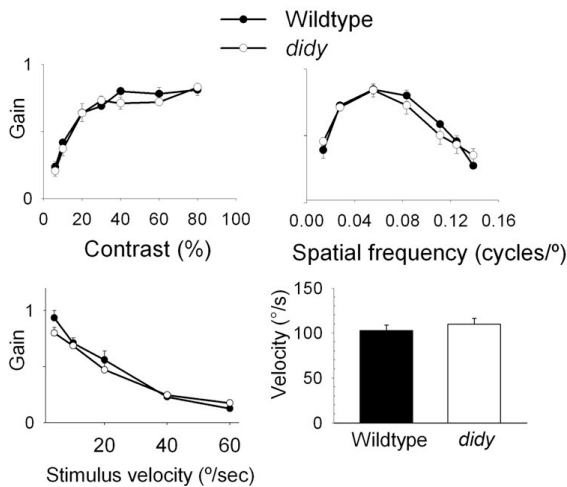
The OKR is evoked by visual stimulation, and any perturbation of its normal performance could be due to disruptions of its sensory inputs or motor outputs.

To test for a visual defect, we determined the gain of the slow phase of *didy* mutant and wildtype larval zebrafish as a function of contrast, spatial frequency, and velocity of the stimulus. We observed no differences in sensitivity or acuity between wildtype and *didy* mutants over the range of stimuli tested (Fig. 5A-C).

These data suggest that the *didy*<sup>s552</sup> mutation does not diminish visual perception.

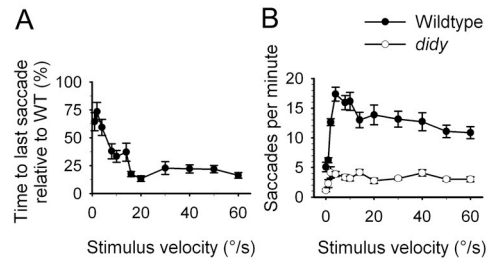
Since slow phase and quick phase of the OKR employ the same set of motor neurons and muscles, and the slow phase is unaltered in the mutant, it seemed likely that the *didy*<sup>s552</sup> mutation does not affect the last stages of motor output. To

further verify this assumption, we measured the ballistics of the saccades in response to a grating moving in a single direction. We found that saccades (if they occur) were very similar between wildtype and *didy* mutants in both amplitude and speed ( $102.6^\circ/\text{s} \pm 6.4$  SEM for wildtype;  $110.1^\circ/\text{s} \pm 6.4$  SEM for *didy*<sup>s552</sup>), indicating that motor neuron discharges and eye muscles are intact in the mutant.



### J Neuro Figure 5

**Normal visual acuity and contrast sensitivity in *didy* mutants.** Fish larvae (n=8 for each genotype) were tested at 5 dpf. Stimulus conditions in all panels were (unless otherwise stated): contrast 100%, velocity  $10^\circ/\text{s}$ , spatial frequency  $0.05$  cycles/°. (A) The slow phase velocity gain (OKR gain) of wildtype and *didy* mutants as a function of stimulus contrast. (B) OKR gain of wildtype and *didy* mutants as a function of spatial frequency. (C) OKR gain of wildtype and *didy* mutants as a function of stimulus velocity.



### J Neuro Figure 6

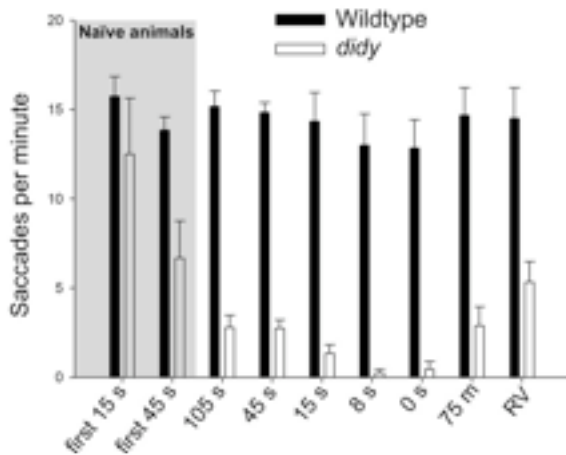
**Exhaustion of saccade production in *didy*<sup>s552</sup> mutants is dependent on the number of prior saccades, not on stimulus velocity.** Stimulus conditions: contrast 100%, spatial frequency  $0.05$  cycles/°; stimulus duration 1 min. (A) Saccade rate of wildtype (solid circle) and *didy* mutant (open circle) during the OKR to a stimulus drifting in one direction as a function of stimulus velocity (n = 10). (B) Time of the last saccade event that occurred during a 2 min exposure to stimulus drifting in one direction (n = 8). Error bars represent SEM.

### **3.6.6 The saccade generation defect does not depend on stimulus velocity and recovers over time**

We asked if the ability to generate saccades in *didy* mutants was dependent on time of exposure to a moving grating (i.e., subsided after a defined time independent of stimulus velocity) or dependent on the number of preceding saccades (i.e., subsided after a defined number of saccades). We distinguished between these possibilities by varying the stimulus velocity over almost two orders of magnitude ( $1^\circ/\text{s}$  to  $60^\circ/\text{s}$ ), while holding the spatial frequency of the grating constant. At each stimulus velocity, *didy* mutants performed about four saccades (Fig. 6A), demonstrating that the ability to sustain saccades was not dependent on time. Responding to faster stimulus velocities, the mutant performed the same number of saccades as for slow velocities, but in a shorter time (Fig. 6B). The mutant was also less likely than wildtype to initiate spontaneous saccades during free viewing when faced with a stationary grating (velocity 0). The rate dropped from about 5 saccades per minute in wildtype to  $<1$  in the mutant (Fig. 6A).

Finally, we tested on what time scales the *didy* mutants recovered from their saccade-exhausted state. Two OKR trials (stimulus velocity  $+10^\circ/\text{s}$ ) were performed in which the interval between exposures to the moving grating was varied. During the interval, the stimulus grating was stationary (velocity 0). We observed that *didy* mutants regained their ability to generate saccades when intervals of longer than 45 seconds were used (Fig. 7). When the two exposures followed each other with an interval shorter than 8 seconds, the *didy* mutants were largely incapable of executing another saccade (Fig. 7). This finding

suggests that the saccade-generating mechanism, once depleted, recovers on the order of tens of seconds in *didy*<sup>s552</sup> mutants.



**Recovery kinetics of saccade generation in *didy* mutants.** Wildtype (solid bars) and *didy* mutants (open bars) were exposed twice, for 45 seconds each, to a stimulus drifting in one direction (velocity 10°/s). The number of saccades during the second exposure was counted ( $n \geq 6$  for each genotype and condition). Time intervals (velocity 0°/s) between exposures to the motion stimulus were varied. The first two bars correspond to saccade rate during first exposure (naïve animals). Following bars show saccade rates during second 45 s trial performed after indicated interval. RV stands for a reversal of the direction of the OKR stimulus (interval 0 s). Error bars represent SEM.

**J Neuro Figure 7**

### 3.6.7 Genetic and functional identification of *didy*<sup>s552</sup> as a null allele of *scn1lab*

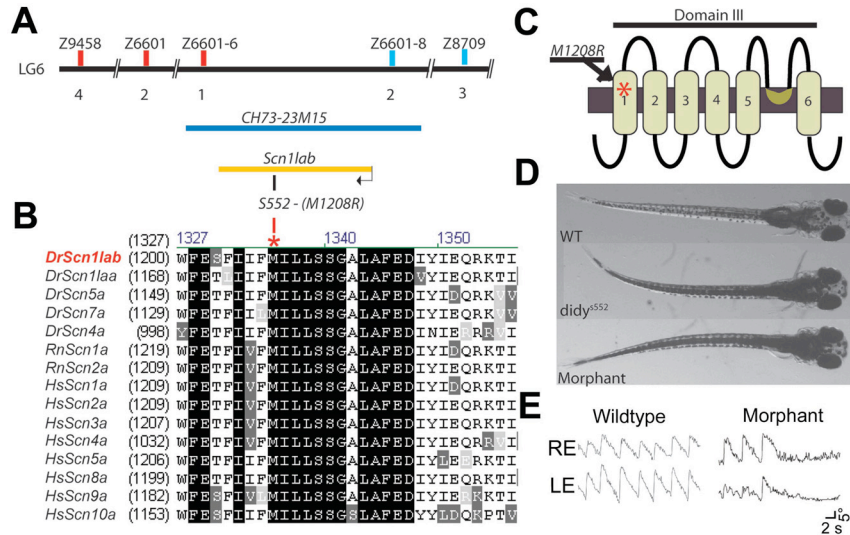
To identify the mutated gene, we used a positional cloning approach. By means of a genome scan using 192 simple sequence repeat length polymorphism (SSLP) markers (Shimoda et al., 1999) distributed over the entire zebrafish genome, we mapped the *didy*<sup>s552</sup> mutation to a region on chromosome 6 between the markers z22712 and z62065. We scanned the genomic region between these two markers for additional simple sequence repeats and found two novel SSLPs, which we called z6601-6 and z6601-8 (see Methods). These markers flank the *didy*<sup>s552</sup> mutation and are located on BAC clone CH73-23M15 (Fig. 8A). Interrogation of the Ensembl database revealed that a single gene was located in this interval, *scn1lab*. Sequencing of the *scn1lab* open reading frame revealed a T to G mutation in the *didy*<sup>s552</sup> cDNA, which results in an amino acid

substitution from a methionine (M) to an arginine (R) at position 1208. The *scn1lab* gene encodes a voltage-gated sodium channel (Nav1.1b), which consists of four domains of six transmembrane helices (Catterall, 2001). The M1208 residue is situated in the predicted first transmembrane helix of the third domain of this channel and is conserved across the family of paralogous genes in mice, rats, humans, and zebrafish (Fig. 8B, C).

To confirm the identity of the gene, we used a morpholino antisense approach to knock down *scn1lab* in wildtype. The morpholino was targeted against the translation start site (ATG) of *scn1lab*. The morphants showed the same external phenotype as the mutants (Fig. 8D). Moreover, morphant fish were impaired in saccade initiation similar to *didy* mutants (Fig. 8E). In summary, genetic linkage, DNA sequence, and morpholino phenocopy indicate that the *didy*<sup>s552</sup> allele is a loss-of-function mutation of *scn1lab*.

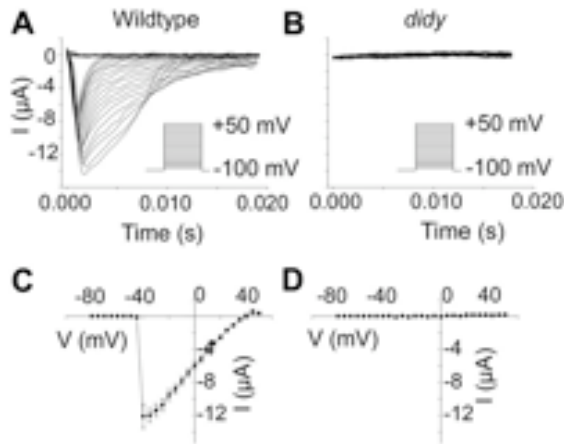
We next studied the effect of the *didy*<sup>s552</sup> mutation on the gating properties of this channel in *Xenopus* oocytes. Genes encoding voltage-gated sodium channels are notoriously difficult to clone due to toxicity in *E. coli*. We therefore took advantage of the available Scn2a clone from *Rattus norvegicus* (*RnScn2a*) (Kearney et al., 2001) and substituted the M with an R at the position equivalent to residue 1208 to generate a mutant channel. We injected wildtype and mutant *Rnscn2a* mRNA into *Xenopus* oocytes and performed two-electrode voltage clamp recordings. Oocytes injected with wildtype *RnScn2a* showed voltage-gated sodium peak currents of approximately 12  $\mu$ A at -40 mV (Fig. 9A, C). Mutant channels, in contrast, were unable to carry currents at any voltage (Fig. 9B, D).

These results corroborate the identity of the *didy* gene as *scn1lab* and indicate that the *didy*<sup>s552</sup> mutation generates a complete loss-of-function allele.



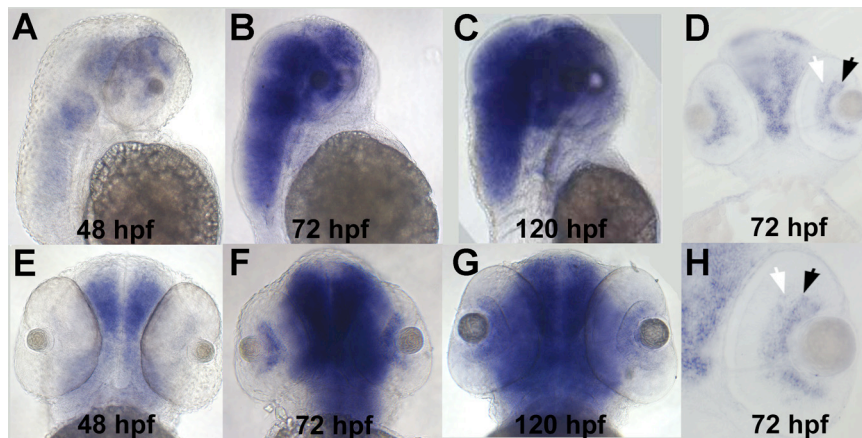
## J Neuro Figure 8

**Molecular identification of *didy* as *scn1lab*.** (A) Positional cloning of the *didy* gene. The *didy*<sup>s552</sup> mutation was mapped between markers z6601-6 and z6601-8, flanking the *scn1lab* gene. Both markers are located on BAC clone CH73-23M15. (B) Alignment of the amino-acid sequence neighboring the M1208R mutation identified in the *didy*<sup>s552</sup> allele to homologues from other vertebrate species. Dr, *Danio rerio* (zebrafish); Rn, *Rattus norvegicus*; Hs, *Homo sapiens*. (C) Predicted location of the M1208R in domain III of the voltage-gated sodium channel Scn1lab (Nav1.1Lb). (D, E) Morpholino knock-down of *scn1lab* transcript in wildtype resulted in a phenocopy of the *didy*<sup>s552</sup> mutation. (D) Both mutant and morphant larvae are dark due to dispersed melanin pigment, indicating a neuroendocrine defect. (E) Unidirectional OKR of *didy* morphant larva shows a failure to sustain saccades similar to *didy*<sup>s552</sup> mutants.



**The mutant *didy* allele likely encodes a non-functional channel.** Two-electrode voltage clamp recordings were performed on *Xenopus* oocytes heterologously expressing rat Scn2a carrying the amino acid substitution equivalent to the *didy*<sup>s552</sup> mutation. Oocytes were voltage-clamped with a holding potential of -100 mV followed by depolarizations in 5 mV increments to +10 mV (A, B) Representative traces of recordings from *Xenopus* oocytes transfected with either wildtype *scn2a* (A) or mutant *scn2a* (B). (C, D) Voltage dependence of activation for wildtype Scn2a (C, n = 12, mean ± SEM) and mutant Scn2a (D, n = 12, mean ± SEM).

**J Neuro Figure 9**



**J Neuro Figure 10**

**Expression pattern of *scn1lab* in zebrafish larvae revealed by anti-sense digoxigenin-labeled RNA *in situ* hybridization.** (A, E) Lateral and ventral view, respectively, of whole-mount staining of 48 hpf embryos. (B, F) Lateral and ventral view, respectively, of whole-mount staining of 72 hpf larvae. (C, G) Lateral and ventral view, respectively, of whole-mount staining of 120 hpf larvae. (D) Vibratome section (20 μm) showing a 72 hpf larval retina and brain. (H) 20x magnification of the eye. Most cells in the ganglion cell layer of the retina (black arrow), close to the lens, express *scn1lab*. Scattered cells in the inner nuclear layer (white arrow) are also *scn1lab*-positive.

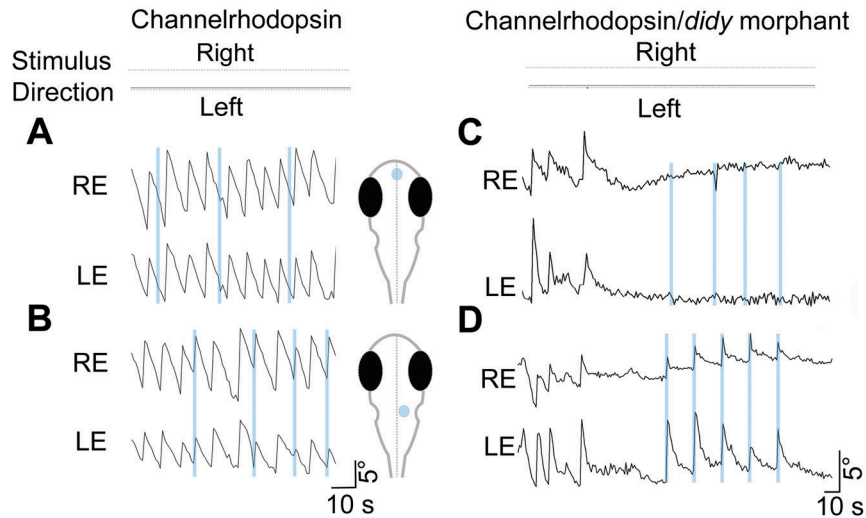
### 3.6.8 The *didy* saccade deficit is reversed by activating ChR2 in the putative saccade generator

Wholemout RNA *in situ* hybridization at 48 hours post fertilization (hpf), 72 hpf, and 120 hpf showed that transcript levels are qualitatively unchanged in *didy*<sup>s552</sup> mutants, suggesting that the mutation does not affect mRNA stability. This was

confirmed by quantitative PCR (data not shown). Similar to other voltage-gated sodium channels (Novak et al., 2006), the gene is broadly expressed in the brain (Fig. 10). The gene product is, however, not ubiquitous. In the retina, *scn1lab* is restricted to retinal ganglion cells and a subset of amacrine cells (Fig. 10D, H). Consistent with the behavioral phenotype, the expression pattern of *scn1lab* overlaps with the saccade-generating region identified above. However, its broad expression pattern is uninformative with regard to its site and mechanism of action in the *didy* mutant.

We hypothesized that depolarization of the saccade-generating neurons with ChR2 might restore saccades in *didy* mutants. For this experiment, *scn1lab* MO was injected into *Et(E1b:Gal4-VP16)s1101t* and *Tg(UAS:ChR2(H134R)-eYFP)s1990t* embryos to generate larvae with a deficit in sustaining saccades. We exposed these larvae to a unidirectional OKR stimulus and waited for their saccades to run down. As before, *didy* morphants performed only about four saccades, but light stimulation at the position of the putative saccade generator rescued saccade initiation (Fig. 11D). Light injection elicited multiple conjugate saccades of normal speeds and amplitudes similar to those in wildtype animals, which were always directed to the stimulated side and precisely time-locked to the light pulse (Fig. 11B, D).





### J Neuro Figure 11

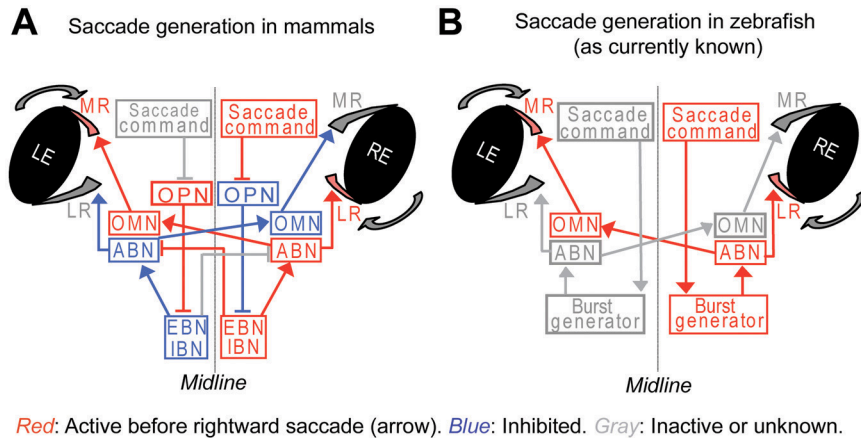
**Restoration of saccades in *didy*<sup>s552</sup> mutants by optical stimulation of the putative saccade-generator region with ChR2.** (A, C) Control: No extra saccades are evoked by photostimulation of a telencephalon region of (A) wildtype larva or (C) *didy* morphants carrying *Et(E1b:Gal4-VP16)s1101t, Tg(UAS:ChR2(H134R)-eYFP)s1990t* during exposure to a drifting grating. (B, D) Saccades are consistently triggered by stimulation of the rhombomere 5 region in the same animals. Representative traces are shown ( $n \geq 3$  animals for each condition).

For wildtype animals, 16 out of 18 and for *didy* morphants 13 out of 15 light injections resulted in a saccade. Optical stimulation of other brain regions was ineffective (Fig. 11A, C). For wildtype animals, 1 out of 20 and for *didy* morphants 0 out of 12 light injections resulted in a saccade. These experiments suggest that the downstream motor neurons or muscles are less, if at all, affected by the *didy*<sup>s552</sup> mutation and locate the defect within or upstream of the putative saccade generator.

### 3.7 Discussion

This work has discovered the location of hindbrain neurons in larval zebrafish that are necessary and sufficient for saccade generation. Properties of this circuitry (Fig. 12) suggest that it is homologous to the one inferred, using electrophysiology, in adult goldfish (Pastor et al., 1994; Aksay et al., 2001; Major et al., 2004; Aksay et al., 2007) and, possibly, to the burst generator in mammals (Fuchs and Kaneko, 1981; Scudder et al., 2002). Optical stimulation of ChR2-expressing neurons on just one side of the hindbrain results in a saccade of both eyes in the direction of the stimulated side. This is in line with the connectivity reported in other vertebrates; the burst neurons activate motor neurons directly (abducens) and indirectly (oculomotor) to drive the ipsilateral lateral rectus muscle and the contralateral medial rectus muscle, thus enabling the production of conjugate eye movements (Fig. 12A). Our data suggest that the quick phase of the OKR in larval zebrafish is generated by a circuit that is comparable in organization to the saccadic burst generator engaged during free viewing in primates (Fig. 12B). This conservation is remarkable, considering the divergent functions of the two behaviors, the phylogenetic distance of zebrafish from mammals, the absence of a fovea in zebrafish, and the well-documented differences in the neural pathways that underlie the initiation of these two types of eye movements (superior colliculus/optic tectum in free viewing and nucleus of the optic tract/pretectum in the OKR) (Ilg and Hoffmann, 1991; Ilg and Hoffmann, 1996; Masseck and Hoffmann, 2009).

From a forward genetic screen, which employed the OKR as a behavioral screening assay (Muto et al., 2005), we isolated a zebrafish mutant in NaV1.1b, which is encoded by the *scn1lab* gene. Heterologous expression and electrophysiology in *Xenopus* oocytes showed that the mutation likely generated a null allele of this voltage-gated sodium channel. Perhaps surprisingly, this “channelopathy” results in a selective defect in the sustenance of saccadic eye movements. Several brain functions tested appear normal, including visual perception and ocular pursuit, as well as swimming scoots and escape responses. However, the mutants fail to inflate their swim bladder, have a deficit in the neural control of pigmentation, and do not survive beyond 14 dpf, indicating that closer analysis will reveal additional neurological defects. Several mutations in genes encoding human Nav1 proteins have been identified and have been shown to result in epilepsy syndromes (Kearney et al., 2001; Goldin, 2003; Ogiwara et al., 2007; Ragsdale, 2008). The zebrafish *didy* mutant may provide an opportunity to study disease aspects that are inaccessible in mammalian models, such as long-term changes in synaptic function or cell-type specific effects. For zebrafish neuroscience, the *didy*<sup>s552</sup> mutant is interesting, because it is one of very few mutations isolated so far that disrupt integrative functions of the brain, while sparing both the sensory surface and the motor output. Most other “behavioral” mutants identified in forward-genetic screens affect neural development, sensory processing, or simple locomotor behaviors (Brockerhoff et al., 1995; Granato et al., 1996; Muto et al., 2005).



## J Neuro Figure 12

### Schematic drawing of circuitry responsible for horizontal saccade generation in mammals and teleosts.

(A) Saccade-generating circuitry in primates. Neurons in the midbrain inhibit the omnipause neurons (OPN), directly or indirectly through activation of inhibitory interneurons. The inhibition of OPN results in short, rapid firing of excitatory burst neurons (EBN), which monosynaptically activate motor neurons in the abducens nucleus (ABN). These motor neurons activate the lateral rectus muscle (LR) on the ipsilateral side. Abducens internuclear neurons in the ABN project to the contralateral oculomotor nucleus (OMN) to activate oculomotor motor neurons. These motor neurons activate the medial rectus muscle (MR) of the contralateral eye. Simultaneously, inhibitory burst neurons (IBN) inhibit the contralateral ABN, which results in a relaxation of the ipsilateral MR and the contralateral LR. (B) Putative framework of the circuitry for horizontal saccade generation in zebrafish larvae. Neurons in the midbrain generate a saccade command that directly or indirectly activates the hindbrain saccade generator on only one side of the animal (right side is shown). The saccade generator activates motor neurons and internuclear neurons in the ipsilateral ABN. The ABN motor neurons activate the lateral rectus muscle (LR) on the ipsilateral side. The ABN internuclear neurons project to the contralateral oculomotor nucleus (OMN) to activate oculomotor motor neurons. The oculomotor motor neurons activate the medial rectus muscle (MR) of the eye contralateral to the activated saccade generator. Thus, a saccade generated in the right side of the hindbrain manifests as rightward eye rotation of both eyes. The circuitry upstream of the saccade generator, especially the existence of neurons homologous to the OPN, has not been demonstrated.

Nav1.1b belongs to a family of at least eight voltage-gated sodium channels encoded in the vertebrate genome (Novak et al., 2006). Although its mutation causes a rather specific behavioral defect, we found that this channel is expressed rather broadly in the CNS. This counterintuitive result is best explained by partial redundancy with other Nav1 channels, which are co-expressed in most neurons and can compensate for absence of one of the channels. We hypothesize that the specificity of the *didy* phenotype arises

primarily from functional compensation of voltage-gated sodium channels in most other neurons outside the saccade generator circuit. Homeostatic regulation of membrane excitability, e. g. downregulation of voltage-gated potassium channels, may further ameliorate the phenotype.

To begin to understand the molecular causes of the behavioral phenotype, we considered known properties of this protein family. Voltage-gated sodium channels exist in either of three states, “closed” (activatable), “open”, and “inactive”. Transitions from one state to another are largely unidirectional, from closed to open, from open to inactive, and from inactive to closed. Neurons become unable to generate action potentials when a large fraction of channels are in the inactive state, e. g., following sustained depolarization or repetitive firing. Importantly, the inactive state comprises at least two distinct conformations with characteristic recovery times, a fast reversible form with recovery kinetics in the millisecond range and a slowly reversible form (Rudy, 1978; Quandt, 1988; Jung et al., 1997; Mickus et al., 1999). The slowly reversible form may be unavailable for activation for seconds or tens of seconds due to a structural rearrangement of the channel protein (Jung et al., 1997; Toib et al., 1998; Carr et al., 2003). Deletion of one of the channels, as in *didy* mutants, is expected to reduce channel density. Prolonged stimulation could deplete the pool of activatable channels and render the neurons unexcitable. This gradual loss of excitability could underlie the mutants’ inability to sustain saccades. Intriguingly, our saccade recovery experiments showed that *didy* mutants needed between 8 and 45 seconds of recovery to be able to perform saccades again, a time that is

in agreement with the recovery time of sodium channels in the slowly reversible inactive state. Optical stimulation of ChR2-expressing neurons in the hindbrain restored saccades. We propose that the Na<sup>+</sup> currents added by activated ChR2 depolarized the affected neurons and thus helped them surpass firing threshold; the remaining endogenous voltage-gated sodium channels were then sufficient to carry the ensuing spikes.

Several lines of evidence suggest that the *didy*<sup>s552</sup> mutation is selective to premotor circuitry. First, in the context of the OKR, the defect appears limited to saccade generation; photoreception, motion detection, and slow-phase eye movements are all intact. Second, photo-activation of the putative saccade generator triggers saccades, even in *didy* mutants whose ability to produce saccades had previously been exhausted, suggesting that motor neurons and eye muscles are unaffected. Third, ChR2 stimulation of abducens motor neurons in the *Et(hsp(600bp):Gal4-VP16)s1020t* line did not elicit saccades, indicating that cells upstream of the motor neurons were triggering the saccades observed in the broadly expressing *Et(E1b:Gal4-VP16)s1101t* line. Fourth, the saccade-generation defect transfers between eyes, but is direction-specific; after exhaustion of saccades in one direction, reversal of the OKR stimulus still elicits saccades in the opposite direction, as one would expect from the connectivity of the burst neurons as shown in our model (Fig. 12). Fifth, assuming evolutionary conservation of the circuit, the deficit is unlikely to be presynaptic to EBNs, because omnipause neuron (OPN) input is inhibitory (see Fig. 12); an inability to spike in OPNs neurons should therefore result in an increased number of

saccades, not in fewer saccades. (For the same reason, we expect optical activation of OPNs to repress saccades and optical silencing of these neurons to facilitate saccades). Based on these five arguments, we favor the burst generator as the site of *didy* action. Alternatively or in addition, a defect of circuit elements inhibiting the OPNs (if they exist in teleosts), such as the dorsal long lead burst neurons described previously (Kamogawa et al., 1996), could also contribute to the *didy* phenotype.

In conclusion, this work has identified a region in the zebrafish larval hindbrain whose activity is necessary and sufficient for saccades to occur. The underlying circuit appears to be homologous, or at least functionally equivalent, to the mammalian burst generator. A newly discovered “channelopathy” perturbs this circuitry, rendering it unable to sustain action potentials over long periods of time. Behavioral experiments involving optical activation have allowed us to infer the basic layout of the saccade-generating circuitry in larval zebrafish, including its bilateral connections and lateralized directional specificity. Finally and more generally, we have shown here that ChR2 stimulation can be employed to mimic neurological functions, several synapses removed from the sensory or motor peripheries. Optogenetic tools can thus complement more conventional approaches to studying circuit function in the zebrafish brain.

### **3.8 Acknowledgements**

We wish to thank A. Goldin, A. Ribera, and K. Deisseroth for providing the rat Nav1.2 plasmid, the zebrafish Scn1lab morpholino, and the NpHR and ChR2 constructs, respectively. T. R. Thiele generated the construct for the

*Tg(UAS:ChR2(H134R)-mCherry)* transgenic line. The *Xenopus* oocyte two-electrode voltage clamp recordings were carried out in L. Y. Jan's laboratory with the help of T. Jin. J. Huisken assisted with the laser setup. This work was supported by NIH R01 NS053358, a Sandler Opportunity Award, the Byers Award for Basic Science, and the NIH Nanomedicine Development Center "Optical Control of Biological Functions" (H. B.). A. B. A. was funded by a stipend from the Boehringer Ingelheim Foundation and a Julius R. and Patricia A. Krevans Fellowship. F. D. B. was supported by an HFSP Postdoctoral Fellowship and a Sandler Postdoctoral Award.



## **Chapter 4 - Optogenetic control of cardiac function**

### **4.1 Authors**

Aristides B. Arrenberg, Didier Y.R. Stainier<sup>\*</sup>, Herwig Baier, Jan Huisken

### **4.2 Abstract**

Organ health and function rely on continuous blood flow and pressure generated by well-paced cardiac output. A method to experimentally control heart function in an animal model would be useful to model common pathological conditions. Here we use optogenetic tools (Miesenbock, 2009), patterned illumination and high-speed selective plane illumination microscopy (Huisken et al., 2004) to localize cardiac pacemaker cells, control the heart rate and modulate cardiac output in embryonic and larval zebrafish. This intervention is local, rapid, reversible, non-invasive, and quantitative. Photostimulation of Halorhodopsin (NpHR) (Zhang et al., 2007) is used to block depolarization, and activation of Channelrhodopsin-2 (ChR2) (Nagel et al., 2003; Zhang et al., 2007) to facilitate it. By automated sequential illumination of small areas of the developing heart with a digital micromirror device (DMD), while simultaneously monitoring heart contractions, we identify the regions responsible for initiating and relaying cardiac conduction. Initially encompassing most of the inflow region, the cardiac pacemaker becomes increasingly confined and comprises less than a dozen cells by the time the heart loops. By directly targeting the pacemaker area with well-defined light pulses, the heart rate can be increased with ChR2 stimulation

or decreased to a full stop with NpHR stimulation. Manipulating the atrioventricular canal induces atrioventricular blocks. Pulsed activation of the distal ventricle reverses cardiac conduction. These studies have greatly advanced our ability to control heart function as well as our understanding of the development, function, and dysfunction of the cardiac conduction system.

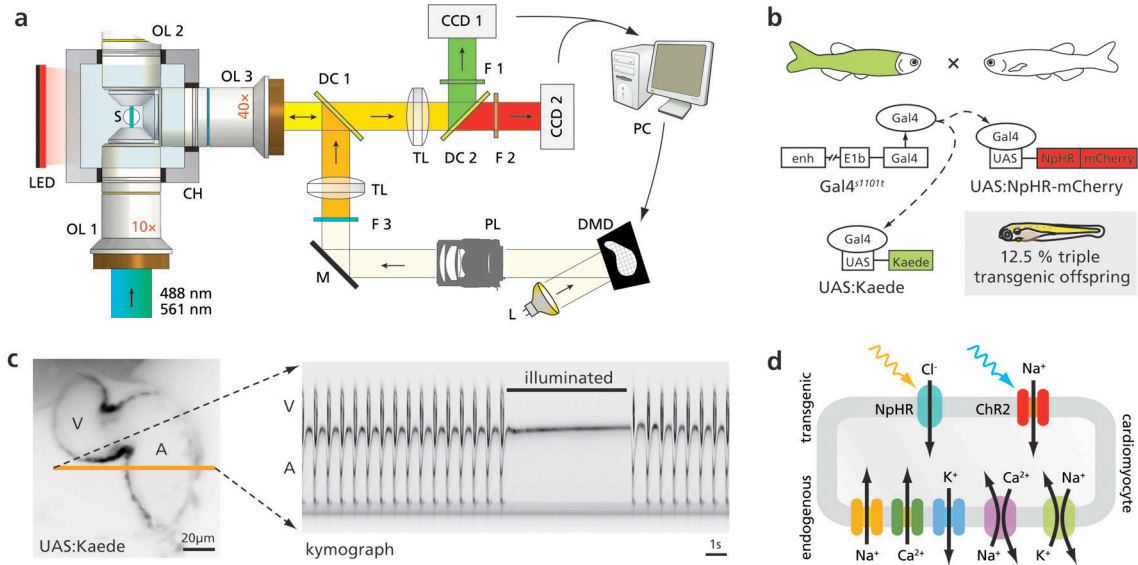
### **4.3 Results and Discussion**

In mammals, the heart rate is controlled by a specialized group of cells in the sinoatrial (SA) node, which act as the primary pacemaker cells. Cells in the atrioventricular (AV) node form the secondary pacemaker cells and together with the primary pacemaker cells, as well as specialized cells in the ventricular walls, constitute the cardiac conduction system (CCS) (Mikawa and Hurtado, 2007; Jongbloed et al., 2008). In non-mammalian vertebrates, a CCS with properties similar to that in mammals has been inferred based on imaging of voltage signals (Kamino et al., 1981; Sedmera et al., 2003) or  $\text{Ca}^{2+}$  transients (Chi et al., 2008): the origin of the conduction wave was located to a region apparently homologous to the SA node. However, it remains unclear whether this presumptive pacemaker is necessary and sufficient for cardiac contractions, and importantly what the consequences of its inactivation are.

To address these shortcomings, we adapted transgenic and optical tools to localize and control cardiac pacemaker cells in the developing zebrafish heart. Light-gated ion channels and pumps have been used in zebrafish to manipulate neurons and modulate behavior (Szobota et al., 2007; Douglass et al., 2008; Arrenberg et al., 2009; Baier and Scott, 2009; Wyart et al., 2009). In contrast to other tools used to change membrane potentials (reviewed by (Asakawa et al., 2008)), Halorhodopsin (NpHR) (Zhang et al., 2007) and Channelrhodopsin-2 H134R (ChR2) (Nagel et al., 2003; Zhang et al., 2007) enable temporally precise (tens of milliseconds) and spatially confined (single cells) control. Localized activation of these proteins has been achieved with well-defined light patterns

generated by laser scanning (Ayling et al., 2009) or fiber optics (Arrenberg et al., 2009). We elected to use a digital micromirror device (DMD) because it enables synchronous, uniform illumination of arbitrary shapes, such as micrometer-sized regions of the heart. Heart function during depolarization (ChR2) or hyperpolarization (NpHR) of the illuminated regions was monitored in real time with high-speed recordings (55-132 frames/s) of optical sections of the heart (Fig. 1a) using a multidirectional selective plane illumination microscope (mSPIM, (Huisken et al., 2004; Huisken and Stainier, 2007; Scherz et al., 2008) ). In our implementation, the DMD provided a resolution of 2.3  $\mu\text{m}$  laterally in the focal plane and ca. 8.9  $\mu\text{m}$  in the z-direction (Fig. S1). In mSPIM, the embryo can be rotated to be illuminated and imaged from different angles. The spectrum of the stimulation light was engineered to match the action spectra of the targeted light-gated proteins without affecting the video recordings (Fig. S2). The light-gated pump NpHR-mCherry was expressed in cardiomyocytes using animals transgenic for *Et(E1b: Gal4-VP16)s1101t; Tg(UAS:NpHR-mCherry)s1989t; Tg(UAS:Kaede)s1999t* ( (Scott et al., 2007; Arrenberg et al., 2009)) (Fig. 1b). Illuminating the entire heart (3 dpf) with orange light instantaneously blocked contractions (Fig. 1c, movie S1), indicating that the strong hyperpolarization induced by the activated chloride pump NpHR perturbed the sensitive, well-balanced interplay of ion channels in the myocardium (Fig. 1d) and prevented depolarizations. Spontaneous  $\text{Ca}^{2+}$  release from the sarcoplasmic reticulum did not appear to play a role in contraction initiation, since no contractions occurred during illumination. The heart recovered to its original beat rate instantaneously

after illumination (in zebrafish, blood circulation is dispensable for survival up to 6 dpf (Sehnert et al., 2002)).



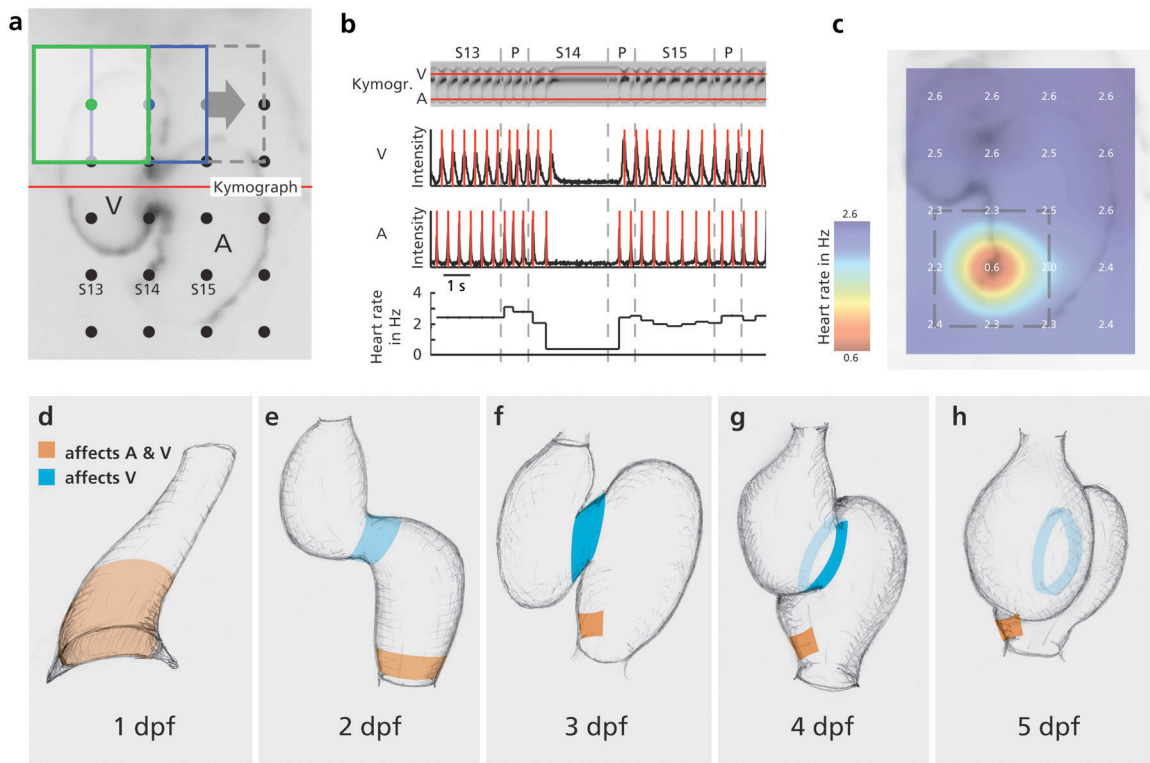
### Manuscript figure 1

#### Zebrafish hearts expressing NpHR are illuminated with a computer-controlled pattern of orange light to induce cardiac arrest.

(a) Microscope layout. The embedded fish (S) can be illuminated with three objective lenses (OL) inside a medium filled chamber (CH). OL1 and OL2 form a sheet of laser light (488 nm or 561 nm) in the focal plane of OL3. A computer-generated pattern is reflected off the digital micromirror device (DMD) and imaged with a photographic lens (PL), a tube lens (TL) and OL3 onto the sample. A red light-emitting diode (LED) provides a uniform transmission light. The fluorescence from the sample and the transmitted light are collected with OL3 and imaged with another TL onto two cameras, CCD1 (green channel) and CCD2 (red channel). Dichroic mirrors (DC), mirrors (M) and filters (F) fold the beam paths and define the spectrum of illumination and detection (see Fig. S2). The sample can be translated and rotated with 4 micro-motors (not shown). (b) The Gal4-UAS system was used to drive tissue specific expression of Kaede as well as NpHR-mCherry. enh, enhancer; E1b, basal promoter. (c) A 3 dpf zebrafish heart expressing NpHR-mCherry stopped beating when illuminated with orange light and recovered instantaneously afterwards. An optical section of the heart was obtained by low-intensity light sheet illumination. The motion of the heart wall along the highlighted line is visualized in the kymograph. V, ventricle; A, atrium; Dark image regions correspond to Kaede fluorescence (inverted image). See movie S1. (d) Besides the endogenous ion channels for Na<sup>+</sup>, Ca<sup>2+</sup> and K<sup>+</sup>, the transgenic lines also express the photo-activatable Cl<sup>-</sup>-pump NpHR or the photo-activatable cation channel ChR2. Application of orange and blue light hyperpolarizes and depolarizes the cardiomyocytes, respectively.

We initially observed that the sinoatrial region was more susceptible to NpHR manipulation than the working myocardium in the atrium and ventricle, a finding most likely attributable to the smaller current densities across the cell membranes of CCS cells (more than 10-fold lower, see ref. (Nygren et al., 1998; Wilders, 2007) and references therein).

In order to sample heart regions in a non-biased way, we sequentially illuminated small, overlapping regions with constant intensity (Fig. 2a, movie S2). Video analysis identified atrial and ventricular systoles, from which the momentary heart rate was calculated (Fig. 2b). Maps showing the heart rate for every illuminated area were generated (Fig. 2c) in order to identify regions in which NpHR activation induced cardiac arrest or ventricular arrhythmia. Pattern generation, data recording and analysis were automated and computer controlled for the fast and reproducible analysis of a large number of hearts.



## Manuscript figure 2

**Automated sequential illumination of 1-5 dpf hearts to locate the areas sensitive to hyperpolarization at the inflow and atrioventricular (AV) canal regions.**

(a) The whole heart was sequentially illuminated with overlapping squares (see movie S2). (b) The intensities in two lines of the kymograph were analyzed to extract the beat rate of the atrium (A) and ventricle (V). A short section of the kymograph, the intensities along the two lines and the heart rate are shown for samples S13-S15, taken at the locations shown in (a); P, illumination pause. (c) False-color image of the observed heart rate after illumination of 20 sampled areas. In this 3 dpf fish, the pacemaker cells are located in the dorsal-right side of the inflow ring. (d-h) Schematics of the pacemaking region (red) and AV region (blue) for 1 to 5 dpf old animals (see main text) as identified by the analysis shown in (a-c).

To follow the maturation of the CCS over embryonic and larval development, we generated heart rate maps for five stages (1 dpf - 5 dpf, n=3 to 15 hearts analyzed, mean 7.4 per stage) from different angles. In 1 dpf animals, the heart stopped beating when a large region at the venous pole of the heart was illuminated at medium light intensities (Fig. 2d). Illumination of the arterial pole of the heart tube did not affect the heartbeat. At higher light intensities, it was possible to block the heartbeat by illuminating smaller patches of the venous pole (Fig. S3a). These findings suggest that cells required to initiate the heartbeat (pacemaker cells) covered a large area at the venous pole. Strong electrical coupling seemed to be present, since the heart could be arrested by illuminating different patches at the venous pole.

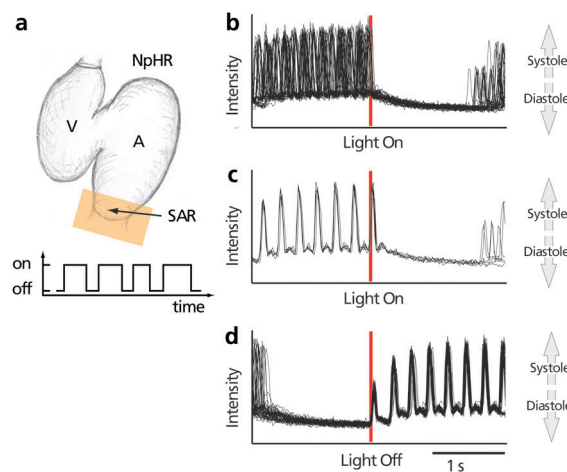
In 2 dpf animals, the pacemaker region was more confined than at 1 dpf (Fig. 2e and S3b) and located around the sinoatrial ring (SAR). While no consistent bias in the location of the pacemaker region was found, individual hearts tended to be more easily arrested by illuminating the right part of the SAR (right-biased: 8 hearts, left-biased: 5 hearts). The atrioventricular canal (AVC) is formed at this stage (Beis et al., 2005) and atrioventricular (AV) blocks could be induced at high illumination intensities. At later stages (3 dpf to 5 dpf), lower light intensities were sufficient to block ventricular systoles, as the AVC continues to mature. However, no bias was detected around the AVC perimeter at any stage, suggesting that all AVC cells contribute equally to the conduction of the beat from the atrium to the ventricle. Upon ablation of the primary pacemaker, downstream pacemakers like the AV node usually take over to maintain heartbeats (Scherf,



1927). Interestingly, in our experiments beating was always blocked when the SAR was silenced, which suggests that pacemaker currents in the AVC and ventricle are not strong enough to drive the larval heart after SAR silencing.

Over the third day of development, the pacemaker region became further defined (Fig. 2f, S3c) and reached a size that remained stable for the next two days (up to 5 dpf). The cells required to initiate heartbeats were confined to the dorsal-right quadrant of the SAR in a majority of the hearts (10 out of 13 hearts). A refinement of the pacemaker area during embryonic development has also been reported in other species, like the chick, where the pacemaker area narrows to a small region as it migrates from the atria to the right sinus primordium (Kamino et al., 1981). In amniotes, the pacemaker is generally situated on the right side, which matches our findings for the larval zebrafish heart. Furthermore, the center of the region (Fig. 2f) appeared to be located about 10  $\mu\text{m}$  (one or two cell diameters) further anterior than the neck of the SAR. Interestingly, the cells that make up the lips of the sinus adjacent to the SAR appear to have an intrinsic pacemaking capability and poor coupling to the SAR, since they continued to contract in the arrested heart (movie S3). However, they were not necessary for heartbeats, since illuminating them only stopped their contractions but not those of the heart. The number of cells required for beating varied between animals. The size of the illuminated area generally corresponded to 10-30 cells but some hearts could be arrested by illuminating just very few cells (3 cells, movies S4 and S5). At 4 and 5 dpf, the pacemaker cells remained at the same relative position (Fig. 2g and 2h, S3d and S3e).

To test whether the heart would be more susceptible to the illumination during pacemaker repolarization rather than depolarization we measured the phase dependency of the NpHR induced arrest by illuminating the SAR with a series of light pulses with randomized onset (Fig. 3a). Hearts always stopped instantaneously after light onset (Fig. 3b), except for a few trials in which one extra beat was observed directly after light onset (Fig. 3c). These immediate escaping beats can be explained by the kinetics of NpHR induced hyperpolarization ( $\tau_{on}=36$  ms, (Zhang et al., 2007)).



### Manuscript figure 3

**The heart stops instantaneously upon illumination and the recovery is precisely timed.**

(a) Schematic of the spatial and temporal pattern of illumination: The sinoatrial ring (SAR) was illuminated with random timing. (b-d) Overlays of motion cardiograms. High fluorescence intensities on the y-axis correspond to atrial systoles and low intensities to atrial diastoles. (b-c) Traces aligned to the onset of illumination. (b) In most cases the heart stopped instantaneously upon illumination. (c) When illuminated during the onset of the systole, one escape beat occurred, since the heart completed the systole. (d) After the light was turned off, the heart started beating instantaneously and was synchronized across trials. A, atrium; V, ventricle; SAR, sinoatrial ring.

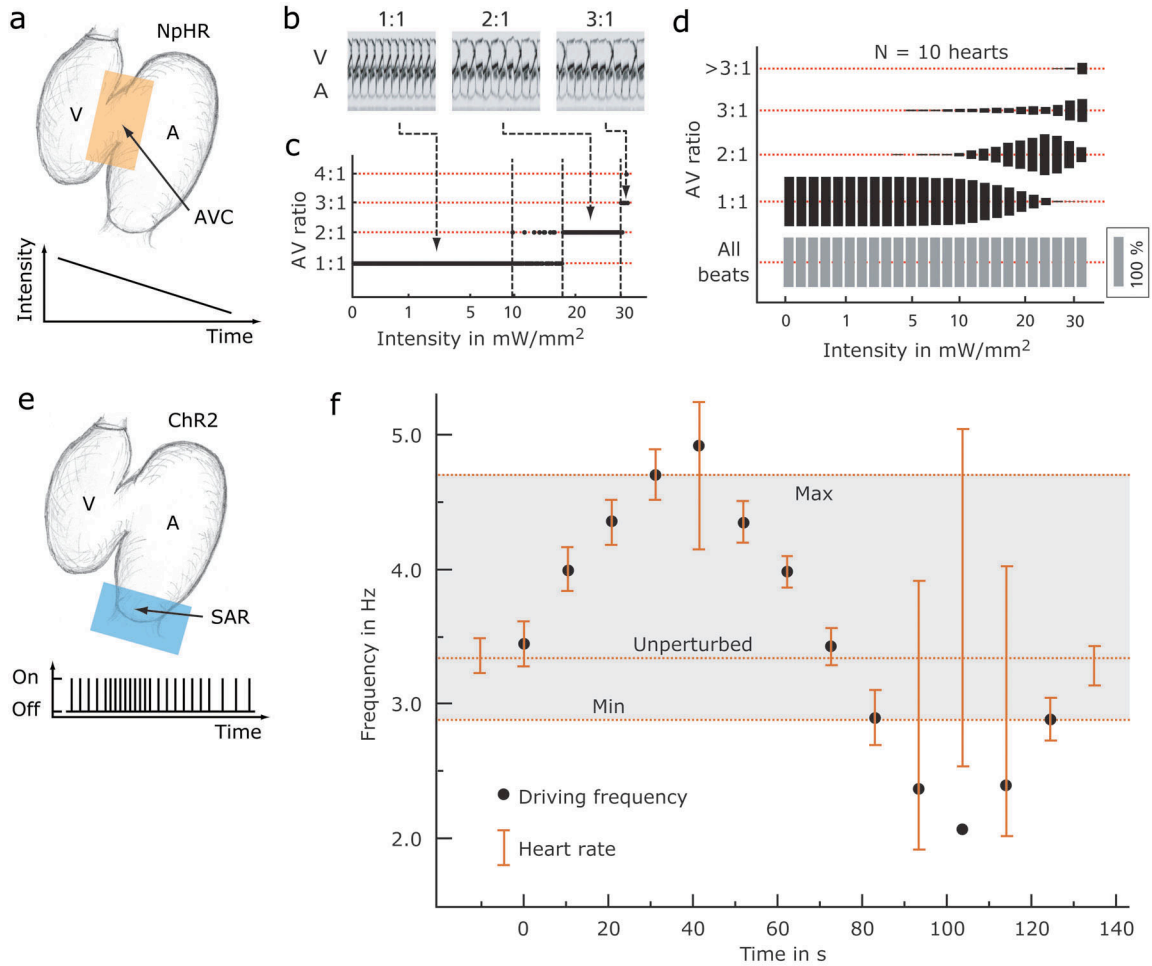
We concluded from this experiment that the pacemaker's susceptibility for membrane potential manipulation was similar over the time course of the heartbeat at the tested light intensity (30 mW/mm<sup>2</sup>). We also characterized the

recovery from illumination (Fig. 3d) and found that the heart started beating at the same time in every trial, meaning that the heart recovers from the same hyperpolarized state and with the same depolarization rate in every trial.

The heart can be manipulated very precisely with the presented tools to switch between a healthy and a diseased state on short time scales. We generated two prominent cardiac dysfunctions, AV blocks and tachy- and bradycardia. When illuminating the AVC (Fig. 4a), we induced different AV blocks by simply varying the light intensity. At high intensities, 3:1 and higher AV blocks could be induced (Fig. 4b and 4c) whereas medium intensities caused 2:1 AV blocks (movie S6). Notably, the 2:1 AV block was stable over a range of intensities (18 – 30 mW/mm<sup>2</sup>, or 55 - 95 % maximal light intensity, see vertical lines in Fig. 4c) and for prolonged periods of time (50 seconds, Fig. 4c). The induction of different AV blocks was reproducible in many different hearts (Fig. 4d), however the required light intensity varied between hearts, probably due to the varying expression levels of NpHR. In some hearts, a full block of ventricular beats could be produced with high light intensities. Generally, plateaus for 3:1 and 2:1 heart blocks could be found.

Next we explored whether the depolarizing ion channel ChR2 could be used to increase the heart rate (tachycardia) by pulsing the illumination of the SAR (Fig. 4e). The heart rate was 3.3 Hz in the 4 dpf animals before perturbation. We found that the heart rate reliably adjusted to the illumination pulses up to a frequency of 4.7 Hz (Fig. 4f, movie S7). When pulsed beyond 4.7 Hz the atrium started to omit pulses. The heart was not capable of maintaining such high

frequency and as a result the heart rate variability increased. Surprisingly, it was also possible to use ChR2 to reduce the heart rate (bradycardia). However, if driven below 2.7 Hz (0.6 Hz below the original heart rate), heartbeats started to be initiated ectopically by cells in the atrium (movie S8). While the experiments with NpHR suggested that the SAR is necessary for heart beating, this experiment with ChR2 showed that cardiomyocytes outside the pacemaker region are capable of autonomous rhythmic contractions in vivo if the SAR does not pace fast enough.



## Manuscript figure 4

### Optically induced atrioventricular arrhythmia, tachycardia and bradycardia.

(a-d) Ventricular blocks of different severity are induced by illuminating the atrioventricular canal (AVC) with well-defined intensities. (a) Schematic of the spatial and temporal pattern of illumination: The atrioventricular ring in NpHR expressing hearts was illuminated with slowly decreasing intensity. (b) Kymograph and (c) AV-ratio for different illumination intensities (the x-axis is scaled according to a power law). High intensities induced a 3:1 block, medium intensities a 2:1 block, and low intensities showed no effect. (d) Summary for 10 different hearts. See movie S6. (e) Schematic of the region and temporal pattern of illumination. The sinoatrial ring in Chr2 expressing hearts was illuminated with short pulses with varying frequency. (f) The heart rate (brown bars) relative to the driving frequency (black dots) during the course of the experiment. The heart rate follows the driving frequency within the indicated dynamic range (between Min and Max). A 40 % increase and a 15 % decrease in heart rate could be achieved. A, atrium; V, ventricle; AVC, atrioventricular canal; SAR, sinoatrial ring.

In mammalian hearts, the conduction direction is determined by the beating rates of primary pacemakers (faster) and downstream pacemakers (slower). Reentry can occur under pathological conditions (Valderrabano et al., 2006) and it is unclear to what extent cellular geometry and rectifying gap junctions (Bukauskas et al., 2002) regulate uni-directional conduction. In some primitive chordates, blood can be pumped in both directions (Kriebel, 1967). We were interested to know whether mechanisms were in place that prevented conduction in the distal-to-proximal direction (rectified conduction) and therefore tested whether cardiac conduction could be reversed at 2 dpf. We applied light pulses to a ventricular region close to the bulbus to rhythmically activate ChR2. Surprisingly, the conduction wave reversed (movie S9, Fig. S4), suggesting that cardiac conduction is not rectified.

In conclusion, we mapped the pacemaker cells in the developing heart and found that they initially cover a large area and subsequently mostly narrow to a small patch in the dorsal-right sinoatrial region. A small number of pacemaker cells is indispensable for heart beat initiation, which makes the embryonic heart very vulnerable. No compensating mechanism seems to be in place on the timescales observed. Our photostimulation methods also allowed us to optically control heart rate, reverse cardiac conduction and induce disease-like states in a reversible manner. In the future, chronic perturbations of the zebrafish pacemaker could be used in small molecule screens for drugs affecting CCS function and to identify intrinsic coping mechanisms of the heart (e.g. shifting of the pacemaker region). Epigenetic factors of heart (Hove et al., 2003) and blood

vessel development (Hahn and Schwartz, 2009) could also be studied under well controlled hemodynamic forces or in the absence of blood flow.

#### **4.4 Methods**

Descriptions of transgenic fish lines, the DMD setup, and data analyses are available in the supplementary information.

#### **4.5 Acknowledgements**

We thank Takashi Mikawa and Robin Shaw for feedback and comments on the manuscript. This work was supported in part by grants from the National Institutes of Health (HL54737) (to D.Y.R.S.), the Packard Foundation (D.Y.R.S.), NIH R01 NS053358 (H.B.), a Sandler Opportunity Award, the Byers Award for Basic Science (H.B.), and the NIH Nanomedicine Development Center “Optical Control of Biological Functions” (H.B.). J.H. was supported by a Human Frontier Science Program (HFSP) cross-disciplinary fellowship. A.B.A. was supported by a Boehringer Ingelheim Fonds (B.I.F.) fellowship and a Krevans fellowship.

#### **4.6 Author contributions**

The optogenetic idea, transgenic lines and original observation originated in H.B.’s lab; follow-up experiments were carried out in D.Y.R.S.’s lab as an equal collaboration between A.B.A. and J.H. All authors worked on the manuscript which was drafted by A.B.A. and J.H.

## **4.7 Author Information**

The authors declare that they do not have competing financial interests. Correspondence and requests for materials should be addressed to D.Y.R.S. (didier.stainier@ucsf.edu).

## **4.8 Supplementary Methods**

### **4.8.1 Transgenic fish**

Zebrafish used for this study were in the TL background and transgenic for a combination of *Tg(E1b:Gal4)s1101t*, *Tg(UAS:NpHR-mCherry)s1989t*, *Tg(UAS:eNpHR-mCherry)s1988t*, *Tg(UAS:ChR2(H134R)-eYFP)s1990t*, *Tg(UAS:Kaede)s1999t*. Transgenic lines were generated using the tol2 transposase system as described elsewhere (Arrenberg et al., 2009). Animals were raised in the dark and treated with PTU on the first day post fertilization to prevent pigment synthesis. Since transgene expression varied between fish of the same clutch and between clutches, animals were sorted about two hours prior to imaging. For sorting, the animals were placed under an epifluorescent dissecting microscope and the magnification changer dial was used to concentrate the light and assess how much light was needed to stop the heart beat (in the case of NpHR fish). Only hearts that responded at relatively low light levels were used in the study. As an estimate, we used the best 20-33 % of the



fish. We did not observe any long-term effects on cardiac function from these manipulations, even after repeated photostimulation over several hours.

#### **4.8.2 DMD stimulation**

**DMD setup.** For patterned illumination, a digital micromirror device (DMD) was coupled into the SPIM microscope (Fig. S2). We used the DMD and light bulb of a consumer market video beamer (IBM iLM300). The video beamer was partially disassembled to remove optical elements in front of the DMD. The DMD was driven via VGA signals from the computer, and the VGA signals were specified from within the custom Labview microscope software.

**DMD pattern generation.** Patterns could be generated in two ways. First, arbitrary regions of interest (ROIs) could be drawn on the live image within Labview, which allowed instantaneous illumination of the sample under visual inspection. Second, a sequence of pre-programmed ROIs could be displayed automatically at pre-defined time points during a recording. For some hearts we did not use automated techniques to localize pacemaker cells. Instead, the rotational axis of the SPIM stage was used to find both i) the optimal angle at which stimulation on one side of the SAR but not the other blocked heartbeats and ii) the angle at which stimulation on either side had the same effect (orthogonal to the optimal angle). With this protocol the location of the pacemaker cells was determined with a precision of 15°.

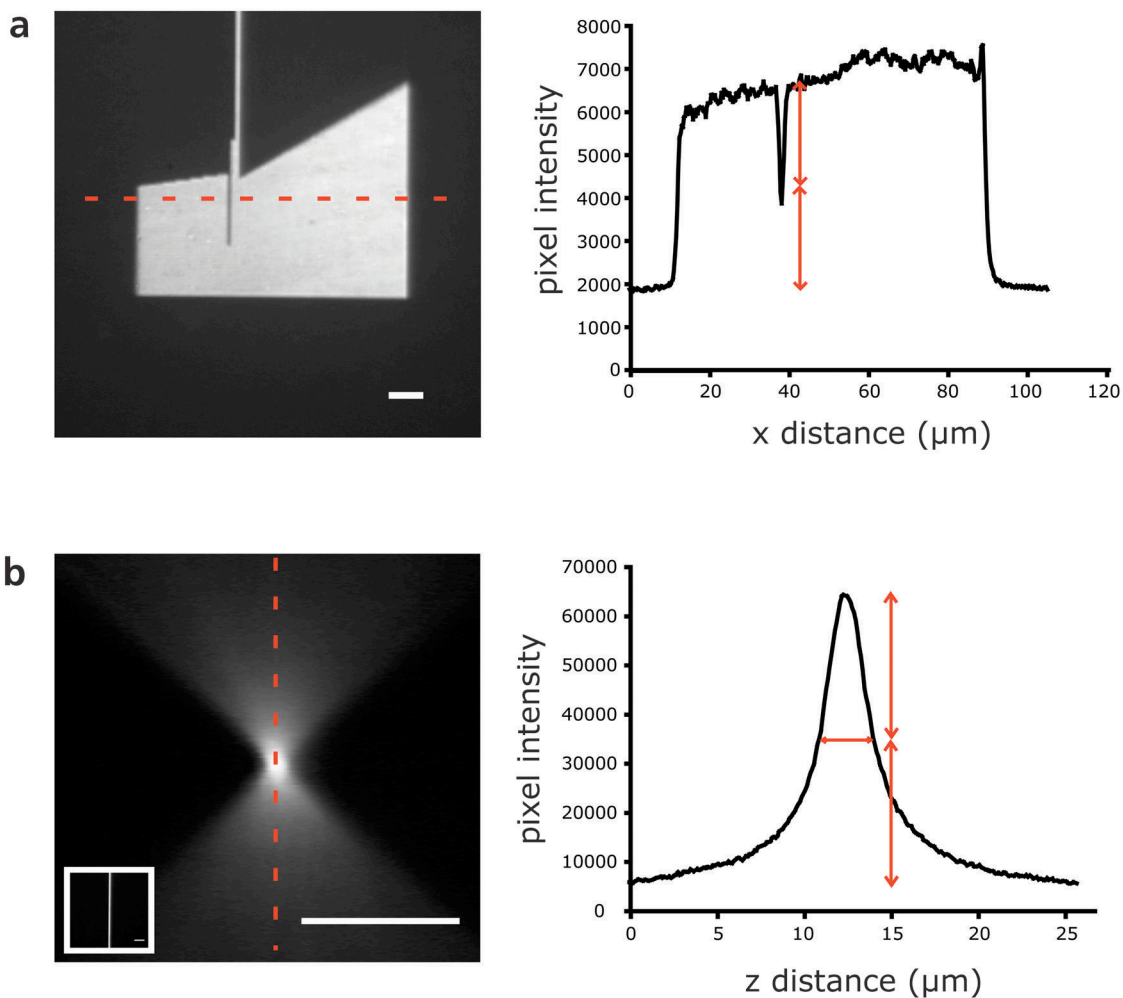
**Cell numbers.** The reported cell numbers in the main text correspond to the number of cells contained in the illuminated ROI. It is likely that adjacent cells were also hyperpolarized to a certain degree due to electrical coupling.

**Light intensities.** At full power (intensity=255), the light intensities were 150 mW/mm<sup>2</sup> (without filter), 60 mW/mm<sup>2</sup> (red filter, NpHR) and 16 mW/mm<sup>2</sup> (blue filter, ChR2). Light intensities used in experiments with NpHR expressing hearts were typically around 30 mW/mm<sup>2</sup>.

### **4.8.3 Analysis**

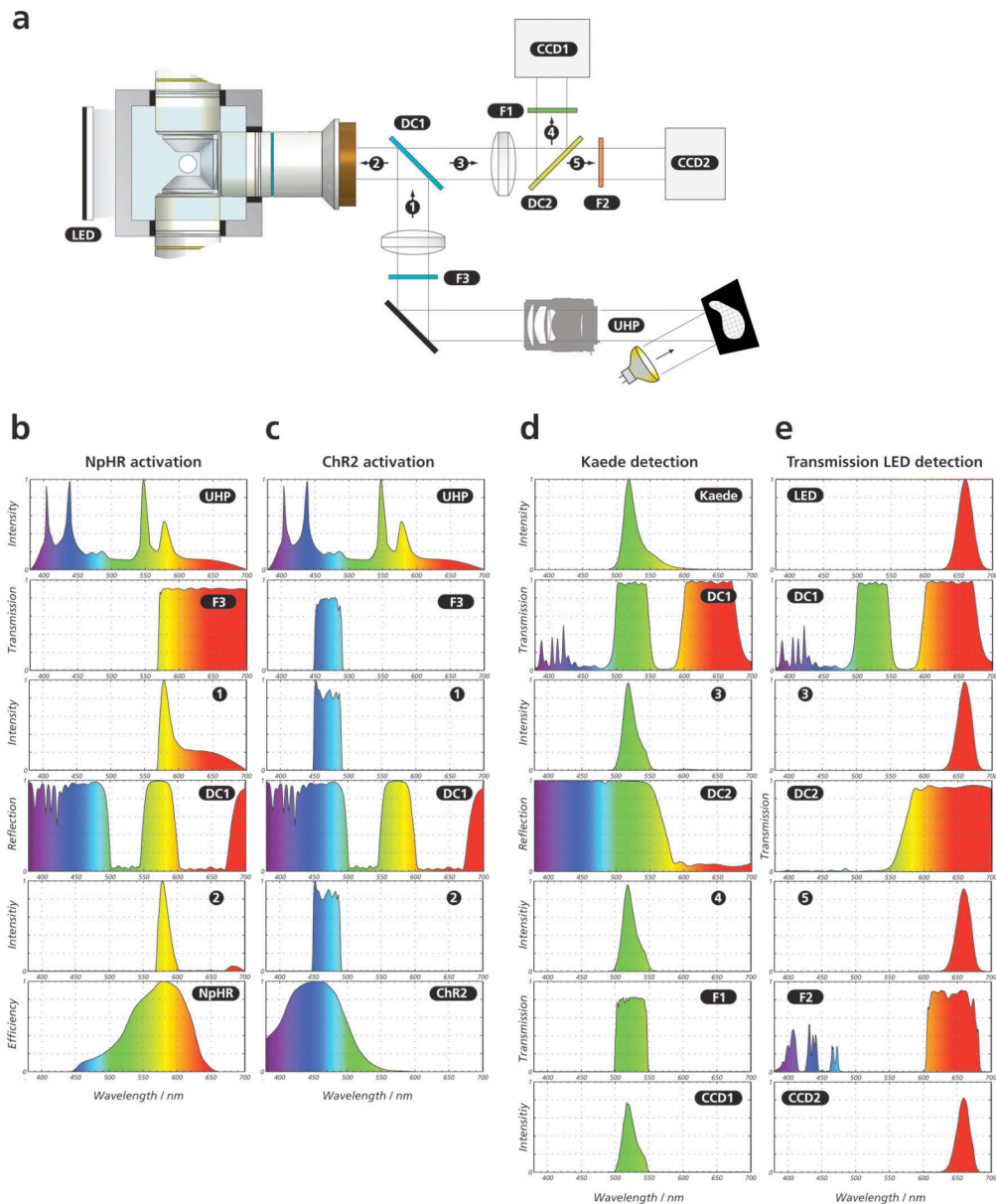
Image analysis was performed in Matlab. The intensity fluctuation of an individual pixel over time was plotted. To find a suitable pixel, a kymograph (x-z projection) of the image time stack was visually inspected, and a line was selected from this kymograph. A peak finder algorithm (O'Haver, 2006) was used to identify peaks automatically. It proved helpful to adjust a single parameter in the peak finder algorithm for every recording empirically since peak shapes could be different in each recording. The identified systolic time points were then combined with the sequence of ROIs used in the recording to create heart rate maps. Sound files were generated using the systolic time points.

#### 4.8.4 Supplementary Figures



#### Manuscript supplementary figure 1

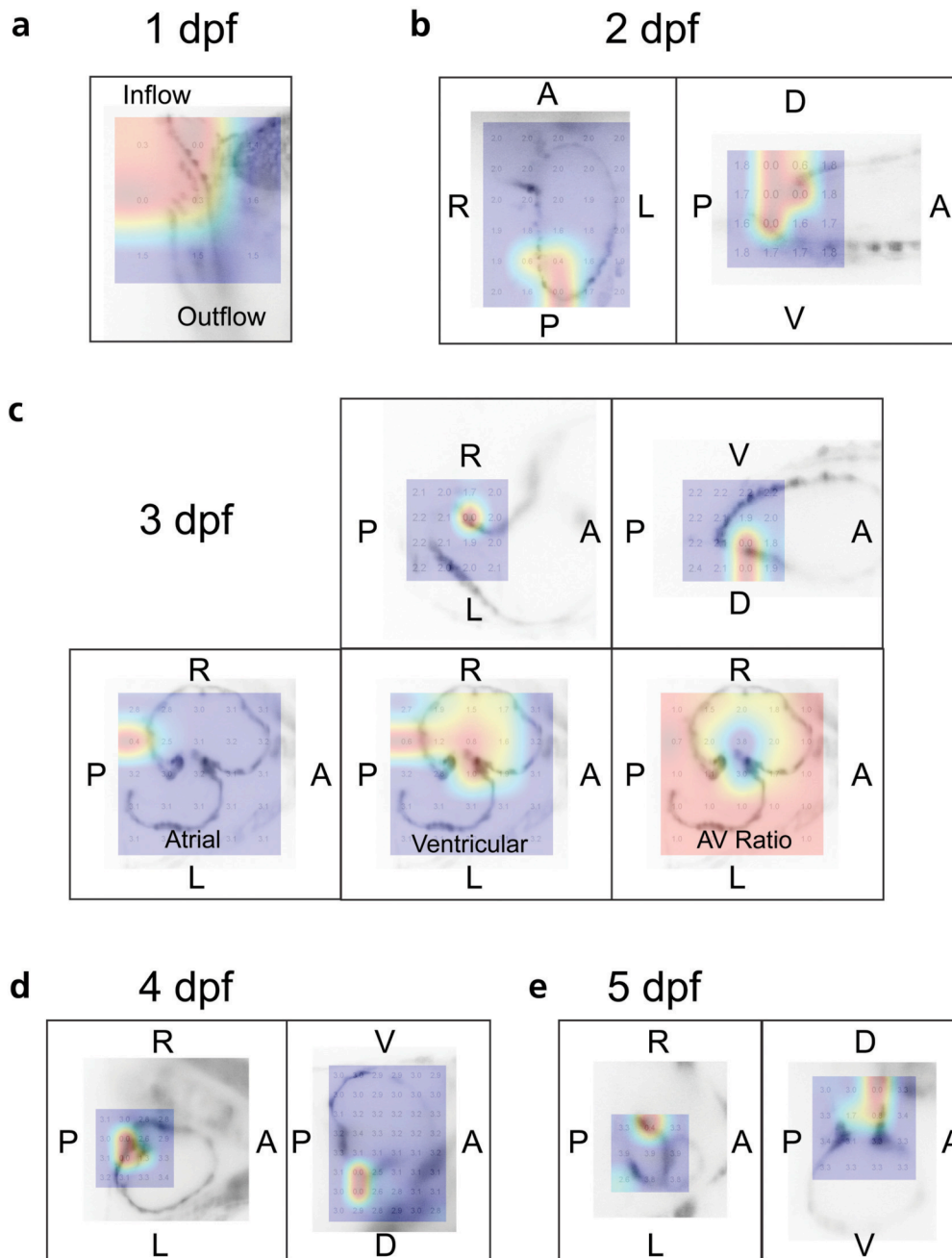
**Resolution of the DMD illumination.** (a) A region of interest containing a 2.3 μm slit was illuminated with the DMD. The pixel intensity along the red dashed line is plotted to the right. The pixel intensity dropped more than 50 % at the slit, indicating that the x-y resolution of the DMD was 2.3 μm or better. (b) A vertical bar was generated with the DMD (inset). A z-stack was recorded and an x-z projection is plotted on the left. The z-resolution was 8.9 μm, which corresponds to the peak width at half maximum. Scale bars, 10 μm.



## Manuscript supplementary figure 2

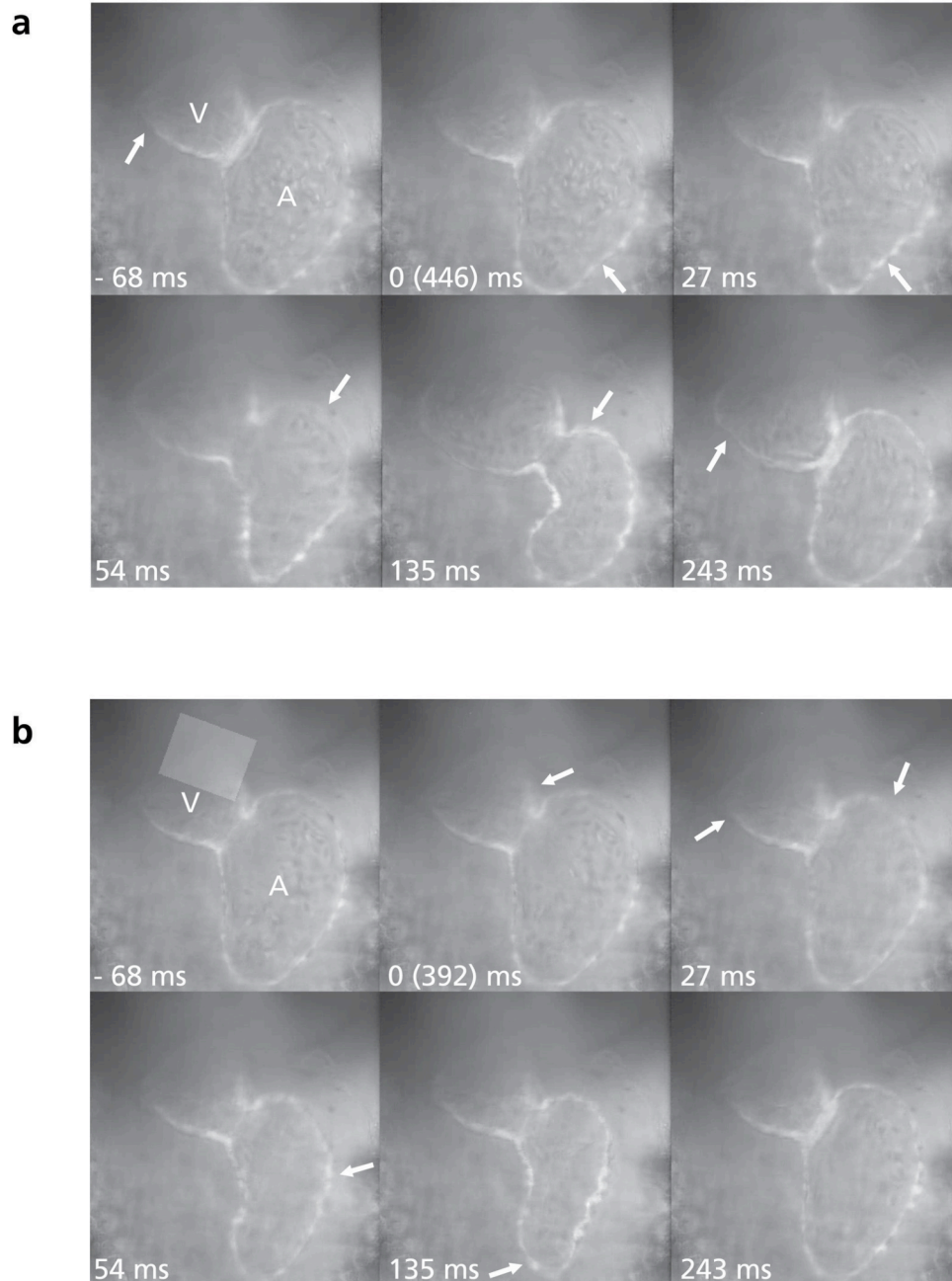
### Optical layout of the microscope with spectra for illumination of NpHR and ChR2 and detection of Kaede and transmission light.

(a) Location and specifications of the three filters F1-F3, the two dichroics DC1-DC2, and five sample points. (b) Spectrum of the ultra high pressure (UHP) lamp as it passes through filter F3 (HQ572LP) used for the activation of NpHR. The dominantly yellow light is reflected by the dichroic DC1 towards OL3. NpHR is efficiently activated around its absorption maximum at 580nm. (c) For activation of ChR2, the bandpass HQ470/40x was chosen for F3. DC1 reflects all of the blue light to activate ChR2 around its maximum at 460nm. (d) The emission spectrum of Kaede passes through DC1 and is reflected off DC2 before it reaches F1 and CCD1. (e) The light from the transmission LED passes through DC1, DC2, and F2 before it reaches CCD2. Both Kaede and the LED are well detected on CCD1 and CCD2, respectively.



### Manuscript supplementary figure 3

**Heart rate maps for hearts ranging from 1 dpf to 5 dpf.** (a) At 1 dpf the heartbeat could be blocked by illumination of the inflow region. (b) In a 2 dpf heart the pacemaker region was slightly biased to the right (*left image*) and more strongly biased towards the dorsal side of the SAR (*right image*). (c) *Top:* The center of the pacemaker region was in the dorsal-right quadrant of the SAR in this 3 dpf heart. *Bottom:* Heartbeats were blocked when the right side of the SAR was illuminated (*left image*). In addition, the heart developed AV blocks when the AV canal was illuminated (*middle and right images*). Also see movie S2 of this heart. (d, e) The pacemaker region remained in the dorsal-right quadrant of the SAR at 4 and 5 dpf. A=anterior, P=posterior, R=right, L=left, D=dorsal, V=ventral.



#### Manuscript supplementary figure 4

**ChR2 stimulation in the distal ventricle reverses cardiac conduction.** (a) Still images from movie S9 show that in the absence of stimulation cardiac conduction progresses from inflow (0 ms) to atrium (54 ms) and ventricle (243 ms). White arrows indicate the location and direction of contraction. Each heartbeat cycle took  $\approx 446$  ms. (b) The same analysis as in (a) for the ChR2 stimulated case. The heart was stimulated at the outflow region (-68 ms, shaded rectangle). Cardiac conduction progressed from ventricle (0 ms) to atrium (27-54 ms). The SAR contracted last (135 ms). A, atrium; V, ventricle.

## Chapter 5 - Discussion

### ***5.1 Optogenetics in zebrafish***

Here, I have presented the application of light-gated ion channels in zebrafish and the identification of cell populations required for a swimming behavior, quick eye movements and cardiac pace making. I generated zebrafish lines transgenic for the light-gated ion channels halorhodopsin (NpHR) and channelrhodopsin-2 (ChR2). They showed acceptable expression on the cell surface and electrophysiological recordings demonstrated potent manipulation of the firing rate. Furthermore I implemented techniques for the local application of light in zebrafish larvae. The use of fiber optics is a versatile and inexpensive approach with a well-defined lateral spread of light but limited resolution in the z direction. The application of a digital-micromirror-device (DMD) in a microscope has superior spatial resolution and allows to illuminate zebrafish tissue with user-defined patterns of light.

The presented tools provide a significant advance over previously available methods for the control of neural activity in the zebrafish. The use of pharmacology is oftentimes limited in larval zebrafish since the larvae are tiny and injected drugs are thus difficult to apply locally. In addition, the induction and reversal of pharmacological manipulations can be slow, dependent on the way of application and on the drug. Most of the transgenic effector lines that were available before only allowed permanent manipulations of neural tissues. Examples are zebrafish lines for the synaptic transmission blocker tetanus toxin

(Asakawa et al., 2008) and for the ablation of neurons using nitroreductase (Curado et al., 2007; Davison et al., 2007; Pisharath et al., 2007). While these manipulations were not reversible, it was already possible to spatially confine the manipulations to neurons of interest, since these tools are genetically encoded and can thus be targeted to identified neuronal populations for which selective promoters are available. The light-gated ion channels used in this study allow an additional way of spatial confinement, namely the use of light. Furthermore, the temporal control that is achievable with light-gated ion channels is unprecedented. Manipulations can be induced and reversed within milliseconds, which enables much better controlled experiments.

## **5.2 Limitations**

Readers will have noted that I was not able to identify the exact cells that controlled the swimming behavior in chapter 2 or the quick eye movements in chapter 3. Rather, I have localized the cells within cylindrical volumes of tissue within the hindbrain. The major reason for this shortcoming is that I made little use of specific expression patterns of light-gated ion channels in the presented work. With a few exceptions, I have been using zebrafish that express the channels broadly in neurons throughout the entire central nervous system. Another reason is the spatial resolution of light application. Activation of multiple identified cells within a dense population of expressing cells is not feasible with our current optical techniques. In the future, the use of advanced optical methods, like holographic illumination (Lutz et al., 2008) or multiphoton



techniques (Mohanty et al., 2008; Papagiakoumou et al., 2008; Rickgauer and Tank, 2009) may surpass this limitation. For the latter techniques it is important to consider the suboptimal activation of currently available light-gated ion channels with multiphoton illumination.

A further caveat that was encountered using the Gal4/UAS system in combination with light-activatable ion channels was variegation: Not all cells that expressed Gal4, also expressed the light-activated ion channel. This situation is especially problematic when working with silencers of activity, like NpHR, since all cells at the studied circuit level must be silenced. If only a fraction is silenced, the remaining active cells might still mediate the behavior. For depolarizing ion channels (ChR2), variegation might be less problematic, because a few activated cells could be enough to trigger the behavior. Using these arguments, a scientist might be in favor of using depolarizing channels, because it is easier to manipulate behaviors. However, caution is necessary, since the depolarization might be less physiologic than hyperpolarization. Hyperpolarization will decrease the membrane potential by a certain amount and any action potentials will be the result of the endogenous, presumably physiologic, excitatory inputs. However, depolarization will force the membrane potential above threshold and lead to firing of action potentials that is dictated by the amount of light and the kinetics of the introduced light-activatable channel. Naturally this firing will have little in common with the spiking that would occur in an unperturbed circuit. (The use of subthreshold depolarization or precisely timed light pulses could ameliorate this caveat.) In this sense, an experiment using hyperpolarization (NpHR) appears to

be a cleaner one, since behaviors are the result of remaining activity in the brain. Overall, the combination of hyperpolarization and depolarization will of course allow the best interpretation of results.

While electrophysiological recordings have been used to characterize the transgenic lines in the presented work, it is important to note that in general electrophysiological techniques are difficult in larval zebrafish. The small size of larval neurons make single-cell recordings hard and the small size of the larva itself, including the absence of bones, complicates any recordings in animals during behavior. While there was no urgent need for advanced electrophysiological experiments in the presented studies, they would help to unlock the full potential of optogenetics in larval zebrafish.

### **5.3 Outlook**

Optogenetic tools have proven to be a valuable addition to the methods of neuroscience. In the zebrafish, we have been using them to identify neural circuits required for behaviors. This approach can be termed functional neuroanatomy, because we are assessing the function of localized cell populations within the brain. This approach allows us to identify the circuit elements of zebrafish behavior and will ultimately lead to a complete functional map of the larval zebrafish brain. For us, one of the most pressing tasks is to identify brain areas in which visual information is transformed into appropriate behaviors. It will be interesting to identify the circuitry in midbrain and

diencephalon required for the Optokinetic response (OKR) and for the hunting of paramecia (prey capture).

So far, we have been using optogenetics in the zebrafish to answer all-or-none questions: Does the animal still perform behavior X when we take circuit Y out of the equation? A different and equally promising approach is to focus on the circuit Y and ask how it manages to generate output B, given input A. This line of research aims at a mechanistic understanding of cell networks and the available optogenetic tools should prove very useful for such experiments. Light-activatable channels allow for very precise and measurable perturbations of firing rates and since the perturbations are reversible, hundreds of trials can be performed in an individual animal to measure input-output functions, exploring the full parameter space and all values a parameter might take. Furthermore, the fast timescale of perturbations can be exploited to understand the importance of spike timing in network processes.

The recent advances regarding genetically encoded sensors of neural activity, e.g. GCaMP-3 (Tian et al., 2009), will hopefully manifest their full potential in translucent larval zebrafish. It seems we are entering an exciting time in zebrafish systems neuroscience.

## Chapter 6 - Bibliography

- Aksay E, Baker R, Seung HS, Tank DW (2000) Anatomy and discharge properties of pre-motor neurons in the goldfish medulla that have eye-position signals during fixations. *J Neurophysiol* 84:1035-1049.
- Aksay E, Gamkrelidze G, Seung H, Baker R, Tank D (2001) *In vivo* intracellular recording and perturbation of persistent activity in a neural integrator. *Nat Neurosci* 4:184-193.
- Aksay E, Olasagasti I, Mensh BD, Baker R, Goldman MS, Tank DW (2007) Functional dissection of circuitry in a neural integrator. *Nat Neurosci* 10:494-504.
- Aravanis AM, Wang LP, Zhang F, Meltzer LA, Mogri MZ, Schneider MB, Deisseroth K (2007) An optical neural interface: in vivo control of rodent motor cortex with integrated fiberoptic and optogenetic technology. *J Neural Eng* 4:S143-156.
- Arrenberg A, Del Bene F, Baier H (2009) Optical control of zebrafish behavior with halorhodopsin. *Proc Natl Acad Sci USA* 106:17968-17973.
- Asakawa K, Kawakami K (2008) Targeted gene expression by the Gal4-UAS system in zebrafish. *Dev Growth Differ* 50:391-399.
- Asakawa K, Suster ML, Mizusawa K, Nagayoshi S, Kotani T, Urasaki A, Kishimoto Y, Hibi M, Kawakami K (2008) Genetic dissection of neural circuits by Tol2 transposon-mediated Gal4 gene and enhancer trapping in zebrafish. *Proc Natl Acad Sci U S A* 105:1255-1260.
- Ayling OG, Harrison TC, Boyd JD, Goroshkov A, Murphy TH (2009) Automated light-based mapping of motor cortex by photoactivation of channelrhodopsin-2 transgenic mice. *Nat Methods* 6:219-224.
- Baier H, Scott EK (2009) Genetic and optical targeting of neural circuits and behavior--zebrafish in the spotlight. *Curr Opin Neurobiol* 19:553-560.
- Banghart M, Borges K, Isacoff E, Trauner D, Kramer RH (2004) Light-activated ion channels for remote control of neuronal firing. *Nat Neurosci* 7:1381-1386.
- Beck JC, Gilland E, Tank DW, Baker R (2004) Quantifying the Ontogeny of Optokinetic and Vestibuloocular Behaviors in Zebrafish, Medaka, and Goldfish. *J Neurophysiol* 92:3546-3561.
- Beck JC, Rothnie P, Straka H, Wearne SL, Baker R (2006) Precerebellar Hindbrain Neurons Encoding Eye Velocity During Vestibular and Optokinetic Behavior in the Goldfish. *J Neurophysiol* 96:1370-1382.
- Beis D, Bartman T, Jin SW, Scott IC, D'Amico LA, Ober EA, Verkade H, Frantsve J, Field HA, Wehman A, Baier H, Tallafuss A, Bally-Cuif L, Chen JN, Stainier DY, Jungblut B (2005) Genetic and cellular analyses of zebrafish atrioventricular cushion and valve development. *Development* 132:4193-4204.

- Borla MA, Palecek B, Budick S, O'Malley DM (2002) Prey capture by larval zebrafish: evidence for fine axial motor control. *Brain Behav Evol* 60:207-229.
- Bourbon HM, Gonzy-Treboul G, Peronnet F, Alin MF, Ardourel C, Benassayag C, Cribbs D, Deutsch J, Ferrer P, Haenlin M, Lepasant JA, Noselli S, Vincent A (2002) A P-insertion screen identifying novel X-linked essential genes in *Drosophila*. *Mech Dev* 110:71-83.
- Brainard DH (1997) The Psychophysics Toolbox. *Spatial Vision* 10:433-436.
- Brand AH, Perrimon N (1993) Targeted gene expression as a means of altering cell fates and generating dominant phenotypes. *Development* 118:401-415.
- Brockhoff SE, Hurley JB, Janssen-Bienhold U, Neuhauss SCF, Driever W, Dowling JE (1995) A behavioral screen for isolating zebrafish mutants with visual system defects. *Proc Natl Acad Sci USA* 92:10545-10549.
- Budick SA, O'Malley DM (2000) Locomotor repertoire of the larval zebrafish: swimming, turning and prey capture. *J Exp Biol* 203:2565-2579.
- Bukauskas FF, Angele AB, Verselis VK, Bennett MV (2002) Coupling asymmetry of heterotypic connexin 45/ connexin 43-EGFP gap junctions: properties of fast and slow gating mechanisms. *Proc Natl Acad Sci U S A* 99:7113-7118.
- Burgess HA, Granato M (2007) Modulation of locomotor activity in larval zebrafish during light adaptation. *J Exp Biol* 210:2526-2539.
- Burrone J, O'Byrne M, Murthy VN (2002) Multiple forms of synaptic plasticity triggered by selective suppression of activity in individual neurons. *Nature* 420:414-418.
- Campagnola L, Wang H, Zylka MJ (2008) Fiber-coupled light-emitting diode for localized photostimulation of neurons expressing channelrhodopsin-2. *J Neurosci Methods* 169:27-33.
- Carr DB, Day M, Cantrell AR, Held J, Scheuer T, Catterall WA, Surmeier DJ (2003) Transmitter modulation of slow, activity-dependent alterations in sodium channel availability endows neurons with a novel form of cellular plasticity. *Neuron* 39:793-806.
- Catterall WA (2001) Structural biology: A 3D view of sodium channels. *Nature* 409:988-991.
- Chambers JJ, Banghart MR, Trauner D, Kramer RH (2006) Light-induced depolarization of neurons using a modified Shaker K(+) channel and a molecular photoswitch. *J Neurophysiol* 96:2792-2796.
- Chi NC, Shaw RM, Jungblut B, Huisken J, Ferrer T, Arnaout R, Scott I, Beis D, Xiao T, Baier H, Jan LY, Tristani-Firouzi M, Stainier DY (2008) Genetic and physiologic dissection of the vertebrate cardiac conduction system. *PLoS Biol* 6:e109.
- Curado S, Anderson RM, Jungblut B, Mumm J, Schroeter E, Stainier DY (2007) Conditional targeted cell ablation in zebrafish: a new tool for regeneration studies. *Dev Dyn* 236:1025-1035.
- Davison JM, Akitake CM, Goll MG, Rhee JM, Gosse N, Baier H, Halpern ME, Leach SD, Parsons MJ (2007) Transactivation from Gal4-VP16 transgenic

- insertions for tissue-specific cell labeling and ablation in zebrafish. *Dev Biol* 304:811-824.
- Douglass AD, Kraves S, Deisseroth K, Schier AF, Engert F (2008) Escape behavior elicited by single, Channelrhodopsin-2-evoked spikes in zebrafish somatosensory neurons. *CurrBiol* 18:1133-1137.
- Drapeau P, Ali DW, Buss RR, Saint-Amant L (1999) In vivo recording from identifiable neurons of the locomotor network in the developing zebrafish. *J Neurosci Methods* 88:1-13.
- Dubnau J, Grady L, Kitamoto T, Tully T (2001) Disruption of neurotransmission in *Drosophila* mushroom body blocks retrieval but not acquisition of memory. *Nature* 411:476-480.
- Easter JSS, Nicola GN (1996) The development of vision in the Zebrafish (*Danio rerio*). *Dev Biol* 180:646-663.
- Fortin DL, Banghart MR, Dunn TW, Borges K, Wagenaar DA, Gaudry Q, Karakossian MH, Otis TS, Kristan WB, Trauner D, Kramer RH (2008) Photochemical control of endogenous ion channels and cellular excitability. *Nat Methods* 5:331-338.
- Fuchs AF, Kaneko CRS (1981) A brain stem generator for saccadic eye movements. *Trends in Neurosci* 4:283-286.
- Gahtan E, Baier H (2004) Of lasers, mutants, and see-through brains: functional neuroanatomy in zebrafish. *J Neurobiol* 59:147-161.
- Gahtan E, Tanger P, Baier H (2005) Visual prey capture in larval zebrafish is controlled by identified reticulospinal neurons downstream of the tectum. *J Neurosci* 25:9294-9303.
- Gahtan E, Sankrithi N, Campos JB, O'Malley DM (2002) Evidence for a widespread brain stem escape network in larval zebrafish. *J Neurophysiol* 87:608-614.
- Gerlitz O, Nellen D, Ottiger M, Basler K (2002) A screen for genes expressed in *Drosophila* imaginal discs. *Int J Dev Biol* 46:173-176.
- Glimcher PW (2003) The neurobiology of visual-saccadic decision making. *Annual Review of Neuroscience* 26:133-179.
- Gnuegge L, Schmid S, Neuhauss SC (2001) Analysis of the activity-deprived zebrafish mutant macho reveals an essential requirement of neuronal activity for the development of a fine-grained visuotopic map. *J Neurosci* 21:3542-3548.
- Goldin AL (1991) Expression of ion channels by injection of mRNA into *Xenopus* oocytes. *Meth Cell Biol* 36:487-509.
- Goldin AL (2003) Mechanisms of sodium channel inactivation. *Curr Op Neurobiol* 13:284-290.
- Gradinaru V, Thompson KR, Deisseroth K (2008) eNpHR: a Natronomonas halorhodopsin enhanced for optogenetic applications. *Brain Cell Biol*.
- Graham-Brown T (1911) The intrinsic factors in the act of progression in the mammal. *Proc R Soc Lond B Biol Sci* 84:308-319.
- Granato M, van Eeden FJ, Schach U, Trowe T, Brand M, Furutani-Seiki M, Haffter P, Hammerschmidt M, Heisenberg CP, Jiang YJ, Kane DA, Kelsh RN, Mullins MC, Odenthal J, Nusslein-Volhard C (1996) Genes controlling

- and mediating locomotion behavior of the zebrafish embryo and larva. *Development* 123:399-413.
- Grillner S, Wallen P, Saitoh K, Kozlov A, Robertson B (2008) Neural bases of goal-directed locomotion in vertebrates--an overview. *Brain Res Rev* 57:2-12.
- Grubb MS, Rossi FM, Changeux JP, Thompson ID (2003) Abnormal functional organization in the dorsal lateral geniculate nucleus of mice lacking the beta 2 subunit of the nicotinic acetylcholine receptor. *Neuron* 40:1161-1172.
- Gurskaya NG, Verkhusha VV, Shcheglov AS, Staroverov DB, Chepurnykh TV, Fradkov AF, Lukyanov S, Lukyanov KA (2006) Engineering of a monomeric green-to-red photoactivatable fluorescent protein induced by blue light. *Nat Biotechnol* 24:461-465.
- Hahn C, Schwartz MA (2009) Mechanotransduction in vascular physiology and atherogenesis. *Nat Rev Mol Cell Biol* 10:53-62.
- Han X, Boyden ES (2007) Multiple-color optical activation, silencing, and desynchronization of neural activity, with single-spike temporal resolution. *PLoS ONE* 2:e299.
- Herrick CJ (1908) On the commissura infima and its nuclei in the brains of fishes. *Journal of Comparative Neurology and Psychology* 18:409-431.
- Hong ST, Bang S, Hyun S, Kang J, Jeong K, Paik D, Chung J, Kim J (2008) cAMP signalling in mushroom bodies modulates temperature preference behaviour in *Drosophila*. *Nature* 454:771-775.
- Hove JR, Koster RW, Forouhar AS, Acevedo-Bolton G, Fraser SE, Gharib M (2003) Intracardiac fluid forces are an essential epigenetic factor for embryonic cardiogenesis. *Nature* 421:172-177.
- Hua J, Smear M, Baier H, Smith S (2005) Regulation of axon growth *in vivo* by activity-based competition. *Nature* 434:1022-1025.
- Huisken J, Stainier DY (2007) Even fluorescence excitation by multidirectional selective plane illumination microscopy (mSPIM). *Opt Lett* 32:2608-2610.
- Huisken J, Swoger J, Del Bene F, Wittbrodt J, Stelzer EH (2004) Optical sectioning deep inside live embryos by selective plane illumination microscopy. *Science* 305:1007-1009.
- Ilg UJ, Hoffmann KP (1991) Responses of monkey nucleus of the optic tract neurons during pursuit and fixation. *Neuroscience Research* 12:101-110.
- Ilg UJ, Hoffmann K-P (1996) Responses of neurons of the nucleus of the optic tract and the dorsal terminal nucleus of the accessory optic tract in the awake monkey. *European Journal of Neuroscience* 8:92-105.
- Jongbloed MR, Mahtab EA, Blom NA, Schaliij MJ, Gittenberger-de Groot AC (2008) Development of the cardiac conduction system and the possible relation to predilection sites of arrhythmogenesis. *ScientificWorldJournal* 8:239-269.
- Jung H-Y, Mickus T, Spruston N (1997) Prolonged sodium channel inactivation contributes to dendritic action potential attenuation in hippocampal pyramidal neurons. *J Neurosci* 17:6639-6646.

- Kalaidzidis IV, Kalaidzidis YL, Kaulen AD (1998) Flash-induced voltage changes in halorhodopsin from *Natronobacterium pharaonis*. *FEBS Lett* 427:59-63.
- Kamino K, Hirota A, Fujii S (1981) Localization of pacemaking activity in early embryonic heart monitored using voltage-sensitive dye. *Nature* 290:595-597.
- Kamogawa H, Ohki Y, Shimazu H, Suzuki I, Yamashita M (1996) Inhibitory input to pause neurons from pontine burst neuron area in the cat. *Neurosci Lett* 203:163-166.
- Kanda T, Iwamoto Y, Yoshida K, Shimazu H (2007) Glycinergic inputs cause the pause of pontine omnipause neurons during saccades. *Neurosci Lett* 413:16-20.
- Kay JN, Finger-Baier KC, Roeser T, Staub W, Baier H (2001) Retinal Ganglion Cell Genesis Requires *lakritz*, a Zebrafish *atonal* Homolog. *Neuron* 30:725-736.
- Kearney JA, Plummer NW, Smith MR, Kapur J, Cummins TR, Waxman SG, Goldin AL, Meisler MH (2001) A gain-of-function mutation in the sodium channel gene *Scn2a* results in seizures and behavioral abnormalities. *Neuroscience* 102:307-317.
- Kimmel CB, Powell SL, Metcalfe WK (1982) Brain neurons which project to the spinal cord in young larvae of the zebrafish. *J Comp Neurol* 205:112-127.
- Kimmel CB, Metcalfe WK, Schabtach E (1985) T reticular interneurons: a class of serially repeating cells in the zebrafish hindbrain. *J Comp Neurol* 233:365-376.
- Kitamoto T (2002) Targeted expression of temperature-sensitive dynamin to study neural mechanisms of complex behavior in *Drosophila*. *J Neurogenet* 16:205-228.
- Kriebel ME (1967) Conduction velocity and intracellular action potentials of the tunicate heart. *J Gen Physiol* 50:2097-2107.
- Lerchner W, Xiao C, Nashmi R, Slimko EM, van Trigt L, Lester HA, Anderson DJ (2007) Reversible silencing of neuronal excitability in behaving mice by a genetically targeted, ivermectin-gated Cl<sup>-</sup> channel. *Neuron* 54:35-49.
- Liu KS, Fetcho JR (1999) Laser ablations reveal functional relationships of segmental hindbrain neurons in zebrafish. *Neuron* 23:325-335.
- Lopez-Barneo J, Darlot C, Berthoz A, Baker R (1982) Neuronal activity in prepositus nucleus correlated with eye movement in the alert cat. *J Neurophysiol* 47:329-352.
- Lutz C, Otis TS, Desars V, Charpak S, Digregorio DA, Emiliani V (2008) Holographic photolysis of caged neurotransmitters. *Nat Methods* 5:821-827.
- Major G, Baker R, Aksay E, Mensh B, Seung HS, Tank DW (2004) Plasticity and tuning by visual feedback of the stability of a neural integrator. *Proc Natl Acad Sci USA* 101:7739-7744.
- Marsh E, Baker R (1997) Normal and Adapted Visuooculomotor Reflexes in Goldfish. *J Neurophysiol* 77:1099-1118.



- Martin JR, Raabe T, Heisenberg M (1999) Central complex substructures are required for the maintenance of locomotor activity in *Drosophila melanogaster*. *J Comp Physiol A* 185:277-288.
- Martin JR, Keller A, Sweeney ST (2002) Targeted expression of tetanus toxin: a new tool to study the neurobiology of behavior. *Adv Genet* 47:1-47.
- Masino MA, Fetcho JR (2005) Fictive swimming motor patterns in wild type and mutant larval zebrafish. *J Neurophysiol* 93:3177-3188.
- Mason L, Scott, E.K., Staub, W., Finger-Baier, K., Baier, H. (2009) Expression patterns from Gal4 enhancer trap screen. ZFIN Direct Data Submission.
- Masseck OA, Hoffmann K-P (2009) Comparative neurobiology of the optokinetic reflex. *Ann N Y Acad Sci* 1164:430-439.
- McDearmid JR, Drapeau P (2006) Rhythmic motor activity evoked by NMDA in the spinal zebrafish larva. *J Neurophysiol* 95:401-417.
- McLaughlin T, Torborg CL, Feller MB, O'Leary DD (2003) Retinotopic map refinement requires spontaneous retinal waves during a brief critical period of development. *Neuron* 40:1147-1160.
- Mendelson B (1986) Development of reticulospinal neurons of the zebrafish. II. Early axonal outgrowth and cell body position. *J Comp Neurol* 251:172-184.
- Metcalfe WK, Mendelson B, Kimmel CB (1986) Segmental homologies among reticulospinal neurons in the hindbrain of the zebrafish larva. *J Comp Neurol* 251:147-159.
- Mickus T, Jung H-Y, Spruston N (1999) Slow sodium channel inactivation in CA1 pyramidal cells. *Ann N Y Acad Sci* 868:97-101.
- Miesenbock G (2009) The optogenetic catechism. *Science* 326:395-399.
- Mikawa T, Hurtado R (2007) Development of the cardiac conduction system. *Semin Cell Dev Biol* 18:90-100.
- Mohanty SK, Reinscheid RK, Liu X, Okamura N, Krasieva TB, Berns MW (2008) In-depth activation of channelrhodopsin 2-sensitized excitable cells with high spatial resolution using two-photon excitation with a near-infrared laser microbeam. *Biophys J* 95:3916-3926.
- Muto A, Orger MB, Wehman AM, Smear MC, Kay JN, Page-McCaw PS, Gahtan E, Xiao T, Nevin LM, Gosse NJ, Staub W, Finger-Baier K, Baier H (2005) Forward genetic analysis of visual behavior in zebrafish. *PLoS Genet* 1:e66.
- Myers PZ (1985) Spinal motoneurons of the larval zebrafish. *J Comp Neurol* 236:555-561.
- Nagel G, Szellas T, Huhn W, Kateriya S, Adeishvili N, Berthold P, Ollig D, Hegemann P, Bamberg E (2003) Channelrhodopsin-2, a directly light-gated cation-selective membrane channel. *Proc Natl Acad Sci U S A* 100:13940-13945.
- Neuhauss SC, Biehlmaier O, Seeliger MW, Das T, Kohler K, Harris WA, Baier H (1999) Genetic disorders of vision revealed by a behavioral screen of 400 essential loci in zebrafish. *J Neurosci* 19:8603-8615.

- Novak AE, Taylor AD, Pineda RH, Lasda EL, Wright MA, Ribera AB (2006) Embryonic and larval expression of zebrafish voltage-gated sodium channel  $\alpha$ -subunit genes. *Dev Dyn* 235:1962-1973.
- Nygren A, Fiset C, Firek L, Clark JW, Lindblad DS, Clark RB, Giles WR (1998) Mathematical model of an adult human atrial cell: the role of K<sup>+</sup> currents in repolarization. *Circ Res* 82:63-81.
- O'Haver T (2006) Findpeaks. [www.mathworks.com/matlabcentral/fileexchange](http://www.mathworks.com/matlabcentral/fileexchange).
- O'Malley DM, Kao YH, Fetcho JR (1996) Imaging the functional organization of zebrafish hindbrain segments during escape behaviors. *Neuron* 17:1145-1155.
- Ogiwara I, Miyamoto H, Morita N, Atapour N, Mazaki E, Inoue I, Takeuchi T, Itohara S, Yanagawa Y, Obata K, Furuichi T, Hensch TK, Yamakawa K (2007) Nav1.1 localizes to axons of parvalbumin-positive inhibitory interneurons: A circuit basis for epileptic seizures in mice carrying an *scn1a* gene mutation. *J Neurosci* 27:5903-5914.
- Orger MB, Kampff AR, Severi KE, Bollmann JH, Engert F (2008) Control of visually guided behavior by distinct populations of spinal projection neurons. *Nat Neurosci* 11:327-333.
- Orger MB, Gahtan E, Muto A, Page-McCaw P, Smear MC, Baier H (2004) Behavioral screening assays in zebrafish. *Methods Cell Biol* 77:53-68.
- Padungchaichot P, Wong JY, Natoli AL, Massalas JS, Finkelstein DI, Lawrence AL, Drago J (2000) Early direct and transneuronal effects in mice with targeted expression of a toxin gene to D1 dopamine receptor neurons. *Neuroscience* 95:1025-1033.
- Papagiakoumou E, de Sars V, Oron D, Emiliani V (2008) Patterned two-photon illumination by spatiotemporal shaping of ultrashort pulses. *Opt Express* 16:22039-22047.
- Pastor AM, De la Cruz RR, Baker R (1994) Eye position and eye velocity integrators reside in separate brainstem nuclei. *Proc Natl Acad Sci USA* 91:807-811.
- Pelli DG (1997) The VideoToolbox software for visual psychophysics: transforming numbers into movies. *Spatial Vision* 10:437-442.
- Pisharath H, Rhee JM, Swanson MA, Leach SD, Parsons MJ (2007) Targeted ablation of beta cells in the embryonic zebrafish pancreas using *E. coli* nitroreductase. *Mech Dev* 124:218-229.
- Pitman JL, McGill JJ, Keegan KP, Allada R (2006) A dynamic role for the mushroom bodies in promoting sleep in *Drosophila*. *Nature* 441:753-756.
- Quandt FN (1988) Modification of slow inactivation of single sodium channels by phenytoin in neuroblastoma cells. *Mol Pharmacol* 34:557-565.
- Quiroga RQ, Nadasdy Z, Ben-Shaul Y (2004) Unsupervised spike detection and sorting with wavelets and superparamagnetic clustering. *Neural Comput* 16:1661-1687.
- Ragsdale DS (2008) How do mutant Nav1.1 sodium channels cause epilepsy? *Brain Res Rev* 58:149-159.
- Rickgauer JP, Tank DW (2009) Two-photon excitation of channelrhodopsin-2 at saturation. *Proc Natl Acad Sci U S A* 106:15025-15030.

- Rudy B (1978) Slow inactivation of the sodium conductance in squid giant axons. Pronase resistance. *J Physiol (Lond)* 283:1-21.
- Scheer N, Campos-Ortega JA (1999) Use of the Gal4-UAS technique for targeted gene expression in the zebrafish. *Mech Dev* 80:153-158.
- Scherf D (1927) Über unvollständigen Sinus-Vorhofblock. *Zeitschrift für Die Gesamte Experimentelle Medizin* 57:188-202.
- Scherz PJ, Huisken J, Sahai-Hernandez P, Stainier DY (2008) High-speed imaging of developing heart valves reveals interplay of morphogenesis and function. *Development* 135:1179-1187.
- Schobert B, Lanyi JK (1982) Halorhodopsin is a light-driven chloride pump. *J Biol Chem* 257:10306-10313.
- Schoonheim PJ, Arrenberg AB, Del Bene F, Baier H Optogenetic localization and genetic perturbation of saccade-generating neurons in zebrafish. *J Neurosci* 30:7111-7120.
- Scott EK, Baier H (2009) The cellular architecture of the larval zebrafish tectum, as revealed by Gal4 enhancer trap lines. *Front Neural Circuits* 3:1-14.
- Scott EK, Mason L, Arrenberg AB, Ziv L, Gosse NJ, Xiao T, Chi NC, Asakawa K, Kawakami K, Baier H (2007) Targeting neural circuitry in zebrafish using GAL4 enhancer trapping. *Nat Methods* 4:323-326.
- Scudder CA, Kaneko CRS, Fuchs AF (2002) The brainstem burst generator for saccadic eye movements; A modern synthesis. *Exp Brain Res* 142:439-462.
- Sedmera D, Reckova M, deAlmeida A, Sedmerova M, Biermann M, Volejnik J, Sarre A, Raddatz E, McCarthy RA, Gourdie RG, Thompson RP (2003) Functional and morphological evidence for a ventricular conduction system in zebrafish and *Xenopus* hearts. *Am J Physiol Heart Circ Physiol* 284:H1152-1160.
- Sehnert AJ, Huq A, Weinstein BM, Walker C, Fishman M, Stainier DY (2002) Cardiac troponin T is essential in sarcomere assembly and cardiac contractility. *Nat Genet* 31:106-110.
- Shimoda N, Knapik EW, Ziniti J, Sim C, Yamada E, Kaplan S, Jackson D, de Sauvage F, Jacob H, Fishman MC (1999) Zebrafish genetic map with 2000 microsatellite markers. *Genomics* 58:219-232.
- Slimko EM, McKinney S, Anderson DJ, Davidson N, Lester HA (2002) Selective electrical silencing of mammalian neurons in vitro by the use of invertebrate ligand-gated chloride channels. *J Neurosci* 22:7373-7379.
- Smear MC, Tao HW, Staub W, Orger MB, Gosse NJ, Liu Y, Takahashi K, Poo M-m, Baier H (2007) Vesicular glutamate transport at a central synapse limits the acuity of visual perception in zebrafish. *Neuron* 53:65-77.
- Sorensen JB, Matti U, Wei SH, Nehring RB, Voets T, Ashery U, Binz T, Neher E, Rettig J (2002) The SNARE protein SNAP-25 is linked to fast calcium triggering of exocytosis. *Proc Natl Acad Sci U S A* 99:1627-1632.
- Straka H, Beck JC, Pastor AM, Baker R (2006) Morphology and Physiology of the Cerebellar Vestibulolateral Lobe Pathways Linked to Oculomotor Function in the Goldfish. *J Neurophysiol* 96:1963-1980.

- Strassman A, Highstein SM, McCrea RA (1986a) Anatomy and physiology of saccadic burst neurons in the alert squirrel monkey. II. Inhibitory burst neurons. *J Comp Neurol* 249:358-380.
- Strassman A, Highstein SM, McCrea RA (1986b) Anatomy and physiology of saccadic burst neurons in the alert squirrel monkey. I. Excitatory burst neurons. *J Comp Neurol* 249:337-357.
- Suster ML, Martin JR, Sung C, Robinow S (2003) Targeted expression of tetanus toxin reveals sets of neurons involved in larval locomotion in *Drosophila*. *J Neurobiol* 55:233-246.
- Szobota S, Gorostiza P, Del Bene F, Wyart C, Fortin DL, Kolstad KD, Tulyathan O, Volgraf M, Numano R, Aaron HL, Scott EK, Kramer RH, Flannery J, Baier H, Trauner D, Isacoff EY (2007) Remote control of neuronal activity with a light-gated glutamate receptor. *Neuron* 54:535-545.
- Tian L, Hires SA, Mao T, Huber D, Chiappe ME, Chalasani SH, Petreanu L, Akerboom J, McKinney SA, Schreiter ER, Bargmann CI, Jayaraman V, Svoboda K, Looger LL (2009) Imaging neural activity in worms, flies and mice with improved GCaMP calcium indicators. *Nat Methods* 6:875-881.
- Toib A, Lyakhov V, Marom S (1998) Interaction between duration of activity and time course of recovery from slow inactivation in mammalian brain Na<sup>+</sup> channels. *J Neurosci* 18:1893-1903.
- Tomlinson RD, Robinson DA (1984) Signals in vestibular nucleus mediating vertical eye movements in the monkey. *J Neurophysiol* 51:1121-1136.
- Valderrabano M, Chen F, Dave AS, Lamp ST, Klitzner TS, Weiss JN (2006) Atrioventricular ring reentry in embryonic mouse hearts. *Circulation* 114:543-549.
- van der Blik AM, Meyerowitz EM (1991) Dynamin-like protein encoded by the *Drosophila shibire* gene associated with vesicular traffic. *Nature* 351:411-414.
- Wallen P, Williams TL (1984) Fictive locomotion in the lamprey spinal cord in vitro compared with swimming in the intact and spinal animal. *J Physiol* 347:225-239.
- Wang S, Szobota S, Wang Y, Volgraf M, Liu Z, Sun C, Trauner D, Isacoff EY, Zhang X (2007) All optical interface for parallel, remote, and spatiotemporal control of neuronal activity. *Nano Lett* 7:3859-3863.
- Wilders R (2007) 25 years of SA nodal cell modeling. *Conf Proc IEEE Eng Med Biol Soc* 2007:152-155.
- Wong JY, Padungchaichot P, Massalas JS, Drago J (2000) Late direct and transneuronal effects in mice with targeted expression of a toxin gene to D1 dopamine receptor neurons. *Neuroscience* 95:1035-1041.
- Wyart C, Bene FD, Warp E, Scott EK, Trauner D, Baier H, Isacoff EY (2009) Optogenetic dissection of a behavioural module in the vertebrate spinal cord. *Nature* 461:407-410.
- Yamamoto M, Wada N, Kitabatake Y, Watanabe D, Anzai M, Yokoyama M, Teranishi Y, Nakanishi S (2003) Reversible suppression of glutamatergic neurotransmission of cerebellar granule cells in vivo by genetically

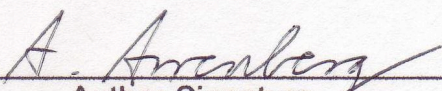
- manipulated expression of tetanus neurotoxin light chain. *J Neurosci* 23:6759-6767.
- Yoshida K, McCrea R, Berthoz A, Vidal PP (1982) Morphological and physiological characteristics of inhibitory burst neurons controlling horizontal rapid eye movements in the alert cat. *J Neurophysiol* 48:761-784.
- Zannino DA, Appel B (2009) Olig2+ precursors produce abducens motor neurons and oligodendrocytes in the zebrafish hindbrain. *J Neurosci* 29:2322-2333.
- Zhang F, Wang L-P, Brauner M, Liewald JF, Kay K, Watzke N, Wood PG, Bamberg E, Nagel G, Gottschalk A, Deisseroth K (2007) Multimodal fast optical interrogation of neural circuitry. *Nature* 446:633-639.
- Zhao S, Cunha C, Zhang F, Liu Q, Gloss B, Deisseroth K, Augustine GJ, Feng G (2008) Improved expression of halorhodopsin for light-induced silencing of neuronal activity. *Brain Cell Biol.*

## Signed library release form

It is the policy of the University to encourage the distribution of all theses, dissertations, and manuscripts. Copies of all UCSF theses, dissertations, and manuscripts will be routed to the library via the Graduate Division. The library will make all theses, dissertations, and manuscripts accessible to the public and will preserve these to the best of their abilities, in perpetuity.

**Please sign the following statement:**

I hereby grant permission to the Graduate Division of the University of California, San Francisco to release copies of my thesis, dissertation, or manuscript to the Campus Library to provide access and preservation, in whole or in part, in perpetuity.

  
\_\_\_\_\_  
Author Signature  
(Aristides Arrenberg)

06/08/2010  
Date